REPORT DOCUMENTATION PAGE

AFOSR-TR-95

CS34

1 AGENCY USE ONLY (Leave blank)	2 REPORT DATE 24 May 1995	3. REPORT TYPE AND DATES COVERED Final Technical Report, 1 March '92 - 28 Feb. '95

4. TITLE AND SUBTITLE
GAS-PHASE METAL REACTIONS

5. FUNDING NUMBERS
PE - 61102F
PR - 2308
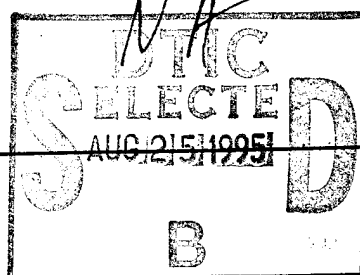SA - AS
G - F49620-92-J-0172

6. AUTHOR(S)

Arthur Fontijn

7. PERFORMING ORGANIZATION NAME(S) AND ADDRESS(ES)

Department of Chemical Engineering
Rensselaer Polytechnic Institute
Troy, NY 12180-3590

9. SPONSORING MONITORING AGENCY NAME(S) AND ADDRESS(ES)

AFOSR/NA
110 Duncan Avenue, Suite B115
Bolling AFB, DC 20332-0001

DTIC ELECTED AUG 25 1995 B

10. SPONSORING MONITORING AGENCY REPORT NUMBER
F49620-92-J-0172

11. SUPPLEMENTARY NOTES

12a. DISTRIBUTION AVAILABILITY STATEMENT

Approved for public release; distribution is unlimited

12b. DISTRIBUTION CODE

13. ABSTRACT (Maximum 200 words)

The use of new advanced solid rocket propellant constituents, such as, e.g., boron as HEDM and ammonium nitrate as replacement for halogen-containing oxidants, requires knowledge of their combustion characteristics. To this end experimental rate coefficient k measurements on individual important Al and B species reactions were made in the 300-1800 K temperature range using a high-temperature fast-flow reactor. Temperature dependent rate coefficient expressions $k(T) = AT^n \exp(-E/RT)$ are found for the reactions between AlO and CH_4, O_2; Al and N_2O; AlCl and N_2O, CO_2, SO_2; BCl and N_2O, SO_2; BO and CO_2. To allow semi-empirical predictions for further metal oxidation reactions, two semi-empirical theories have been developed and utilized. These are Semi-Empirical Configuration Interaction theory for prediction of E from one species to another and Metals-Transition State Theory for prediction of k(T) from k at one temperature. Dual military-civilian applications of this work are discussed.

14. SUBJECT TERMS			15. NUMBER OF PAGES 51
Combustion Kinetics	HEDMs	Rocket Propulsion	
High-Temperature	AlO	Technology Transfer	16. PRICE CODE
Boron Compounds	Kinetic Theory	Hydrocarbon Conversion	

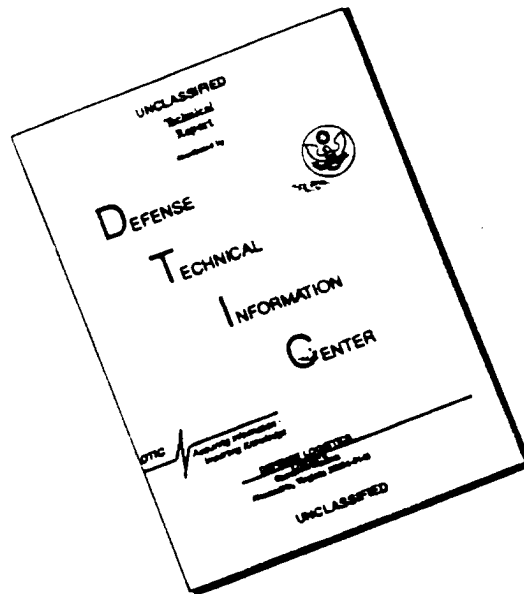| 17. SECURITY CLASSIFICATION OF REPORT Unclassified	18. SECURITY CLASSIFICATION OF THIS PAGE Unclassified	19. SECURITY CLASSIFICATION OF ABSTRACT Unclassified	20. LIMITATION OF ABSTRACT UL

Standard Form 298 (Rev. 2-89)

DISCLAIMER NOTICE

THIS DOCUMENT IS BEST QUALITY AVAILABLE. THE COPY FURNISHED TO DTIC CONTAINED A SIGNIFICANT NUMBER OF PAGES WHICH DO NOT REPRODUCE LEGIBLY.

CONTENTS

APPENDIX A   "Gas-Phase Metal Reactions"

APPENDIX B   "Gas-Phase Reactions between Hydrocarbons and Metal Oxides: The AlO + CH_4 Reaction from 590 to 1380 K"

APPENDIX C   "Experimental and Transition-State Theory Studies of the Gas-Phase Reactions of AlCl with N_2O, CO_2, and SO_2"

APPENDIX D   "Wide Temperature Range Kinetics of the Gas-Phase Reactions of BCl with SO_2, N_2O, O_2, and CO_2"

APPENDIX E   "Activation Barriers for Series of Exothermic Homologous Reactions. IV. Comparison of Measurements to Theory for Reactions s^2p^1 Atoms with N_2O"

APPENDIX F   "The AlO + O_2 Reaction System Over a Wide Temperature Range"

I. RESEARCH OBJECTIVES

Advances in solid-fuel propellant technology for the late nineteen nineties depend critically on an understanding and quantitative description of a number of combustion processes. These include the combustion of metallic, particularly boron, HEDMs and environmentally clean Al and B propellants, containing, e.g. ammonium nitrate instead of perchlorate. In this context the present work had several objectives. Unique high-temperature, fast-flow reactors HTFFR, which allow measurements of the kinetics of isolated reactions in the 300-1900 K temperature range, were employed to provide a kinetic data base for metallic species reactions in propulsion system models. The results obtained enhance the understanding of the chemistry involved, which in turn allowed making predictions for further reactions. This enables faster model development than experimental work by itself can provide. To this end establishing correlations in series of similar reactions and understanding the fundamental basis for these was emphasized. Where appropriate dual military-civilian use aspects of the work have been emphasized (see especially Section III A).

II. RESULTS

A. Cumulative Chronological List of Publications

APPENDIX A

1. Arthur Fontijn, Ed. *Gas-Phase Metal Reactions*, North-Holland, Amsterdam, 1992, 700 pages, preface v-vi

APPENDIX B

2. David P. Belyung, Arthur Fontijn and Paul Marshall, "Gas-Phase Reactions Between Hydrocarbons and Metal Oxides. The AlO+CH_4 reaction from 590 to 1380 K", *The Journal of Physical Chemistry*, <u>97</u>, 3456-3459 (1993).

APPENDIX C

3. Peter M. Futerko and Arthur Fontijn, "Experimental and Transition-State Theory Studies of the Gas-Phase Reactions of AlCl with N_2O, CO_2, and SO_2," *The Journal of Physical Chemistry*, <u>97</u>, 7222-7227 (1993).

APPENDIX D

4. Peter M. Futerko, Aleksandar G. Slavejkov, and Arthur Fontijn, "Wide Temperature Range Kinetics of the Gas-Phase Reactions of BCl with SO_2, N_2O, O_2, and CO_2," *The Journal of Physical Chemistry* <u>97</u>, 11950-11955 (1993).

APPENDIX E

5.   David P. Belyung, Peter M. Futerko, and Arthur Fontijn, "Activation Barriers for Series of Exothermic Homologous Reactions IV. Comparison of Measurements to Theory for Reactions of s^2p^1 Atoms with N_2O," *The Journal of Chemical Physics* 102, 155-160 (1995).

APPENDIX F

6.   David P. Belyung and Arthur Fontijn, "The AlO + O_2 Reaction System Over a Wide Temperature Range," *J. Phys. Chem.*, submitted, April 1995.

In addition the following Ph.D. thesis resulted from this grant:

7.   Peter M. Futerko, "Experimental and Theoretical Studies of BCl, AlCl, and Metal Atom Reactions with O_2, CO_2, SO_2, and N_2O," Rensselaer Polytechnic Institute, 1993, University Microfilm No. 9325242.

III. SIGNIFICANCE OF THE RESULTS

Here we discuss the significance of the papers given in the preceding section in the chronological sequence given there.

A.   General and Military-Civilian Dual-Use (Publications 1 and 2)

The general significance of Publication 1, should be clear from its Preface given. It has become very widely quoted.

A few dual military-civilian aspects are illustrated here. Publication 2 is one example of this; another is the use of our unique family of reactors developed for wide temperature range studies on isolated reactions. The development of these reactors was prompted by the needs of the military for kinetic data on metal combustion. With support of NSF we are now also applying the reactors to waste incineration problems. In that area we showed the presence of several paths for chromium oxidation.[1] As chromium is in its highest oxidation state highly toxic, but relatively harmless in lower oxidation states, knowledge of the various reaction pathways is needed to hinder the complete oxidation. An understanding of high-temperature reactions of metals is important to many more applications. These include decreasing slag formation in coal combustion, preventing hot corrosion in jet engine turbines, alleviation of soot formation in all sorts of combustion devices, as well as new chemical synthesis processes for refractory materials.

The direct conversion of methane, i.e. natural gas, to liquid fuels and chemicals of commercial interest is a long-sought goal. A major approach being followed is to pass methane over solid-state catalysts consisting of mixtures of metal oxides with dopants. The first step in this process is to abstract a hydrogen atom from methane CH_4 to produce a highly reactive methyl radical CH_3 to form C-C bonds. To understand these surface reactions better, gas-phase studies of the reactions between methane and metal oxides are desired. Theoretical studies have suggested that such

abstraction reactions should occur at elevated temperatures. Because of our experience with AlO from studies for rocket propellants, we decided to use that oxide to experimentally investigate this. Publication 2 provides the first experimental confirmation, but also shows that at least in this instance the theoretically predicted mechanism is not dominant. In general, such gas-phase studies provide essential input for gas-solid catalytic reactions.

B. k(T) Predictions for Model Development (Publications 3-5)

Combustion models, whether for the plume or chamber, require reliable kinetic input data at realistic temperatures. The data needed are rate coefficients k(T) and mechanisms. Measurements with our HTFFR (high-temperature fast-flow reactor) and MHTP (metals high-temperature photochemistry) techniques are providing such information for metallic species. However, experiments alone are a rather slow way to obtain information on all the reactions needed. It is therefore desirable to develop predictive techniques. Fully theoretical a priori techniques have not yet reached the state of making meaningful predictions. We have therefore chosen to develop semi-empirical techniques for metallic species. These predictions allow either extrapolation of our measured data from one species to another (SECI theory), or for one reaction, from one temperature to a wide range of temperatures (MTST theory). Another way of expressing the scope of these theories is that in rate coefficient expressions

$$k(T) = AT^n \exp(-E/RT) \tag{1}$$

SECI predicts the exponential, MTST the pre-exponential part. The theories are semi-empirical in that for SECI the E factor (activation barrier) of a similar reaction needs to be known and that for MTST an experimental rate coefficient measurement at one temperature is required.

The left hand side of Figure 1 illustrates SECI the right hand side MTST, each of which will now be discussed.

1. Semi-empirical Configuration Interaction (SECI) Theory

The E factor in eq. (1) is the difference in the potential energy of the activated complex (transition state), formed from the reactants, and the sum of the potential energies of the reactants. It represents the highest potential energy on the path from reactants to products. It can be calculated, using resonance theory, from the properties of three hypothetical resonating activated complexes, i.e. that resulting from purely ground state interaction for which the barrier is q, the interaction involving the lowest excited state of the atomic reaction partner, and ionic interaction. The wave function of the actual complex resulting from these structures is given by

$$\Psi = c_1\Psi_1 + c_2\Psi_2 + c_3\Psi_3 \tag{2}$$

where the c factors give the contributions of each structure. The actual Ψ will be that for which $E = \int \Psi^* H \Psi d\tau$ is at a minimum. The condition can be expressed as a set of simultaneous linear equations, ultimately resulting in
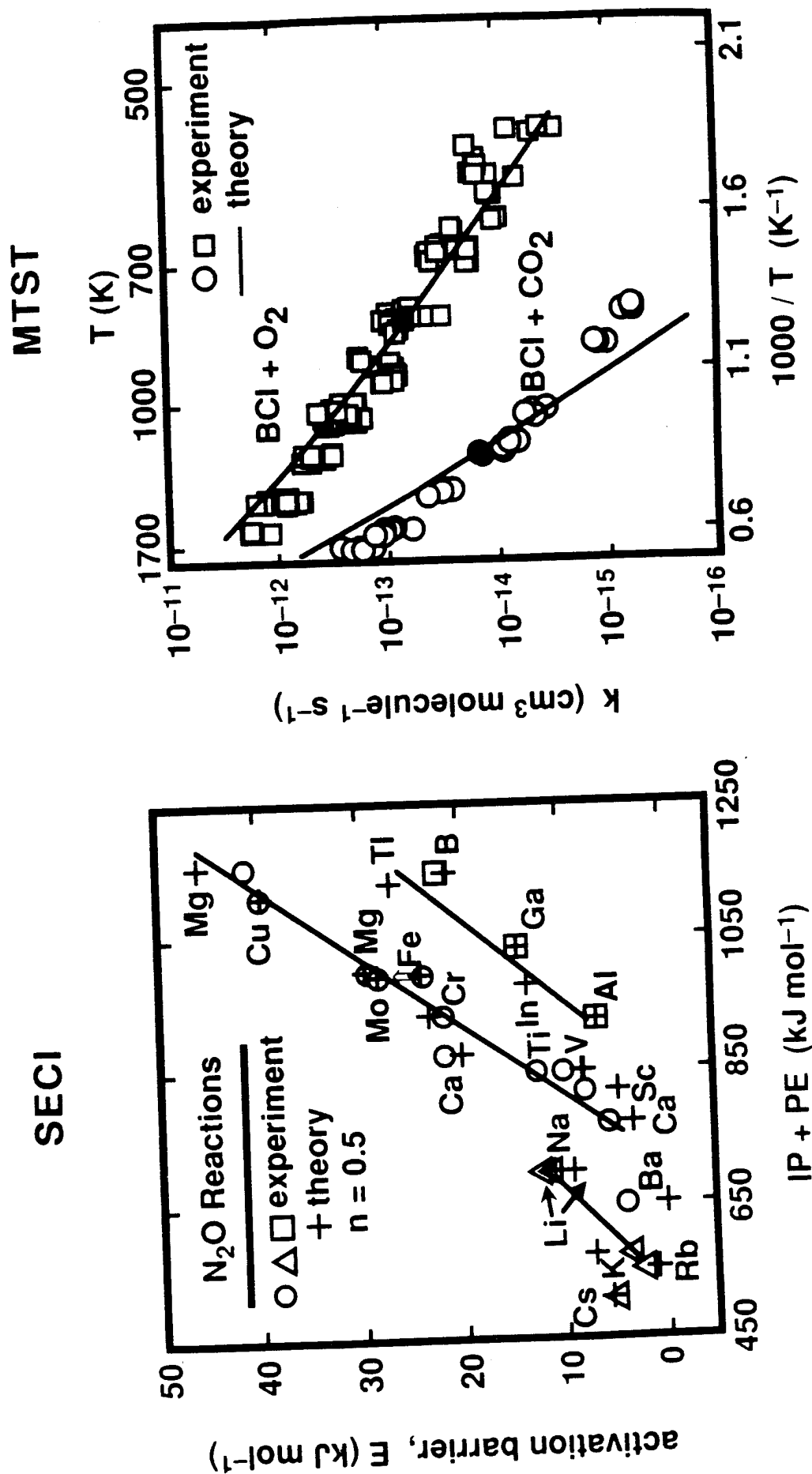
3

k(T) Predictions For Model Development

SECl

MTST

Fontijn / RPI

Figure 1

4

$$aq + bq^2 + cqE + dq^2E + fE + gE^2 + hE^3 = 0 \qquad (3)$$

where a, b, c, d, e, f, g, h are constants derived from tabulated physical properties of the individual reaction partners.

E and q can not simultaneously be calculated from first principles. For a series of similar reactions, e.g. the boron group atoms with N_2O (see the figure) we therefore obtain E for one atomic partner. This is done by fixing n for the series, which allows finding E from eq. (1) used as the fitting expression for the experimental k(T) measurements. Eq. (3) then yields q, which according to the Hirschfelder theory is the same for all members of the series. E for the other members of the series can now be calculated from eq. 3 using q and the constants appropriate for each of the atoms.

The SECI figure shows E plotted against I.P. (the ionization potential related to the 3rd structure) plus P.E. (the promotion, or excitation, energy representative of the 2nd structure). It shows good correlation with IP + PE and excellent agreement between theory and experiment obtained for three groups of atom reactions with N_2O. The left hand line is for the one-electron alkali metal group and is of interest for example to hot turbine combustion corrosion problems. The middle line is for two electron atoms, and contains metals of interest, e.g. to toxic emission problems. The right hand line, for two s one p electron atoms, has most recently been obtained and includes metals of most importance to rocket propulsion.

2. Metals Transition State Theory (MTST)

As shown in Fig. 1, by taking one experimental point (the solid symbol) at mid-temperature range for the reaction of interest, we can predict the shape of the Arrhenius plot in good agreement with measurements, thus reducing the work required for data taking.

In general transition state theory (TST) k(T) is given by:

$$k(T) = \frac{k_B T}{h} \frac{q^{\neq}}{q_{AB}q_{CD}} \exp(-\Delta E^{\neq}/RT) \qquad (4)$$

where k_B and h are, respectively, the Boltzmann and Planck constants, and q_{AB} and q_{CD} are the partition functions of the reactants. $q^{\neq}$ and $\Delta E^{\neq}$ are, respectively, the partition function of the transition state and its energy above the reactant ground states, both of which are unknown. By using simple ab initio methods for estimating $q^{\neq}$, and equating eq. (4) with an experimental rate coefficient at one temperature, $\Delta E^{\neq}$ can be found.

The basic TST approach was developed primarily for reactions of more commonly studied reactants, such as hydrocarbons. There, the transition state structure and hence $q^{\neq}$ can be found readily by comparison to known stable compounds, which information is generally lacking for refractory species. The advance is that we have made the method useful for such species as well.

C. AlO and BO Oxidation Reactions (Publication 6)

Oxidation reactions of Al and B species are essential input to various rocket combustion models. In further experimental work, we have thoroughly studied the AlO oxidation by O_2 (Publication 6) and obtained a significant preliminary result for BO oxidation (not published).

The AlO + O_2 reaction system was originally thought to proceed as a simple abstraction reaction leading to AlO_2 + O.[2] However, in recent years we have found several examples of reactions, considered in the literature as simple abstraction to proceed by addition or insertion at lower temperatures, with abstraction becoming more significant, but not necessarily dominant, at higher temperatures. Examples of this are publication 2 and Ref. 1. These observations and the vast improvements in HTFFR technique since then,[2] prompted this new investigation. For temperatures below about 1000 K the AlO consumption now is found to be pressure-dependent, with a negative temperature dependence; log k (305-1010 K) = -25.36-1.69 log (T/K) $cm^6 molecule^{-2} s^{-1}$. At higher temperatures the system becomes pressure-independent and the AlO consumption rate coefficients increase; k(1200-1690 K) = $7.7 \times 10^{-10} exp$ (-10008 K/T) $cm^3 molecule^{-1} s^{-1}$.

The following mechanism describes these findings:

$$AlO + O_2 \xrightleftharpoons{\qquad} AlO_3^* \xrightarrow{M} AlO_3 \qquad\qquad (5)$$
$$\downarrow$$
$$AlO_2 + O$$
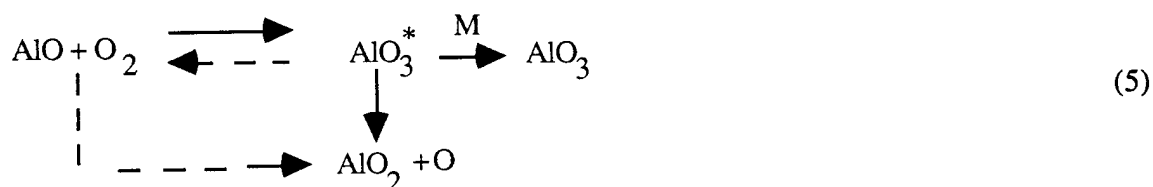
Here, the dotted lines indicate the paths unlikely to contribute significantly. Thus, the reaction is thought to proceed through an intermediate AlO_3^* complex, which can be collision-stabilized or dissociate to AlO_2 + O. The latter process is 96 $\pm$ 40 kJ mol^{-1} endothermic.

It is interesting to observe that in a room temperature study of the AlO + CO_2 reaction, competition between an addition and abstraction reaction was observed.[3] This suggests that in that system abstraction will become dominant at lower temperatures than for AlO + O_2. The O_2 reaction should be primarily of interest for plume models, while the CO_2 reaction is of both plume and chamber interest.

The AlO + O_2 behavior contrasts with that of the iso-electronic exothermic BO + O_2 reaction system, for which no pressure dependence was found over the 300-1000 K range, but again a negative temperature dependence was observed;[4] k(T) = $7.0 \times 10^{-12} exp$ (259 K/T) $cm^3 molecule^{-1} s^{-1}$. This suggests a

$$BO + O_2 \rightleftharpoons BO_3^* \rightarrow BO_2 + O \qquad\qquad (6)$$
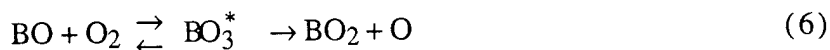
mechanism. We have made a series of BO oxidation measurements in the HTFFR apparatus. In this environment accurate rate coefficients could not be obtained, apparently due to BO wall-dimerization. We are about to continue this work in one of our MHTP (metals high-temperature photochemistry) reactors, where such problems should not arise.[6] Nonetheless, the HTFFR work has already yielded some interesting

6

information. Our results on BO + O_2 between 400 and 1000 K are in essential agreement with the earlier measurements from an MHTP-like reactor.[4] For the hypothesized reaction BO + $CO_2 \rightarrow BO_2$ + CO a slow pressure-dependent process was observed at room temperature, but no measurable BO consumption occurred from 780 to 1200 K. This indicates rate coefficients less than about 1×10^{-15} $cm^3 molecule^{-1} s^{-1}$. This is four orders of magnitude lower than found for the BO + O_2 reaction. It further is two to three orders of magnitude lower than the guestimated values in the current models for boron-hydrocarbon slurry (air-breathing) combustion, where it is indicated to be a highly sensitive reaction. Those models should now be reconsidered.

IV. PROFESSIONAL PERSONNEL

For two Ph.D. students, P.M. Futerko and D.P. Belyung this grant and the parallel AASERT grant were their principal projects. Additionally, Dr. P.N. Bajaj and Mr. W.F. Flaherty helped with the work, as did two M.Sc. students M.G. Santana and G.T. Dalakos, and an undergraduate A.M. Zinacola. My former students, Professor P. Marshall and Dr. A.G. Slavejkov contributed significantly to publications 2 and 4, respectively.

V. CUMULATIVE CHRONOLOGICAL LIST OF PRESENTATIONS AND OTHER INTERACTIONS

We presented papers and seminars in which results of our AFOSR-sponsored work were discussed, at the:

1. HEDM Contractors Conference, Lancaster, CA (April 1992).

2. Russian Academy of Sciences, Chernogolovka, Russia (May 1992).

3. American Chemical Society, National Meeting, Washington, DC (August 1992).

4. Department of Chemistry, University of Auckland, New Zealand (March 1993).

5. AFOSR Contractors Meeting in Propulsion, Atlantic City, NJ (June 1993).

6. Third International Conference on Chemical Kinetics, NIST, Gaithersburg, MD (July 1993).

7. CNRS Laboratory for Photophysics and Molecular Photochemistry, University of Bordeaux, France (July 1993).

8. AFOSR Workshop on "Radiation Signature Predictions, Ultraviolet Kinetics," Washington, DC (April 1994).

9. AFOSR Contractors Meeting in Propulsion, Lake Tahoe, CA/NV (June 1994).

10. AIChE National Meeting, San Francisco, CA (November 1994).

11. Eastern States Meeting, The Combustion Institute, Clearwater Beach, FL (December 1994).

GAS-PHASE
METAL REACTIONS

edited by

ARTHUR FONTIJN

Department of Chemical Engineering
Rensselaer Polytechnic Institute
Troy, NY 12180-3590
U.S.A.

". . . here's metal more attractive."
W. Shakespeare: Hamlet

PREFACE

The study of reactions of metallic species in the gas phase impinges on a variety of basic, technical and socio-technical fields. Spread over the currently "developed world" there are a sizeable number of scientists and engineers occupied with gas-phase metal reactions. Yet, there has been little interaction among them; apparently no book or major meeting has previously been dedicated to the subject. A number of conversations I had with colleagues on both sides of the Atlantic during a recent sabbatical clearly brought out the need to try to bundle our knowledge. The present volume has come about as a response to this. It brings together overviews from most of the groups concerned with fundamental research, both of an experimental and theoretical nature. Still, much of this work has been stimulated by very practical problems. The individual authors show these connections. To further emphasize this aspect, a few of the final chapters primarily address such problems, but show what the research needs are, or how fundamental information can be used toward their solution. The introductory chapter outlines the connection between the various contributions and mentions significant further efforts and applications.

If one compares the present field to other areas of chemical reaction studies, such as hydrocarbon oxidation, it is striking how little theoretical effort there has been. In fact, several of the theory chapters in this volume came about primarily because the plans for it stimulated the research. Another gap that shows clearly is that between the kinetic and dynamic aspects; much work needs to be done before a proper synthesis of the results obtained can be achieved. Many of the chapters indicate current shortcomings and potential areas where important contributions can be made. This book therefore not only summarizes most of the present knowledge, but also provides a proper starting point for far more extensive further research and interdisciplinary collaboration.

The birth of this volume has proceeded in stages. The authors submitted preliminary chapters, which were then presented and discussed at a symposium held before the Physical Chemistry Division of the American Chemical Society, in New York in August 1991. Following the meeting, many of the chapters were revised and all were then refereed and usually further improved. Thus this work already includes the benefit of much interaction on an international scale.

I thank the authors and referees for their timely contributions and Mrs. Rose Primett for all the typing, organizing, faxing and telephoning that this work has involved. Finally, I thank several of the agencies of the United States Government that have over the years allowed me to continue my efforts on, and expand my interest in, metallic species reactions. Particularly, the support I have received from the Air Force Office of Scientific Research and the National Science Foundation is gratefully acknowledged.

<div align="right">

Arthur Fontijn
Rensselaer Polytechnic Institute
Troy, NY 12180-3590
U.S.A.

</div>

GAS-PHASE
METAL REACTIONS

edited by

ARTHUR FONTIJN
Department of Chemical Engineering
Rensselaer Polytechnic Institute
Troy, NY 12180-3590
U.S.A.

N·H

". . . here's metal more attractive."
W. Shakespeare: Hamlet

PREFACE

The study of reactions of metallic species in the gas phase impinges on a variety of basic, technical and socio-technical fields. Spread over the currently "developed world" there are a sizeable number of scientists and engineers occupied with gas-phase metal reactions. Yet, there has been little interaction among them; apparently no book or major meeting has previously been dedicated to the subject. A number of conversations I had with colleagues on both sides of the Atlantic during a recent sabbatical clearly brought out the need to try to bundle our knowledge. The present volume has come about as a response to this. It brings together overviews from most of the groups concerned with fundamental research, both of an experimental and theoretical nature. Still, much of this work has been stimulated by very practical problems. The individual authors show these connections. To further emphasize this aspect, a few of the final chapters primarily address such problems, but show what the research needs are, or how fundamental information can be used toward their solution. The introductory chapter outlines the connection between the various contributions and mentions significant further efforts and applications.

If one compares the present field to other areas of chemical reaction studies, such as hydrocarbon oxidation, it is striking how little theoretical effort there has been. In fact, several of the theory chapters in this volume came about primarily because the plans for it stimulated the research. Another gap that shows clearly is that between the kinetic and dynamic aspects; much work needs to be done before a proper synthesis of the results obtained can be achieved. Many of the chapters indicate current shortcomings and potential areas where important contributions can be made. This book therefore not only summarizes most of the present knowledge, but also provides a proper starting point for far more extensive further research and interdisciplinary collaboration.

The birth of this volume has proceeded in stages. The authors submitted preliminary chapters, which were then presented and discussed at a symposium held before the Physical Chemistry Division of the American Chemical Society, in New York in August 1991. Following the meeting, many of the chapters were revised and all were then refereed and usually further improved. Thus this work already includes the benefit of much interaction on an international scale.

I thank the authors and referees for their timely contributions and Mrs. Rose Primett for all the typing, organizing, faxing and telephoning that this work has involved. Finally, I thank several of the agencies of the United States Government that have over the years allowed me to continue my efforts on, and expand my interest in, metallic species reactions. Particularly, the support I have received from the Air Force Office of Scientific Research and the National Science Foundation is gratefully acknowledged.

Arthur Fontijn
Rensselaer Polytechnic Institute
Troy, NY 12180-3590
U.S.A.

Gas-Phase Reactions between Hydrocarbons and Metal Oxides: The AlO + CH₄ Reaction from 590 to 1380 K

David P. Belyung and Arthur Fontijn*

*High-Temperature Reaction Kinetics Laboratory, The Isermann Department of Chemical Engineering,
Rensselaer Polytechnic Institute, Troy, New York 12180-3590*

Paul Marshall*

Department of Chemistry, University of North Texas, Denton, Texas 76203-5068

Received: November 16, 1992; In Final Form: February 2, 1993

A recent ab inito study suggested that gaseous metal oxides can directly abstract H atoms from hydrocarbons, but with considerable barriers. To try to confirm the occurrence of such reactions, the title reaction has been studied in a high-temperature fast-flow reactor. The data are well described by the fitting expression $k(590-1380$ K$) = 9.6 \times 10^{-39}(T/K)^{7.96} \exp(2468$ K$/T)$ cm³ molecule⁻¹ s⁻¹, with 2σ precision limits varying with temperature from ±4% to ±12%. The corresponding 2σ accuracy limits are about ±25%. Comparison of this result to further ab initio and conventional transition-state theory calculations suggests that direct abstraction indeed can occur at the higher temperatures but that one or more other channels, possibly involving AlO insertion into a C-H bond, dominate in the initial attack step. The potential implications of this work for catalytic conversion of methane to higher hydrocarbons are considered.

Introduction

In a recent ab initio study Børve and Pettersson[1] predicted that some gaseous metal oxides, LiO, MgO, and AlO, can directly abstract an H atom from methane to produce methyl radicals. Such exothermic reactions have not been observed in the gas phase, and their studies suggested these to have considerable barriers, 25–67 kJ mol⁻¹. However, solid metal oxides have been found to be effective catalysts for H abstraction from methane, leading to C₂H₄ and C₂H₆ in significant yields,[2] a process of considerable commercial promise. The basis for this catalytic reaction has been strongly suggested to be the surface reaction of the O⁻ ion to remove a hydrogen atom, a process which appears to proceed to a significant degree only above about 1000 K.[3] Theoretical studies of cluster models of the MoO₃ oxide structure have supported this hypothesis.[4] If the occurrence of the gas-phase processes could be experimentally confirmed, it would not only establish a new class of reactions but also could lead to a better understanding of the heterogeneous catalytic processes. We therefore decided to investigate one of these suggested reactions:

$$AlO + CH_4 \rightarrow AlOH + CH_3 \qquad (1)$$
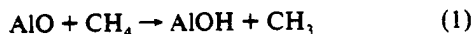
for which $\Delta H^\circ = -27$ kJ mol⁻¹.[5,6] While this reaction has a higher predicted barrier than those of the other oxides,[1] we have had extensive experience with the study of the gas-phase reactions of AlO at temperatures up to 1600 K in HTFFRs (high-temperature fast-flow reactors)[7] and therefore selected this oxide.

Technique

The HTFFR facility used in this work and the data handling procedures have been previously described.[7] Briefly, a vertical mullite (McDanel MV-30) reaction tube (60 cm long, 2.2 cm i.d.) is heated to the desired temperature by columns of resistively heated SiC rods inside an insulated, water-cooled vacuum housing. Al vapor is produced by resistively heating an Al-wetted W coil in a flow of Ar carrier gas. A trace of oxidizer, 0.5% N₂O or 5% O₂ in Ar, at ≈4 × 10⁻³% of the main Ar flow, is passed through a Pt side tube to a location just downstream from the vapor source to rapidly convert Al to AlO.[8-10] Further downstream CH₄/Ar mixtures at flow rates of 4–8% of the main Ar flow rate are introduced through a movable inlet. Rate coefficient measurements are made under pseudo-first-order conditions, [AlO] ≪ [CH₄], in the stationary inlet mode,[11] at reaction zone lengths of 10 or 20 cm.

Relative AlO concentrations were monitored by laser-induced fluorescence (LIF) using a pulsed Lambda Physik EMG 101 excimer/FL 2002 dye laser in combination with a KDP doubling crystal. Two transitions B²Σ–X²Σ and C²Σ–X²Σ were used. In the former, AlO is pumped on the 464.8-nm (1,0) band and the fluorescence is observed through a 482-nm (20-nm fwhm) interference filter, i.e., mainly at the 486.6-nm (1,1) band.[12] The B²Σ–X²Σ system could only be used up to 1200 K because of interference by the background radiation from the reactor walls. For measurements above 1200 K and some checks at lower temperatures, the C²Σ–X²Σ (0,0) transition at 302.2 nm[12] was used in combination with a 301-nm (11-nm fwhm) interference filter. The fluorescence was detected by an EMI 9813QA photomultiplier tube, connected to a Data Precision Analogic 6000/620 100-MHz transient digitizer.

The gases used were 99.998% Ar from the liquid Ar (Linde), 0.5% N₂O (99.99%) in Ar (99.999%) from Matheson, 5% O₂ (99.99%) in Ar (99.995%) from Scott, and CH₄ (99.99%) from Matheson.

Results

Plots of ln[AlO]ᵣₑₗₐₜᵢᵥₑ versus [CH₄] yield straight lines with slopes $-kt$, where t is reaction time. For each individual measurement, k and σ_k were determined by a weighted linear regression.[11,13] The k values and the experimental conditions under which they were obtained are summarized in Table I. The measurements may be seen to be independent of the following: pressure varied from 13.1 to 63.3 mbar, corresponding to total concentrations [M] from 8.0 × 10¹⁶ to 6.4 × 10¹⁷ molecules cm⁻³; average gas velocity $\bar{v}$ varied from 12 to 98 m s⁻¹; reaction zone length selected at 10 or 20 cm; initial fluorescence intensity F (a measure of initial [AlO]) varied from 9 to 65 in arbitrary units. The temperature range covered is 590–1380 K. The lower limit was determined by the heating effect of the Al vaporizer, and the upper limit by the dissociation of CH₄. An Arrhenius

TABLE I: Summary of Rate Coefficient Measurements on the AlO + CH₄ Reaction[a]

reaction zone length (cm)	P (mbar)	[M] (10^{17} cm^{-3})	[CH₄]$_{max}$ (10^{15} cm^{-3})	F[b]	$\bar{V}$ (m s^{-1})	T (K)	$k \pm \sigma_k$ (cm^3 molecule^{-1} s^{-1})
20	26.7	2.1	9.4	17	32	913	4.42 ± 0.33 (−14)[c,d]
20	26.5	2.1	9.4	17	33	912	4.93 ± 0.41 (−14)[d]
20	43.3	3.3	10.3	24	29	928	3.19 ± 0.31 (−14)[d]
20	20.0	1.5	4.8	33	62	932	5.22 ± 0.63 (−14)[d]
20	20.0	1.5	4.8	24	62	935	6.78 ± 0.93 (−14)[d]
20	15.5	1.0	5.0	22	98	1083	1.67 ± 0.21 (−13)[d]
20	15.5	1.0	5.0	20	98	1083	1.83 ± 0.21 (−13)[d]
20	13.1	0.8	4.4	30	90	1135	1.76 ± 0.23 (−13)[d]
20	17.2	1.1	3.8	47	68	1098	1.72 ± 0.21 (−13)[d]
20	17.2	1.1	3.8	32	68	1102	1.75 ± 0.17 (−13)[d]
20	28.9	1.9	4.7	38	48	1103	1.09 ± 0.12 (−13)[d]
20	19.2	1.2	5.8	41	56	1139	1.58 ± 0.19 (−13)[d]
20	16.7	1.1	4.9	64	67	1144	1.81 ± 0.22 (−13)[d]
20	20.1	1.6	9.9	53	46	882	3.30 ± 0.53 (−14)[d]
20	36.7	2.6	4.4	30	29	1001	8.15 ± 0.90 (−14)[d]
20	30.4	2.1	5.8	41	33	1051	8.53 ± 0.79 (−14)[d]
20	32.8	2.2	5.1	38	31	1053	1.11 ± 0.08 (−13)[d]
20	32.8	2.3	8.5	35	30	1031	8.82 ± 0.97 (−14)[d]
10	36.3	2.5	9.4	32	28	1034	8.62 ± 0.81 (−14)[d]
10	19.6	1.4	6.4	64	51	1034	1.43 ± 0.16 (−13)[d]
10	19.6	1.4	7.7	63	51	1037	9.28 ± 1.07 (−14)[d]
20	19.6	1.3	5.0	54	52	1061	1.28 ± 0.14 (−13)[d]
20	19.6	1.3	5.0	53	52	1063	1.29 ± 0.15 (−13)[d]
20	31.7	2.3	7.0	48	37	985	7.38 ± 0.53 (−14)[d]
20	33.6	2.5	7.5	34	35	982	7.22 ± 0.55 (−14)[d]
10	34.3	2.6	9.6	37	34	961	7.91 ± 0.69 (−14)[d]
10	34.3	2.6	9.5	39	34	963	8.18 ± 0.66 (−14)[d]
10	34.3	2.6	7.4	29	44	962	7.11 ± 0.63 (−14)[d]
10	34.3	2.6	7.4	24	44	961	8.19 ± 0.85 (−14)[d]
20	34.4	2.5	5.7	25	46	1000	1.09 ± 0.09 (−13)[d]
20	34.4	2.5	5.7	23	46	1003	1.09 ± 0.09 (−13)[d]
20	24.1	2.1	13.7	26	38	827	2.10 ± 0.21 (−14)[d]
20	24.9	2.5	18.4	28	29	721	1.16 ± 0.15 (−14)[d]
20	24.9	2.5	18.1	24	29	734	1.34 ± 0.14 (−14)[d]
10	25.1	2.5	18.6	28	28	717	1.31 ± 0.12 (−14)[d]
10	25.7	2.5	18.8	28	28	734	1.65 ± 0.22 (−14)[d]
10	36.0	3.3	15.5	52	34	781	2.67 ± 0.32 (−14)[d]
10	35.7	3.3	15.2	38	35	795	3.12 ± 0.39 (−14)[d]
20	16.0	1.2	5.6	53	58	945	7.05 ± 0.83 (−14)[e]
20	16.0	1.2	4.5	35	58	953	7.84 ± 0.97 (−14)[e]
10	16.3	1.3	6.9	39	57	938	1.10 ± 0.12 (−13)[e]
10	16.3	1.3	8.1	65	57	942	1.07 ± 0.14 (−13)[e]
10	21.2	2.4	14.0	34	28	651	1.44 ± 0.18 (−14)[e]
10	39.5	4.3	17.1	9	15	660	1.62 ± 0.20 (−14)[e]
10	39.5	4.3	17.2	9	15	663	1.99 ± 0.14 (−14)[e]
20	34.1	4.1	21.1	42	19	602	5.60 ± 0.64 (−15)[e]
20	34.0	4.0	17.1	30	19	618	9.95 ± 1.27 (−15)[e]
20	34.0	3.9	16.9	25	19	628	1.02 ± 0.13 (−14)[e]
20	53.1	5.3	6.2	9	21	727	2.11 ± 0.23 (−14)[e]
20	24.5	2.9	20.6	15	19	603	7.78 ± 0.91 (−15)[e]
20	24.5	2.9	20.0	27	20	621	8.11 ± 0.65 (−15)[e]
20	14.3	1.7	11.0	33	24	598	6.71 ± 0.77 (−15)[e]
20	14.3	1.7	11.1	20	23	591	6.23 ± 0.78 (−15)[e]
20	63.3	6.4	9.9	11	20	718	1.72 ± 0.20 (−14)[e]
20	15.3	1.4	8.7	34	37	780	2.40 ± 0.26 (−14)[e]
20	15.3	1.4	8.8	40	37	770	2.43 ± 0.31 (−14)[e]
20	21.9	1.8	5.9	25	33	893	4.94 ± 0.54 (−14)[e]
20	56.0	4.8	4.7	23	20	845	3.02 ± 0.31 (−14)[e]
20	13.7	1.2	4.7	20	55	846	4.64 ± 0.53 (−14)[e]
20	13.7	1.2	4.7	16	56	853	3.87 ± 0.47 (−14)[e]
10	14.1	1.2	7.0	24	56	866	5.81 ± 0.75 (−14)[e]
20	44.5	2.3	1.1	19	30	1374	4.57 ± 0.32 (−13)[e]
20	44.7	2.5	1.2	20	28	1380	3.49 ± 0.34 (−13)[e]
20	41.7	4.5	7.4	32	13	668	1.46 ± 0.11 (−14)[f]
20	41.6	4.6	7.5	45	12	650	1.36 ± 0.10 (−14)[f]
20	53.9	5.3	6.8	62	14	736	1.71 ± 0.11 (−14)[f]
20	54.3	5.6	8.3	65	13	707	1.68 ± 0.14 (−14)[f]
20	54.3	5.7	8.5	58	13	686	1.45 ± 0.11 (−14)[f]
20	17.5	1.0	1.5	40	60	1232	3.44 ± 0.37 (−13)[e]
10	24.1	1.4	2.0	37	46	1283	5.07 ± 0.44 (−13)[e]
10	24.1	1.3	2.0	37	47	1296	5.87 ± 0.50 (−13)[e]
20	24.0	1.3	1.3	38	48	1317	4.52 ± 0.35 (−13)[e]
20	24.0	1.3	1.3	39	48	1324	5.21 ± 0.44 (−13)[e]

[a] The measurements are reported in the sequence in which they were obtained. [b] In arbitrary units. [c] Should be read as (4.42 ± 0.33) × 10^{-14}. [d] Data obtained by using the C$^2\Sigma$–X$^2\Sigma$ transition and an alumina ring inlet. [e] Data obtained by using the C$^2\Sigma$–X$^2\Sigma$ transition and a quartz ring inlet. [f] Data obtained by using the B$^2\Sigma$–X$^2\Sigma$ transition and a quartz ring inlet.
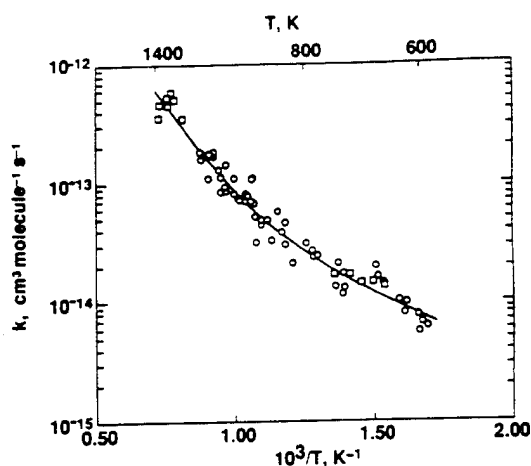
Figure 1. Arrhenius plot of the rate coefficient data of the AlO + CH₄ reaction: □, 5% O₂ used as AlO precursor; O, 0.5% N₂O used as AlO precursor.

plot of these data, Figure 1, shows strong curvature. Several different expressions were tried to fit the ln k versus T^{-1} data. Using Marquardt's method,[14] a regression fit to a $k(T) = A(T/K)^n \exp(-B/T)$ expression yields

$$k(590-1380\ K) = 9.6 \times 10^{-39}(T/K)^{7.96} \times$$
$$\exp(2468\ K/T)\ \ cm^3\ molecule^{-1}\ s^{-1}\ \ (2)$$

Equation 2 must be seen as a fitting expression only, as the numbers are unrealistic for a single channel reaction. This $k(T)$ expression most likely indicates competition between several reaction channels. We next attempted a similar regression for a double-exponential expression $k(T) = A \exp(-B/T) + C \exp(-D/T)$, which yielded

$$k(590-1380\ K) = 2.0 \times 10^{-10} \exp(-8299\ K/T) +$$
$$4.2 \times 10^{-13} \exp(-2402\ K/T)\ \ cm^3\ molecule^{-1}\ s^{-1}\ \ (3)$$

This fitting expression also does not seem to be representative of individual actual reaction paths, because of the high preexponential of the first term. This term appears too large for a metathesis reaction between a diatomic radical and a molecule.[15] While molecular insertion reactions, e.g., of singlet CH₂ and SiH₂, are known with A factors of this magnitude, these reactions proceed with an activation energy close to zero.[16-18]

Calculating the uncertainties of these fitting expressions by combining[19] variances and covariances, similarly as in our earlier studies,[7] yields precision limits of ±4% to ±12% for eq 2 and of ±5% to ±12% for eq 3, depending upon temperature. Both expressions lead to essentially equal accuracy limits of ±23% to ±26%, when combined with a ±10% uncertainty in the reactor flow profile[11,20] and ±20% for potential systematic errors. The simpler expression (2) is therefore preferred for the present temperature range.

Discussion

There has been one previous attempt to observe reaction 1. In that room temperature study no reaction could be detected, and an upper limit for the rate coefficient of 5×10^{-14} cm³ molecule⁻¹ s⁻¹ was derived.[8] Equations 2 and 3 suggest much lower values; hence, the results do not contradict one another.

The activation energies, i.e., the local slopes of the Arrhenius plot, Figure 1, reach the 67 kJ mol⁻¹ calculated by Børve and Pettersson[1] only at the highest temperatures investigated. For example, from eq 2 these energies are 46, 59, 66, and 71 kJ mol⁻¹ at 1000, 1200, 1300, and 1380 K, respectively. Also, the fitting expressions suggest that the reaction follows several paths. Further mechanistic considerations thus appear in order. To this end we first assess the likely importance of H-atom abstraction.
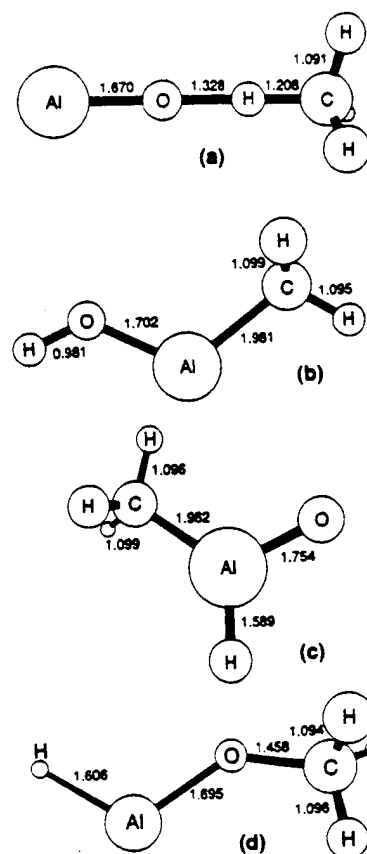

Figure 2. MP2/3-21G(*) structures of (a) C_{3v} TS for H-atom abstraction by AlO from CH₄, ∠AlCH = 106.6°; (b) C_s CH₃AlOH adduct, ∠AlOH = 128.8°, ∠OAlC = 116.2°, ∠AlCH = 112.2°, 109.4°(2); (c) C_s CH₃-Al(O)H adduct, ∠OAlH = 113.7°, ∠HAlC = 127.2°, ∠CAlH = 112.4°, 110.3°(2); (d) C_s CH₃OAlH adduct, ∠HAlO = 114.7°, ∠AlOC = 138.2°, ∠OCH = 112.2°, 109.5°(2). Distances are in 10⁻¹⁰ m.

Børve and Pettersson carried out a partial CASSCF optimization of an assumed C_{3v} transition state (TS) but did not obtain enough information to predict rate coefficients. In order to estimate these, we have analyzed abstraction by conventional transition-state theory (CTST), which requires vibrational and rotational data to estimate the partition function of the TS. Accordingly, we reoptimized the complete TS structure, at the MP2/3-21G(*) level,[21] and obtained the vibrational frequencies. The geometry is shown in Figure 2a and confirms their[1] work; the frequencies are 1574i, 175(2), 441(2), 570, 1030, 1357(2), 1394, 1561(2), 3109 and 3226(2) cm⁻¹. For an energy barrier at 0 K (i.e., including zero-point energy, ZPE) of E_0, the CTST abstraction rate coefficient is

$$k(590-1380\ K) = 1.43 \times 10^{-22}(T/K)^{3.30} \times$$
$$\exp(-940\ K/T)\exp(-E_0/RT)\ \ cm^3\ molecule^{-1}\ s^{-1}\ \ (4)$$

Preliminary estimates showed that quantum mechanical H-atom tunneling has little effect when $k \gtrsim 1 \times 10^{-14}$ cm³ molecule⁻¹ s⁻¹. Agreement between eqs 2 and 4 at 825 K, the midpoint of the range of T^{-1} investigated, is obtained when $E_0(4) = 12.4$ kJ mol⁻¹. This yields $k(1380\ K)$ within 5% of the experimental value, while $k(590\ K)$ is too small by a factor of 2.3. Though accord at low temperatures might be improved by adjustment of the TS frequencies, the fitted $E_0(4)$ is much lower than the $E_0(1) = 67$ kJ mol⁻¹ from the earlier ab initio estimate.[1] Use of that value together with the observed total AlO removal rate coefficient, eq 2, implies a branching ratio for direct abstraction of about 9×10^{-3} at 1380 K and about 6×10^{-6} at 590 K. In order to estimate the uncertainty in the $E_0(1)$ value that Børve and Pettersson derived at the CCI + Q level of theory, we compare their estimates of $\Delta H°$ for reaction 1 and the Li and Mg analogues[1] with the

experimental values.[5,6] The mean error is about ± 25 kJ mol^{-1}, which is a minimum estimate of the uncertainty in $E_0(1)$. We also allow for a possible factor of 3 uncertainty in the TS partition functions. These uncertainties imply that branching ratios for direct abstraction, i.e., without formation of an intermediate bound complex, as large as 0.23 at 1380 K and 0.003 at 590 K cannot be excluded, but another reaction channel, which is totally dominant at the lower temperatures, is definitely indicated.

The alternative abstraction channel leading to HAlO + CH$_3$ would be 192 ± 93 kJ mol^{-1} endothermic[5,6] and can on that basis be excluded from further consideration. The likelier prospects for further channels involve additions of AlO to CH$_4$. Particularly, insertion of AlO (a doublet species) into a C–H bond offers an intriguing prospect, by analogy to the suggested insertion of Al and other group 13 doublet ground-state atoms into such bonds.[22,23] To test this, we have employed theoretical methods to characterize possible insertion products and estimated the likely pressure dependence of these to see whether they are consistent with our observations. Ab initio geometries of three potential insertion species obtained by means of MP2/3-21G(*) theory are shown in Figure 2b–d. Structure d was previously proposed as the product of insertion of Al into CH$_3$OH,[24] similar to such insertion into H$_2$O.[24,25] To confirm that these structures are true energy minima, we calculated the vibrational frequencies, which are all real.[26] These frequencies are also used to derive the zero-point energy (ZPE), to obtain the temperature dependence of the enthalpies in the kinetic calculations outlined below. The enthalpies of CH$_3$AlOH, CH$_3$Al(O)H, and CH$_3$OAlH, relative to AlO + CH$_4$ at 0 K, are predicted at the MP4SDQ/6-31G*+ZPE//MP2/3-21G(*) level to be -166, -46, and -87 kJ mol^{-1}, respectively.[27] Equilibrium constant calculations with these enthalpies indicate that CH$_3$AlOH is stable under our experimental conditions, that the second adduct is too weakly bound to be a significant final sink for AlO, and that formation of the third adduct cannot be ruled out at the lowest temperatures studied. There is a possibility that these adducts decompose to new products. For example, CH$_3$AlOH might dissociate to AlOH + CH$_3$, perhaps with a lower overall energy barrier than proposed for direct abstraction.

Next, the likely pressure dependence of AlO + CH$_4 \rightarrow$ CH$_3$AlOH at 825 K was investigated by means of QRRK theory.[28] The addition rate coefficient is predicted to be within 25% of the high-pressure limit at 15 mbar of Ar and would show only a small pressure variation over the experimental range with assumed Arrhenius parameters for insertion of $A = 10^{-12}$ cm^3 molecule^{-1} s^{-1} and $E_a = 0$. This is consistent with the lack of an observed pressure dependence of the experimental rate coefficients. If there were a significant barrier to insertion ($E_a > 0$), then dissociation of the excited adduct back to AlO + CH$_4$ would be less competitive with collisional stabilization and the predicted rate coefficients would be even closer to the high-pressure limit. The observed pressure independence is also consistent with a mechanism where the adduct fragments to new products before stabilization. Further QRRK calculations suggest that formation of any adduct, which is sufficiently thermodynamically stable to be significant in our experiments, will have a rate coefficient that is in the falloff region or close to the high-pressure limit.

Conclusions

These experiments are in accord with the suggestion by Børve and Pettersson[1] that gas-phase reactions between AlO and CH$_4$ occur and may provide insight in the heterogeneous catalytic conversion of methane to C$_2$ hydrocarbons. However, use of their calculated barrier suggests that the branching ratio for direct abstraction is small and therefore that other reaction channels are important. Our calculations demonstrate that insertion leading to CH$_3$AlOH is a reasonable candidate for the initial step, although other channels are not excluded. The insertion

products (Figure 2b–d) might model the products of dissociative adsorption of CH$_4$ onto an alumina catalyst, where their energies are likely to differ from gas-phase values. More detailed experimental and theoretical investigations of the present reaction system, as well as of other metal oxide–hydrocarbon reactions, are needed to obtain an understanding of this new class of gas-phase reactions and their potential importance for methane conversion.

References and Notes

(1) Børve, K. J.; Pettersson, L. G. M. *J. Phys. Chem.* **1991**, *95*, 3214.

(2) Feng, Y.; Niiranen, J.; Gutman, D. *J. Phys. Chem.* **1991**, *95*, 6564.

(3) Hutchings, G. J.; Woodhouse, J. R.; Scurrell, M. S. *J. Chem. Soc., Faraday Trans. 1* **1989**, *85*, 2507.

(4) Mehandru, S. P.; Anderson, A. B.; Brazdil, J. F.; Grasselli, R. K. *J. Phys. Chem.* **1987**, *91*, 2930.

(5) Pedley, J. B.; Naylor, R. D.; Kirby, S. P. *Thermochemical Data of Organic Compounds*; Chapman and Hall: New York, 1986; p 89.

(6) Chase, M. W., Jr.; Davies, C. A.; Downey, Jr.; Frurip, D. J.; McDonald, R. A.; Syverup, A. N. *JANAF Thermochemical Tables; J. Phys. Chem. Ref. Data* **1985**, *14* (Suppl. No. 1).

(7) Slavejkov, A. G.; Stanton, C. T.; Fontijn, A. *J. Phys. Chem.* **1990**, *94*, 3347 and references therein.

(8) Parnis, J. M.; Mitchell, S. A.; Kanigan, T. S.; Hackett, P. A. *J. Phys. Chem.* **1989**, *93*, 8045.

(9) Fontijn, A.; Futerko, P. M. In *Gas-Phase Metal Reactions*; Fontijn, A.. Ed.; North-Holland: Amsterdam, 1992; Chapter 6.

(10) Garland, N. L.; Nelson, H. H. *Chem. Phys. Lett.* **1992**, *191*, 269.

(11) Fontijn, A.; Felder, W. In *Reactive Intermediates in the Gas Phase. Generation and Monitoring*; Setser, D. W., Ed.; Academic Press: New York, 1979; Chapter 2.

(12) Pearse, R. W. B.; Gaydon, A. G. *The Identification of Molecular Spectra*; Chapman and Hall: London, 1976; p 41.

(13) Irvin, J. A.; Quickenden, T. I. *J. Chem. Educ.* **1983**, *60*, 711.

(14) Press, W. H.; Flannery, B. P.; Teukolsky, S. A.; Vetterling, W. T. *Numerical Recipes*; Cambridge University: Cambridge, 1986; Chapter 14.

(15) Benson, S. W. *Thermochemical Kinetics*, 2nd ed.; John Wiley: New York, 1976; Chapter 4.

(16) Wagener, R.; Wagner, H. Gg. *Ber. Bunsen-Ges. Phys. Chem.* **1990**, *94*, 1096.

(17) Chu, J. O.; Beach, D. B.; Jasinski, J. M. *J. Phys. Chem.* **1987**, *91*, 5340.

(18) Becerra, R.; Frey, H. M.; Mason, B. P.; Walsh, R.; Gordon, M. S. *J. Am. Chem. Soc.* **1992**, *114*, 2752.

(19) Wentworth, W. E. *J. Chem. Educ.* **1965**, *42*, 96.

(20) Fontijn, A.; Felder, W. *J. Phys. Chem.* **1979**, *83*, 24.

(21) Frisch, M. J.; Head-Gordon, M.; Trucks, G. W.; Foresman, J. B.; Schlegel, H. B.; Raghavachari, K.; Robb, M. A.; Binkley, J. S.; Gonzalez, C.; Defrees, D. J.; Fox, D. J.; Whiteside, R. A.; Seeger, R.; Melius, C. F.; Baker, J.; Martin, R. L.; Kahn, L. R.; Stewart, J. J. P.; Topiol, S.; Pople, J. A. *Gaussian 90*; Gaussian: Pittsburgh, PA, 1990.

(22) Yu, H.; Goddard, J. D. *Can. J. Chem.* **1990**, *68*, 663.

(23) Jeong, G. H.; Klabunde, K. J. *J. Am. Chem. Soc.* **1986**, *108*, 7103.

(24) Jordan, K. D.; Kurtz, H. A. In *Metal Bonding and Interactions in High Temperature Systems*; ACS Symposium Series 179; Gole, J. L., Stwalley, W. C., Eds.; American Chemical Society: Washington, DC, 1982; Chapter 26.

(25) Oblath, S. B.; Gole, J. L. *J. Chem. Phys.* **1979**, *70*, 581; *Combust. Flame* **1980**, *37*, 293.

(26) Unscaled MP2/3-21G(*) frequencies ν for CH$_3$AlOH are 21, 220, 387, 520, 618, 662, 759, 935, 1322, 1549, 1559, 3054, 3130, 3155, and 3674 cm^{-1}. ν for CH$_3$Al(O)H are 44, 192, 411, 581, 655, 744, 781, 908, 1356, 1555, 1557, 2016, 3057, 3125, and 3150 cm^{-1}; ν for CH$_3$OAlH are 87, 151, 242, 630, 726, 1158, 1203, 1275, 1557, 1607, 1613, 1910, 3061, 3126, and 3142 cm^{-1}. The CH$_3$ groups in these species are essentially free rotors.

(27) Difficulties in describing AlO with a single reference wave function make these estimates uncertain, although the energy difference between the three adducts is unaffected. See e.g.: Marshall, P.; O'Connor, P. B.; Chan, W. T.; Kristof, P. V.; Goddard, J. D. In *Gas-Phase Metal Reactions*; Fontijn, A., Ed.; North-Holland: Amsterdam, 1992; Chapter 8.

(28) (a) Dean, A. M. *J. Phys. Chem.* **1985**, *89*, 4600. (b) Westmoreland, P. R. QRRK EGA Program, 1988.

Experimental and Transition-State Theory Studies of the Gas-Phase Reactions of AlCl with N₂O, CO₂, and SO₂

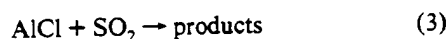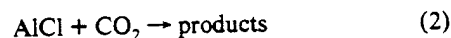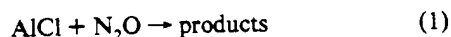**Peter M. Futerko[†] and Arthur Fontijn[*]**

*High-Temperature Reaction Kinetics Laboratory, The Isermann Department of Chemical Engineering,
Rensselaer Polytechnic Institute, Troy, New York 12180–3590*

Received: February 4, 1993; In Final Form: April 19, 1993

The high-temperature fast-flow reactor technique has been used to make kinetic measurements. A weighted fit to the AlCl + N₂O data gives $k(700–990 \text{ K}) = 5.6 \times 10^{-11} \exp(-7380 \text{ K}/T)$ cm³ molecule⁻¹ s⁻¹. A weighted fit to the AlCl + CO₂ measurements leads to the expression $k(900–1790 \text{ K}) = 4.4 \times 10^{-23} (T/\text{K})^{3.0} \exp(-3900 \text{ K}/T)$ cm³ molecule⁻¹ s⁻¹. 2σ accuracy limits are about ±25%. An upper limit $k(800–1100 \text{ K}) < 5 \times 10^{-14}$ cm³ molecule⁻¹ s⁻¹ has been determined for the AlCl + SO₂ reaction. An alternate form of classical transition-state theory is developed to allow predictions on the preexponential part of rate coefficient expressions for metallic species. This model-based transition-state-theory (MTST) method uses a valence-force molecular model to estimate rotational constants and vibrational frequencies of the transition state and is applicable to reactions with early barriers, typical of many exothermic charge-transfer reactions. The geometrical parameters and force constants that describe the molecular model are derived from properties of the reactants. For the N₂O reaction good agreement between MTST and experiment is obtained, based on the assumption of an O atom abstraction reaction leading to OAlCl. No such agreement is found for the CO₂ reaction, which indicates adduct formation as the main AlCl consumption channel. For the previously measured AlCl + O₂ reaction MTST calculations suggest that abstraction can be of some significance above about 1500 K; however, adduct formation appears to dominate over most of the 490–1750 K range.

Introduction

As part of an ongoing study of the temperature dependence of the rate coefficients of reactions of small Al- and B-containing species, we report here experiments on the reactions

$$\text{AlCl} + \text{N}_2\text{O} \rightarrow \text{products} \quad (1)$$

$$\text{AlCl} + \text{CO}_2 \rightarrow \text{products} \quad (2)$$

$$\text{AlCl} + \text{SO}_2 \rightarrow \text{products} \quad (3)$$

We previously studied the AlCl reactions with O₂,[1] CO₂,[2] Cl₂,[3] and HCl,[4] the results of which have been summarized.[5] The measurements of reaction 2 are repeated here, as the high-temperature fast-flow reactor (HTFFR) technique used has been much improved[5,6] since the previous[2] study, where the data showed wide scatter. The O₂ and CO₂ reactions were originally thought to lead directly to OAlCl. However, a recent ab initio study of the thermochemistry[7] of OAlCl suggests these two channels to be too endothermic[8] for reaction along this path with the observed rate coefficients.

To investigate the mechanism of all these AlCl reactions with oxygen-containing oxidants, we present here a semiempirical transition-state theory based method for predicting the temperature dependence of rate coefficients. In this model-based transition-state theory (MTST) the rotational constants and vibrational frequencies of the transition state are derived from molecular models based on the assumption of valence forces. This approach, the limitations of which are discussed, should be widely applicable to reactions with early activation barriers since the required input data, namely, geometrical parameters and force constants, of the transition state can be estimated from reactant properties in accord with Hammond's postulate.[9] Reactions occurring by a crossing of neutral and ionic potential

energy surfaces, typical of oxidation reactions of metal species, are included. MTST is thus useful for such reactions when the input data for the widely used semiempirical TST method developed by Benson,[10] principally for H/C/O/N species reactions, are not available.

Experimental Section

Detailed descriptions of the HTFFR used in this work have been given elsewhere.[5,6] The reactor consists of a vertical mullite reaction tube (2.2-cm i.d.) surrounded by SiC heating elements. This assembly is sealed inside an insulated water-cooled vacuum housing. Two methods were used to produce AlCl. In the first, previously used method, a trace amount of Cl₂ or HCl was added to the Ar bath gas flowing over the Al-wetted resistively-heated tungsten vaporization coil, located 7–17 cm upstream from the reaction zone.[1,3] In the second method, similar to that used in the BCl studies,[6,11] AlCl₃ was vaporized from a quartz crucible (4-mm i.d.) into a stream of Ar. This stream then flowed through a 2450-MHz, nominally 100-W, microwave discharge in a quartz tube (1.2-cm i.d.) and then into the reaction tube. Both methods were used in the AlCl + CO₂ study in the 1200–1690 K temperature range and found to yield identical results. The second method would in general be especially useful for HTFFR studies near room temperature; such temperatures are not accessible by the first method because the heat generated by the vaporization coil heats the reaction tube to temperatures greater than 450 K. Downstream from the source, a mixture of Ar and the oxidant gas (N₂O, CO₂, or SO₂) was introduced into the reaction tube through a movable inlet. The molar flow rate of gas through the inlet was kept constant during a given rate coefficient determination, which consisted of five or six measurements at varying oxidant concentrations. A small amount of O₂ was added to the inlet gas to rapidly[5] remove any remaining Al atoms entering the reaction zone. Such atoms otherwise may continue to produce AlCl and hence interfere with the measurements.

Relative AlCl concentrations were monitored by laser-induced fluorescence using a pulsed Lambda Physik EMG 101 excimer/Fl 2002 dye laser combined with a KDP doubling crystal. The

[†] Present address: Department of Chemical Engineering, Massachusetts Institute of Technology, Cambridge, MA 02139.

TABLE I: Summary of Rate Coefficient Measurements for AlCl + N₂O[a]

reaction zone length (cm)	P (mbar)	[M] (10^{17} cm^{-3})	[N₂O]$_{max}$ (10^{15} cm^{-3})	F	$\bar{v}$ (m s^{-1})	T (K)	$k \pm \sigma_k$ (cm³ molecule^{-1} s^{-1})
20	50.9	4.0	16.4	40[b]	20	919	2.01 ± 0.13 (−14)[c]
10	50.9	4.0	16.5	73	20	919	2.16 ± 0.17 (−14)
20	50.9	4.0	13.7	36	21	921	2.01 ± 0.12 (−14)
10	50.9	4.0	13.6	27	21	924	2.18 ± 0.19 (−14)
10	101.0	7.7	14.1	34	14	948	2.29 ± 0.22 (−14)
10	101.2	7.6	13.9	37	14	964	2.08 ± 0.22 (−14)
20	29.6	2.2	14.3	50	39	984	2.75 ± 0.21 (−14)
20	29.7	2.2	14.2	62	39	991	2.82 ± 0.25 (−14)
20	54.1	5.3	23.9	23	16	735	2.40 ± 0.33 (−15)
20	54.1	5.4	24.2	22	16	726	2.19 ± 0.32 (−15)
20	78.6	8.1	52.3	30	7	704	1.44 ± 0.14 (−15)
20	78.6	8.1	52.3	17	7	704	1.80 ± 0.13 (−15)
20	66.7	6.9	40.0	49	14	704	1.31 ± 0.22 (−15)
20	66.7	6.8	39.7	48	14	709	1.11 ± 0.22 (−15)
20	41.6	4.2	22.2	35	13	726	2.23 ± 0.22 (−15)
20	41.6	4.1	22.1	33	13	731	2.45 ± 0.21 (−15)
20	55.2	5.4	28.9	34	10	740	2.80 ± 0.21 (−15)
20	55.2	5.3	28.6	41	10	748	3.13 ± 0.22 (−15)
20	78.5	7.2	35.6	31	12	795	4.17 ± 0.35 (−15)
20	62.9	5.5	32.7	50	17	830	7.68 ± 0.72 (−15)
20	62.9	5.4	32.2	54	17	842	9.51 ± 0.64 (−15)
10	62.9	5.5	32.3	59	17	836	9.35 ± 0.67 (−15)
10	49.9	4.2	15.0	23	19	856	1.04 ± 0.08 (−14)
20	49.9	4.2	15.1	26	19	853	9.80 ± 0.70 (−15)
20	42.5	3.6	13.5	31	21	846	9.20 ± 0.79 (−15)
20	42.8	3.6	13.5	24	21	852	1.08 ± 0.08 (−14)
20	44.3	3.6	17.3	42	32	879	1.30 ± 0.16 (−14)
20	44.3	3.6	17.3	34	32	882	1.48 ± 0.10 (−14)
20	35.2	2.9	13.9	17	40	873	1.50 ± 0.15 (−14)
20	50.7	4.2	20.0	9	27	871	8.86 ± 0.82 (−15)
20	68.4	5.7	17.3	52	16	875	1.07 ± 0.07 (−14)

[a] The measurements are reported in the sequence in which they were obtained. [b] In arbitrary units. [c] Should be read as (2.01 ± 0.13) × 10^{-14} cm³ molecule^{-1} s^{-1}.

AlCl(A$^1\Pi$–X$^1\Sigma^+$) transition[12] was pumped on the (0,0) band at 261.4 nm, and the fluorescence intensity was observed through a 262-nm (26-nm fwhm) filter by an EMI 9813QA photomultiplier tube coupled to a Data Precision Analogic 6000/620 100-MHz transient digitizer. Rate coefficient measurements were made in the stationary inlet mode[13] with observed reaction zone lengths of 10 or 20 cm. The oxidant concentrations were maintained in great excess over the AlCl concentrations. Rate coefficients and their uncertainties were obtained from the slopes of linear plots of ln [AlCl]$_{relative}$ vs oxidant concentration by a weighted linear regression.[14]

The gases used were 99.998% Ar from the liquid, "Precision Aquarator" 99.99% CO₂, Cl₂ (1% in Ar) and "Atomic Absorption" 99.0% N₂O from Linde, "Ultra High Purity" 99.99% N₂O and "Anhydrous" 99.98% SO₂ from Matheson, HCl (5% in He) from Spectra, and O₂ (5.0% in Ar) from Scott.

Results

The AlCl + N₂O Reaction. Reaction 1 was studied from 700 to 990 K. No measurements at higher temperatures are included as thermal dissociation of N₂O is sufficiently large to interfere with rate coefficient measurements.[11] Below 700 K the reaction was too slow to measure. Table I summarizes the rate coefficients and the temperatures at which they were obtained along with the experimental parameters: reaction zone length, total pressure P, total concentration [M], maximum oxidant concentration [N₂O]$_{max}$, fluorescence intensity F (a measure of [AlCl] at the start of the reaction zone), and average velocity $\bar{v}$. The independence of the individual rate coefficients k_i of these parameters was checked by examining plots of $[k(T) - k_i]/k(T)$, where $k(T)$ is obtained from the fitted rate coefficient expression given below, vs the above experimental parameters. It can be seen from Figure 1 that over the limited temperature range studied
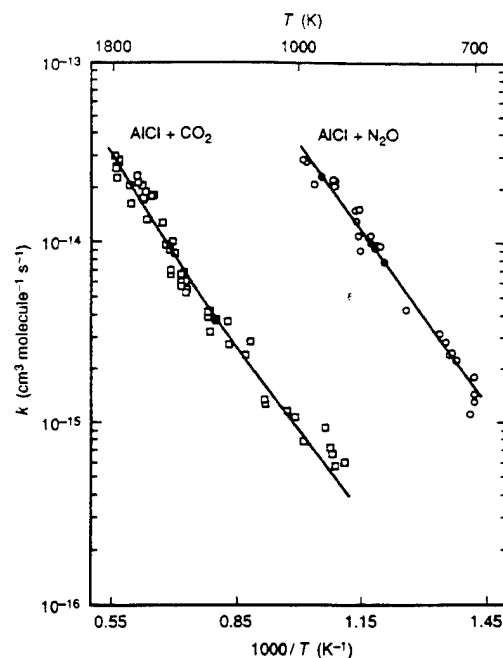

Figure 1. Arrhenius plots of experimental rate coefficients for the AlCl + N₂O (open circles) and AlCl + CO₂ (open squares) reactions. The experimental rate coefficient expressions are shown as full lines.

the k_i measurements show no deviation from Arrhenius behavior. A weighted nonlinear fit[15] of the data to the expression $k(T) = A \exp(-E/RT)$ gives

$$k_1(700\text{–}990 \text{ K}) = 5.6 \times 10^{-11} \times$$
$$\exp(-7380 \text{ K}/T) \quad \text{cm}^3 \text{ molecule}^{-1} \text{ s}^{-1} \quad (4)$$

with covariance matrix elements[16]

$$(\sigma_A/A)^2 = 0.113, \quad \sigma_E^2 = 79\,900 \text{ K}^2, \quad \sigma_{AE}/A = 94.6 \text{ K} \quad (5)$$

Combining these matrix elements by the propagation of errors technique[4,10] yields ±2σ_k precision limits of 15% at 700 K, 6% at 850 K, and 12% at 990 K. Allowing 10% uncertainty associated with the flow profile factor and 20% for further systematic errors yields ±2σ_k accuracy limits of 27% at 700 K, 23% at 850, and 25% at 990 K.

The AlCl + CO₂ Reaction. Reaction 2 was studied over the 900–1790 K temperature range. The rate coefficient data summarized in Table II are again independent of reaction zone length, P, [M], [CO₂]$_{max}$, F, and $\bar{v}$. The Arrhenius plot of the rate coefficients shown in Figure 1 exhibits slight upward curvature. The rate coefficient data were fitted to the three-parameter expression $k(T) = AT^n \exp(-E/RT)$. The goodness of the fit χ^2 is found to be relatively insensitive to the value of the parameter n over the approximate range 2.0–4.0. We therefore fix n at 3.0. A two-parameter nonlinear regression analysis of the data gives

$$k_2(900\text{–}1790 \text{ K}) = 4.4 \times 10^{-23} (T/\text{K})^{3.0} \times$$
$$\exp(-3900 \text{ K}/T) \quad \text{cm}^3 \text{ molecule}^{-1} \text{ s}^{-1} \quad (6)$$

with covariance matrix elements

$$(\sigma_A/A)^2 = 0.0182, \quad \sigma_E^2 = 38\,000 \text{ K}^2, \quad \sigma_{AE}/A = 26.0 \text{ K} \quad (7)$$

Combining the covariance matrix elements by the propagation of errors technique yields ±2σ_k precision limits of 17% at 900 K, 5% at 1350 K, and 6% at 1790 K. Allowing 10% uncertainty associated with the flow profile factor and a conservative 20% for further systematic errors yields ±2σ_k confidence limits of 28% at 900 K, 23% at 1350, and 23% at 1790 K. The present rate

TABLE II: Summary of Rate Coefficient Measurements for AlCl + CO₂[a]

reaction zone length (cm)	P (mbar)	[M] (10^{17} cm⁻³)	[CO₂]$_{max}$ (10^{15} cm⁻³)	F	$\bar{v}$ (m s⁻¹)	T (K)	$k \pm \sigma_k$ (cm³ molecule⁻¹ s⁻¹)
20	43.3	2.5	18	18[b]	25	1273	4.20 ± 0.55 (−15)[c,d]
20	78.4	4.5	33	71	13	1254	3.73 ± 0.50 (−15)[d]
20	78.6	4.5	32	64	14	1273	3.21 ± 0.22 (−15)[d]
10	78.6	4.4	32	62	14	1281	3.86 ± 0.53 (−15)[d]
10	78.6	4.4	32	108	14	1284	4.15 ± 0.28 (−15)[d]
10	63.5	3.2	17	33	14	1429	8.71 ± 0.98 (−15)[d]
10	63.7	3.2	21	47	14	1440	9.99 ± 0.91 (−15)[d]
20	62.8	3.1	12	50	14	1475	9.69 ± 0.98 (−15)[d]
20	62.8	3.0	12	54	14	1493	1.28 ± 0.13 (−14)[d]
20	43.5	2.8	16	13	19	1132	2.84 ± 0.30 (−15)[d]
20	43.5	2.7	15	18	19	1149	2.38 ± 0.98 (−15)[d]
20	58.1	4.3	23	10	13	990	7.83 ± 2.20 (−15)[d]
20	57.7	4.1	23	23	13	1010	1.06 ± 0.18 (−15)[d]
20	88.1	6.2	27	27	11	1031	1.15 ± 0.17 (−15)[d]
20	46.4	3.1	20	59	22	1091	1.27 ± 0.34 (−15)[d]
20	46.1	3.1	20	48	22	1094	1.34 ± 0.45 (−15)[d]
20	53.5	2.4	14	21	31	1584	1.33 ± 0.19 (−14)[d]
10	53.3	2.4	14	24	31	1602	1.74 ± 0.21 (−14)[d]
10	53.2	2.4	14	21	31	1609	2.04 ± 0.18 (−14)[d]
10	92.0	4.0	20	21	15	1679	1.67 ± 0.24 (−14)[d]
10	92.0	4.0	20	17	15	1686	2.05 ± 0.21 (−14)[d]
20	53.7	4.2	21	55	11	930	7.20 ± 3.38 (−16)[d]
20	53.7	4.1	21	43	11	942	9.32 ± 3.11 (−16)[d]
20	65.3	5.1	27	74	16	920	5.70 ± 2.62 (−16)[d]
20	65.7	5.1	27	54	16	925	6.69 ± 1.47 (−16)[d]
20	78.6	6.3	36	39	16	900	5.97 ± 1.34 (−16)[d]
20	43.1	2.3	17	19	34	1368	5.49 ± 1.38 (−15)[d]
20	43.1	2.3	17	40	35	1373	5.24 ± 0.71 (−15)[d]
10	43.1	2.3	17	68	35	1374	6.10 ± 2.76 (−15)[d]
10	43.1	2.3	17	66	35	1386	6.77 ± 0.83 (−15)[d]
10	85.8	4.5	33	40	18	1397	6.66 ± 0.68 (−15)[d]
10	85.4	4.4	33	19	18	1399	6.00 ± 0.95 (−15)[d]
20	83.6	4.3	17	30	18	1401	5.74 ± 1.00 (−15)[d]
20	99.6	6.0	30	113	18	1210	3.69 ± 0.41 (−15)[e]
20	113.3	6.8	30	87	18	1204	2.72 ± 0.28 (−15)[e]
20	73.3	4.2	25	59	17	1250	3.75 ± 0.32 (−15)[e]
20	60.4	2.8	12	36	45	1540	1.81 ± 0.15 (−14)[e]
20	60.4	2.8	12	39	46	1556	1.80 ± 0.23 (−14)[e]
20	91.4	4.2	16	39	25	1590	1.83 ± 0.10 (−14)[e]
20	91.6	4.2	16	78	25	1590	1.90 ± 0.11 (−14)[e]
10	92.8	4.2	21	53	25	1599	1.71 ± 0.12 (−14)[e]
10	93.0	4.2	21	54	25	1599	1.74 ± 0.12 (−14)[e]
10	61.9	2.7	18	62	22	1632	2.14 ± 0.15 (−14)[e]
20	60.5	2.7	12	65	22	1638	2.32 ± 0.14 (−14)[e]
20	52.9	2.6	17	87	33	1448	6.59 ± 0.54 (−15)[e]
20	52.8	2.6	16	59	33	1449	6.98 ± 0.64 (−15)[e]
10	52.8	2.6	16	60	33	1454	9.33 ± 1.11 (−15)[e]
10	52.8	2.6	16	60	33	1454	9.08 ± 1.06 (−15)[e]
10	75.0	3.1	12	70	37	1765	2.75 ± 0.28 (−14)[e]
10	75.2	3.1	12	69	36	1765	2.81 ± 0.20 (−14)[e]
20	74.8	3.0	7	87	37	1777	2.26 ± 0.14 (−14)[e]
20	74.8	3.0	12	88	37	1777	2.57 ± 0.24 (−14)[e]
20	41.9	1.7	8	91	68	1787	2.61 ± 0.21 (−14)[e]
20	42.1	1.7	8	125	67	1787	2.55 ± 0.16 (−14)[e]
20	42.1	1.7	8	39	67	1791	2.98 ± 0.26 (−14)[e]

[a] The measurements are reported in the sequence in which they were obtained. [b] In arbitrary units. [c] Should be read as (4.20 ± 0.55) × 10⁻¹⁵ cm³ molecule⁻¹ s⁻¹. [d] AlCl produced by the microwave-discharge method. [e] AlCl produced by the reacting Cl₂ or HCl with an Al-wetted vaporization coil.

coefficient recommendation is in good agreement with that determined in the previous investigation;[2] however, the scatter in the measurements is now greatly reduced.

The AlCl + SO₂ Reaction. The rate coefficients of reaction 3 could not be accurately determined because of absorption and emission of laser radiation by SO₂,[12] which greatly lowered the sensitivity of AlCl detection. Corrections were made to the integrated fluorescence signal to remove the SO₂ contribution. Over the 800–1100 K temperature range no significant change in the AlCl signal could be observed as the SO₂ concentration was varied, which indicates an upper limit to the rate coefficient

$$k_3(800\text{–}1100 \text{ K}) < 5 \times 10^{-14} \text{ cm}^3 \text{ molecule}^{-1} \text{ s}^{-1} \quad (8)$$

We were unable to investigate reaction 3 at higher temperatures because the emitted radiation from species other than AlCl was too intense. Thermochemical[8] equilibrium calculations indicate that above 1100 K SO, which also absorbs and emits radiation near the AlCl transition,[12] can be present in significant quantities.

Model-Based Transition-State Theory (MTST)

According to conventional transition-state theory the rate coefficient for a reaction occurring on a single potential energy surface is given by[17]

$$k(T) = \frac{k_B T}{h} \frac{q_{\ddagger}}{q_A q_B} \exp(-\Delta E^{\ddagger}/RT) \quad (9)$$

in which $q_{\ddagger}$ is the partition function for the transition state, q_A and q_B are partition functions for the reactants, and $\Delta E^{\ddagger}$ is the difference in zero-point levels of the transition state and the reactants. q_A and q_B are readily evaluated from experimental values of the rotational constants and vibrational frequencies of the reactants. The data needed to evaluate $q_{\ddagger}$ are seldom available and must therefore be estimated. The MTST approach for this evaluation is suitable for transition states which arise from an early crossing of neutral and ionic potential surfaces, such as is the case for many metal species reactions. For such a transition state reasonably good estimates of the geometrical parameters and vibrational frequencies can be made using Hammond's postulate.[9] It can then be assumed that the internuclear distances, valence angles, and force constants of the transition states are closely related to the properties of the reactants for an exothermic reaction and properties of the products for an endothermic reaction.

Vibrational frequencies for transition states are obtained from molecular models. The molecular model used here assumes that harmonic restoring forces oppose changes in bond lengths, angles between valence bonds, and dihedral angles. The potential energy V in the region near the transition state is thus given by[18]

$$2V = \sum_i F_{ri} \Delta r_i^2 + \sum_j F_{\theta j} \Delta \theta_j^2 + \sum_k F_{\tau k} \Delta \tau_k^2 \quad (10)$$

where F_r, F_θ, and F_τ are force constants for changes in internuclear distances r, valence angles θ, and dihedral angles σ from their respective equilibrium values. A normal-coordinate analysis of the model, which procedure has been described in detail by Pauling and Wilson,[19] is carried out. The secular equation thus obtained is solved numerically by reducing the determinant to the tridiagonal form using Householder's algorithm.[15] The characteristic polynomial of the resulting matrix is then evaluated by the QL algorithm with implicit shifts.[15] Vibrational frequencies ν_i are obtained from the relation[19]

$$\nu_i = \lambda_i^{0.5}/2\pi c \quad (11)$$

in which λ_i are the eigenvalues of the secular equation. Rotational constants B_i for the transition state are obtained from the eigenvalues of the inertia tensor,[20] that is, from the principal moments of inertia I_i by the relation[21]

$$B_i = h/(8\pi^2 c I_i) \quad (12)$$

Several examples of accordingly estimating transition-state parameters for AlCl reactions are given in the Discussion.

Some limitations of MTST are that force constants arising from the reaction, which includes one stretching force constant and one or more bending or torsional force constants, must be estimated from the available ab initio calculations on similar reactions. The most important of these are the torsional force constants, since the torsions can be of low frequency and hence influence the TST rate expression. Also, MTST is not suitable

TABLE III: Transition-State Parameters for ClAlONN‡

| geometrical parameter[a,b]		force constant[c]	
r(ClAl)	2.13	F_r(ClAl)	2.1
r(AlO)	2.25	F_r(AlO)	−2.0
r(ON)	1.18	F_r(ON)	5.85
r(NN)	1.13	F_r(NN)	18.7
θ(ClAlO)	120	F_θ(ClAlO)	0.2
θ(AlON)	90	F_θ(AlON)	0.6
θ(ONN)	160	F_θ(ONN)	0.67
τ(ClAlON)	0	F_τ(ClAlON)	0.02
τ(AlONN)	0	F_τ(AlONN)	0.02

rotational constants $(B_1B_2B_3)$: 9.51×10^{-4} cm^{-3}

vibrational frequencies ν_i: 39, 89, 150, 291, 478, 605, 991, 2221 cm^{-1}

[a] We assume trans arrangements for the atoms in the ClAlON and AlONN groups. [b] Units of r are 10^{-10} m; units of θ and τ are deg. [c] Units of F_r are 10^2 N m^{-1}; units of F_θ and F_τ are 10^{-18} N m rad^{-2}.

for reactions with a centrally located transition state, e.g., H + HCl → H₂ + Cl, because the potential energy function (cf. eq 10) would have to be modified to include a cross-term for the interaction between the H–H and H–Cl bonds.[22] Furthermore, the transition state would resemble both the reactants and the products in part; hence, there would be considerable uncertainty in estimating geometrical parameters and force constants.

Discussion

The AlCl + N₂O Reaction. The lowest channel of the abstraction reaction

$$AlCl + N_2O \rightarrow OAlCl + N_2 \qquad (1a)$$
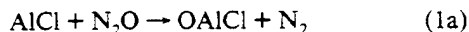
is spin-allowed and 267 kJ mol^{-1} exothermic.[23] The parameters of the transition state ClAlONN‡ are derived from properties of the reactants and are summarized in Table III. The distances r(ClAl), r(ON), and r(NN) are from values for the AlCl and N₂O molecules. The internuclear distance along the reaction coordinate r(AlO) is estimated by

$$r(AlO) = [r(Al^+) + r(O^-)]0.50^{1/(\delta-1)} \qquad (13)$$

Equation 13 is based on a relation given by Pauling[24] between univalent radii and the bond distances of diatomic alkali-metal halide molecules. We assume that the relation applies to charge-transfer complexes and hence to transition states, which are located fairly close to the complexes. Values for the univalent radii r(Al$^+$) and r(O$^-$) and the average Born exponent δ are obtained as described in ref 25. The constant 0.50 is obtained such that eq 13 gives good agreement with ab initio computations[26–28] of B–O, Al–O, and H–O distances for transition states of the respective BCl + O₂, Al + CO₂, and H + N₂O reactions. Lacking information on the valence and dihedral angles of the transition state, we assume the values given in Table III based on optimized geometries from ab initio computations.[26–28] The force constant F_r(ClAl) is taken as that in AlCl,[29] while F_r(NN) and F_θ(ONN) are obtained from data for N₂O.[30] The remaining force constants in Table III are estimated by a scheme that gives good agreement with ab initio computations[26–28] of vibrational frequencies. For example, F_r(ON) is taken as one-half the N–O stretching force constant in N₂O. In addition, all torsional force constants are taken as 0.02×10^{-18} N m rad^{-2} and the stretching force constants corresponding to reaction coordinates are taken as -2.0×10^2 N m^{-1}. These data are used to calculate the transition-state rotational constants and vibrational frequencies, which are summarized in Table III.

To allow comparison between theory and experiment, the preexponential factor of eq 9 is calculated for the 500–2000 K temperature range and fitted to the expression AT^n. To calculate the barrier height, the experimental rate coefficient expression is set equal to the TST equation (9) at 820 K, the temperature
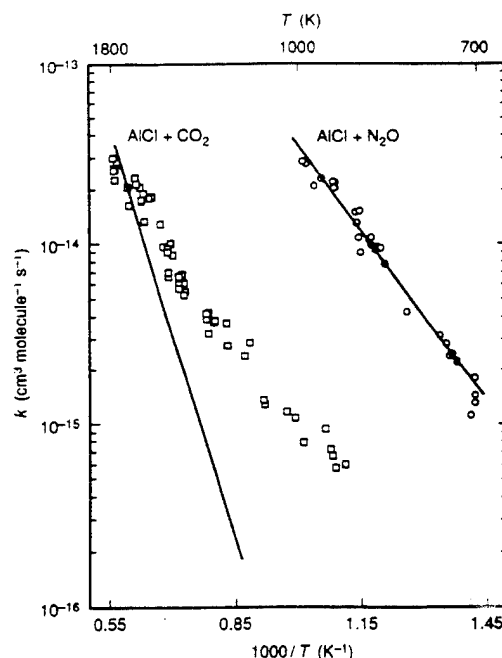

Figure 2. Arrhenius plots of experimental rate coefficients for the AlCl + N₂O (open circles) and AlCl + CO₂ (open squares) reactions. Rate coefficient expressions for the O atom abstraction channels for these reactions derived using the MTST method are shown as solid lines.

TABLE IV: Transition-State Parameters for ClAlOCO‡

geometrical parameter[a,b]		force constant[c]	
r(ClAl)	2.08	F_r(ClAl)	3.2
r(AlO)	1.63	F_r(AlO)	4.2
r(OC)	1.81	F_r(OC)	−2.0
r(CO)	1.13	F_r(CO)	19.0
θ(ClAlO)	160	F_θ(ClAlO)	0.3
θ(AlOC)	90	F_θ(AlOC)	0.6
θ(OCO)	120	F_θ(OCO)	0.2
τ(ClAlOC)	0	F_τ(ClAlOC)	0.02
τ(AlOCO)	0	F_τ(AlOCO)	0.02

rotational constants $(B_1B_2B_3)$: 9.46×10^{-4} cm^{-3}

vibrational frequencies ν_i: 75, 91, 141, 216, 231, 523, 908, 2164 cm^{-1}

[a] We assume trans arrangements for the atoms in the ClAlOC and AlOCO groups. The parameters of the transition state are based on the products of the endothermic reaction AlCl + CO₂ → CO + OAlCl. [b] Units of r are 10^{-10} m; units of θ and τ are deg. [c] Units of F_r are 10^2 N m^{-1}; units of F_θ and F_τ are 10^{-18} N m rad^{-2}.

corresponding to the middle of the T^{-1} range of the experiments. The value $\Delta E^{\ddagger} = 45.9$ kJ mol^{-1} is thus obtained, which yields

$$k_{MTST} = 5.74 \times 10^{-18} \, (T/K)^{2.06} \times$$
$$\exp(-5520 \, K/T) \quad cm^3 \, molecule^{-1} \, s^{-1} \quad (14)$$

A comparison between eq 14, the MTST rate coefficient for reaction 1a, and experiment is shown in Figure 2. Over the temperature range of the experimental data the agreement can be seen to be excellent, which suggests that the dominant channel for reaction 1 is abstraction, i.e., channel 1a.

The AlCl + CO₂ Reaction. The abstraction reaction

$$AlCl + CO_2 \rightarrow OAlCl + CO \qquad (2a)$$

is 98 kJ mol^{-1} endothermic.[23] The parameters of the transition state ClAlOCO‡, which are summarized in Table IV, have been derived based on properties of the products OAlCl + CO. The estimation scheme is very similar to that for the AlCl + N₂O transition state so only the differences will be discussed here. The r(CO), r(ClAl), and r(AlO) distances are taken as those in CO and OAlCl. The internuclear distance along the reaction coordinate is estimated by r(OC) = $[r(O^-) + r(C^+)]0.50^{1/(\delta-1)}$.

The force constant $F_r(CO)$ is taken as that in the CO molecule, while $F_r(ClAl)$ and $F_\theta(ClAlO)$ are taken as equal to force constants derived from ab initio calculations[7] of the vibrational frequencies of OAlCl. Table IV summarizes the resulting rotational constants and vibrational frequencies.

We calculate the preexponential factor of eq 9 in the 500–2000 K temperature range and fit the results to the expression AT^n expression. A barrier height of 118 kJ mol⁻¹ for the forward reaction is estimated based on the endothermicity of reaction 2a plus a barrier height for the reverse reaction of 20 kJ mol⁻¹, which is probably too small in view of the fact that CO + OAlCl is isoelectronic with AlCl + N₂O, for which we obtained a barrier height of 45.9 kJ mol⁻¹. Combining the calculated A, n, and $\Delta E^\ddagger$ values leads to the expression

$$k_{MTST} = 1.27 \times 10^{-18} \, (T/K)^{2.44} \times$$
$$\exp(-14190 \, K/T) \quad cm^3 \, molecule^{-1} \, s^{-1} \quad (15)$$

Equation 15 is plotted in Figure 2 to allow for comparison with experiment. It may be seen that the rate coefficients thus calculated are too low to account for the experimental data below about 1400 K. If a higher barrier for the reverse reaction were to be included, the calculated rate coefficients would decrease further, reinforcing this conclusion. We thus speculate that at least below 1400 K the main products of reaction 2 are adducts correlating with the singlet and triplet potential energy surfaces of AlCl⁺ with CO₂⁻.

The AlCl + SO₂ Reaction. The abstraction reaction

$$AlCl + SO_2 \rightarrow OAlCl + SO \quad (3a)$$
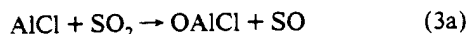
has an endothermicity[23] of 119 kJ mol⁻¹ and is spin-forbidden. For temperatures between 800 and 1100 K the rate coefficient for abstraction is much lower than the upper limit determination (cf. eq 8) because of the large endothermicity. There may be channels leading to the formation of adducts. However, since no reaction could be detected, the adducts must have low binding energies and the addition channels may have significant activation barriers.

The AlCl + O₂ Reaction. In the study[1] of the rate coefficients of the AlCl + O₂ reaction from 490 to 1750 K, it was speculated that the dominant low temperature channel could be

$$AlCl + O_2 \rightarrow AlO_2 + Cl \quad (16a)$$
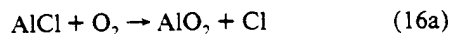
while at higher temperatures the channel

$$AlCl + O_2 \rightarrow OAlCl + O \quad (16b)$$
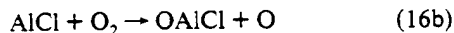
was considered a possibility. Thermochemical data available at that time indicated that the thermochemistry of channel 16a was uncertain, while channel 16b was thought to be exothermic.[1] Recent high-level ab initio computations[7] on AlO₂ now indicate that channel 16a is 87 kJ mol⁻¹ endothermic, confirming the $\Delta H_f(AlO_2)$ assumed in the JANAF tables.[8] That theoretical work[23] also suggests that channel 16b is 66 kJ mol⁻¹ endothermic. These data and the use of MTST allow a reevaluation of the measurements of the AlCl + O₂ reaction.

The parameters for the molecular model as well as the rotational constants and vibrational frequencies of the transition state for channel 16a are summarized in Table V. The geometry and force constants have been obtained based on the assumption that the transition state resembles the products OAlO + Cl, with the halogen atom attacking the Al atom by a side-on approach. We assume the AlO distance and force constants $F_r(AlO)$ and F_θ (OAlO) for the transition state are equal to those of AlO₂.[8] The remaining parameters have been obtained similarly to those for the AlCl + N₂O, CO₂ reactions. If the barrier height for the

TABLE V: Transition-State Parameters for AlO₂Cl‡

geometrical parameter[a,b]		force constant[c]	
$r(AlCl)$	2.34	$F_r(AlCl)$	−2.0
$r(AlO)$	1.69	$F_r(AlO)$	4.2
$\theta(OAlO)$	160	$F_\theta(OAlO)$	0.24
$\theta(OAlCl)$	100	$F_\theta(OAlCl)$	0.2
$\tau(AlO_2Cl)$	0	$F_\tau(AlO_2Cl)$	0.02

rotational constants $(B_1B_2B_3)$: $1.72 \times 10^{-3} \, cm^{-3}$

vibrational frequencies v_i: 119, 176, 200, 678, 981 cm⁻¹

[a] We assume a C_{2v} arrangement for the atoms. The parameters of the transition state are based on the products of the endothermic reaction AlCl + O₂ → OAlO + Cl. [b] Units of r are 10^{-10} m; units of θ and τ are deg. [c] Units of F_r are 10^2 N m⁻¹; units of F_θ and F_τ are 10^{-18} N m rad⁻².

TABLE VI: Transition-State Parameters for ClAlOO‡

geometrical parameter[a,b]		force constant[c]	
$r(ClAl)$	2.08	$F_r(ClAl)$	3.2
$r(AlO)$	1.63	$F_r(AlO)$	4.2
$r(OO)$	1.72	$F_r(OO)$	−2.0
$\theta(ClAlO)$	160	$F_\theta(ClAlO)$	0.3
$\theta(AlOO)$	90	$F_\theta(AlOO)$	0.6
$\tau(ClAlOO)$	0	$F_\tau(ClAlOO)$	0.02

rotational constants $(B_1B_2B_3)$: $3.27 \times 10^{-3} \, cm^{-3}$

vibrational frequencies v_i: 125, 131, 245, 522, 907 cm⁻¹

[a] We assume a trans arrangement for the atoms. The parameters of the transition state are based on the products of the endothermic reaction AlCl + O₂ → O + OAlCl. [b] Units of r are 10^{-10} m; units of θ and τ are deg. [c] Units of F_r are 10^2 N m⁻¹; units of F_θ and F_τ are 10^{-18} N m rad⁻².
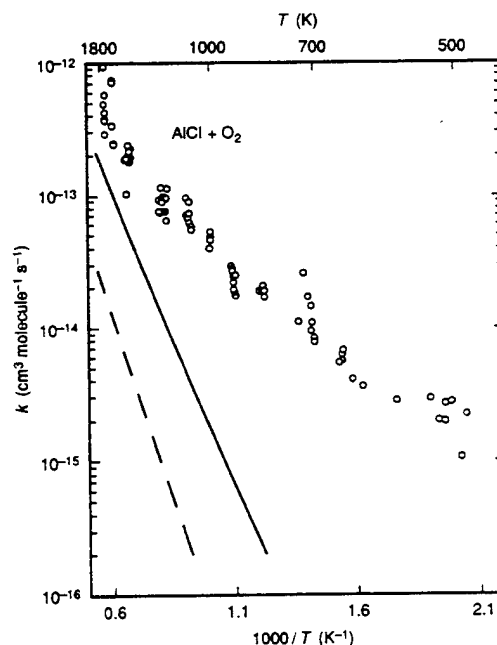
Figure 3. Arrhenius plot of experimental rate coefficients for the previously[1] studied AlCl + O₂ (open circles) reaction. Rate coefficient expressions for the AlCl + O₂ → OAlCl + O (full line) and AlCl + O₂ → AlO₂ + Cl (dashed line) channels derived using the MTST method are shown for comparison with experiments.

reverse reaction is neglected, MTST calculations give

$$k_{MTST} = 2.75 \times 10^{-17} \, (T/K)^{1.76} \times$$
$$\exp(-10460 \, K/T) \quad cm^3 \, molecule^{-1} \, s^{-1} \quad (17)$$

As can be seen in Figure 3 the MTST calculations given by the dashed line indicate that channel 16a is insignificant at all temperatures.

The MTST parameters for channel 16b are summarized in Table VI and have been obtained similarly to those for the AlCl

+ CO_2 reaction. If we assume a negligible barrier height for the reverse reaction, the MTST expression obtained is

$$k_{MTST} = 1.18 \times 10^{-17} (T/K)^{1.87} \times \exp(-7938 \text{ K}/T) \text{ cm}^3 \text{ molecule}^{-1} \text{ s}^{-1} \quad (18)$$

In Figure 3 the experimental rate coefficient measurements are shown along with those from eq 18. This comparison suggests that channel 16b can be of significance above about 1500 K in agreement with the earlier speculation.[1]

Recent ab initio calculations[26] have indicated the existence of a stable adduct $AlClO_2$, which correlates with the reactants AlCl + O_2. Hence, the dominant reaction pathway at temperatures below 1750 K is likely to be addition with the abstraction reaction 16b becoming of greater importance with increasing temperature.

References and Notes

(1) Rogowski, D. F.; Fontijn, A. *21st Symposium (International) on Combustion*; The Combustion Institute: Pittsburgh, 1988; p 943.
(2) Rogowski, D. F.; Fontijn, A. *Chem. Phys. Lett.* **1986**, *132*, 413.
(3) Rogowski, D. F.; Marshall, P.; Fontijn, A. *J. Phys. Chem.* **1989**, *93*, 1118.
(4) Slavejkov, A. G.; Fontijn, A. *Chem. Phys. Lett.* **1990**, *165*, 375.
(5) Fontijn, A.; Futerko, P. M. In *Gas-Phase Metal Reactions*; Fontijn, A., Ed.; North-Holland: Amsterdam, 1992; Chapter 6.
(6) Slavejkov, A. G.; Futerko, P. M.; Fontijn, A. *23rd Symposium (International) on Combustion*; The Combustion Institute: Pittsburgh, 1991; p 155.
(7) Chen, W.; Hase, W. L.; Schlegel, H. B. In *Gas-Phase Metal Reactions*; Fontijn, A., Ed.; North-Holland: Amsterdam, 1992; Chapter 9.
(8) *JANAF Thermochemical Tables*; *J. Phys. Chem. Ref. Data* **1985**, *14* (Suppl. No. 1).
(9) Hammond, G. S. *J. Am. Chem. Soc.* **1955**, *77*, 334.
(10) Benson, S. W. *Thermochemical Kinetics*, 2nd ed.; Wiley: New York, 1976.
(11) Futerko, P. M.; Slavejkov, A. G.; Fontijn, A. To be submitted.
(12) Pearse, R. W. B.; Gaydon, A. G. *The Identification of Molecular Spectra*, 4th ed.; Wiley: New York, 1976.
(13) Fontijn, A.; Felder, W. In *Reactive Intermediates in the Gas Phase*; Setser, D. W., Ed.; Academic Press: New York, 1979; Chapter 2.
(14) Irvin, J. A.; Quickenden, T. I. *J. Chem. Educ.* **1983**, *60*, 711.
(15) Press, W. H.; Flannery, B. P.; Teukolsky, S. A.; Vetterling, W. T. *Numerical Recipes*; Cambridge University: Cambridge, 1986.
(16) Wentworth, W. E. *J. Chem. Educ.* **1965**, *142*, 96, 162.
(17) Laidler, K. J. *Chemical Kinetics*, 3rd ed.; Harper & Row: New York, 1987; pp 94–106.
(18) Harzberg, G. *Molecular Spectra and Molecular Structure. II. Infrared and Raman Spectra of Polyatomic Molecules*; Van Nostrand: New York, 1945; pp 168–186.
(19) Pauling, L.; Wilson, E. B., Jr. *Introduction to Quantum Mechanics*; Dover: New York, 1963; pp 282–288.
(20) Goldstein, H. *Classical Mechanics*, 2nd ed.; Addison-Wesley: Reading, MA, 1980; pp 188–203.
(21) In ref 19, p 274.
(22) Glasstone, S.; Laidler, K. J.; Eyring, H. *The Theory of Rate Processes*; McGraw-Hill: New York, 1941; pp 119, 120, 222–224.
(23) As discussed in ref 7, the heat of formation of OAlCl in ref 8 is probably inaccurate. Reaction enthalpies are thus calculated using the ab initio values of the atomization energy of OAlCl in ref 7 and heats of formation at 0 K, in ref 8, for all other species.
(24) Pauling, L. *The Nature of the Chemical Bond*, 3rd ed.; Cornell University: Ithaca, NY, 1960; pp 511–532.
(25) Futerko, P. M.; Fontijn, A. *J. Chem. Phys.* **1991**, *95*, 8065.
(26) Chen, W.; Hase, W. L.; Schlegel, H. B. Work in progress communicated to us by H. B. Schlegel.
(27) Marshall, P.; O'Connor, P. B.; Chan, W.-T.; Kristof, P. V.; Goddard, J. D. In *Gas-Phase Metal Reactions*; Fontijn, A., Ed.; North-Holland: Amsterdam, 1992; Chapter 8.
(28) Marshall, P.; Fontijn, A.; Melius, C. F. *J. Chem. Phys.* **1987**, *86*, 5540.
(29) Huber, K. P.; Herzberg, G. *Molecular Spectra and Molecular Structure. IV. Constants of Diatomic Molecules*; Van Nostrand: New York, 1979.
(30) Shimanouchi, T. In *Physical Chemistry: An Advanced Treatise*; Eyring, H., Henderson, D., Jost, W., Eds.; Academic: New York, 1970; Vol. IV.

Wide Temperature Range Kinetics of the Gas-Phase Reactions of BCl with SO_2, N_2O, O_2, and CO_2

### Peter M. Futerko,[†] Aleksandar G. Slavejkov,[‡] and Arthur Fontijn[*]

High-Temperature Reaction Kinetics Laboratory, The Isermann Department of Chemical Engineering, Rensselaer Polytechnic Institute, Troy, New York 12180-3590

Rate coefficients for the title reactions have been measured in a high-temperature fast-flow reactor (HTFFR). Weighted fits give for BCl + SO_2 $k(470–1690 \text{ K}) = 7.7 \times 10^{-22}(T/\text{K})^{3.0} \exp(-1680 \text{ K}/T)$ cm^3 molecule^{-1} s^{-1} and for BCl + N_2O $k(670–1000 \text{ K}) = 5.1 \times 10^{-12} \exp(-6340 \text{ K}/T)$ cm^3 molecule^{-1} s^{-1}. 2σ accuracy limits are about ±25%. Model-based transition-state theory (MTST) is used to calculate rate coefficients for the O-atom abstraction channels of these reactions, as well as for the previously measured BCl reactions with O_2 and CO_2. Approximate agreement between theory and experiment is obtained for the four reactions, indicating abstraction to be dominant for each reaction. The reactions are compared to the corresponding AlCl reactions.

Introduction

In previous work, the high-temperature fast-flow reactor (HTFFR) technique has been used to make rate coefficient measurements on the reactions BCl + O_2, in the 540–1670 K range,[1] and BCl + CO_2, over the 770–1830 K range.[2] Here we extend this series by reporting measurements on the reactions

$$\text{BCl} + \text{SO}_2 \rightarrow \text{products} \qquad (1)$$

$$\text{BCl} + \text{N}_2\text{O} \rightarrow \text{products} \qquad (2)$$
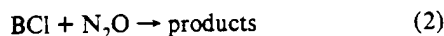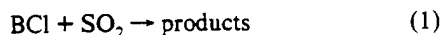
in the respective 470–1690 K and 670–1000 K temperature ranges.

In another recent paper, we reported on the AlCl reactions with these same four oxygen-containing oxidants and developed a variant of classical transition-state theory (CTST).[3] This model-based transition-state theory (MTST) is applicable to reactions with early activation barriers and is particularly useful when the input data for the CTST methods originated by Benson[4] are not available. MTST was used in that work[3] to determine the AT^n part of the rate coefficient $k(T) = AT^n \exp(-E/RT)$ expressions for abstraction reactions. Here we continue the comparison between experiment and MTST calculations for reactions of BCl, isoelectronic with AlCl.

Experimental Section

The HTFFR technique, as used for BCl studies, has been described in detail elsewhere.[2,5] Briefly, BCl was generated by passing 20–40 ppm BCl_3/Ar through a microwave discharge in a Pyrex tube (1.2-cm i.d.) and fed into the reaction tube. The reactor consisted of a vertically positioned mullite tube (2.2-cm i.d.) sealed inside a water-cooled, steel vacuum housing. Two parallel series of SiC heating elements were used to maintain uniform temperatures in the reaction tube. Efficient heating of the bath gas was achieved by fixing the smaller mullite tube (1.8-cm o.d.) in the reaction tube upstream from the reaction zone. The oxidant gas, SO_2 or N_2O mixed with N_2, was introduced into the reaction tube through a movable alumina ring inlet with eight circular openings (0.1-cm diameter) through which the oxidant gas mixtures were injected into the BCl/Ar stream. Gas flow through the inlet was maintained at a constant molar rate

for rate coefficient determinations, each of which consisted of five or six measurements at different oxidant concentrations. At 10 or 20 cm downstream from the ring, relative concentrations of BCl were monitored by laser-induced fluorescence (LIF) using four different transitions of the ($A^1\Pi–X^1\Sigma^+$) band, namely, (1,0)Q at 266.0 nm, (0,0)Q at 272.0 nm, (0,0)P at 272.16 nm, and (1,1)P at 272.21 nm.[6] Laser pulses at these wavelengths were generated by a Lambda Physik EMG 101 excimer laser/FL 2002 dye laser/KDP doubling crystal combination. The pulses were directed through two 4-mm-diameter holes in the mullite reaction tube. The BCl fluorescence, which passed through a third hole in the reaction tube positioned normal to the laser pulse path, was recorded with an EMI 9813 QA photomultiplier tube (PMT)/LeCroy VV100B wide-band pulse amplifier/Data Precision Analogic 6000/620 100-MHz transient digitizer combination. A 270-nm interference filter (24-nm fwhm) was positioned in front of the PMT to remove background radiation.

Rate coefficient measurements were made in the stationary inlet mode[7] with reaction zone lengths of 10 or 20 cm, under pseudo-first-order conditions with BCl as the minor reactant. Plots of ln $[\text{BCl}]_{\text{relative}}$ vs $[\text{SO}_2]$ or $[\text{N}_2\text{O}]$, in which $[\text{BCl}]_{\text{relative}}$ is the time-integrated LIF signal averaged over 200 laser pulses, were linear with slopes proportional to the rate coefficients. For each individual measurement, k_i and σ_{k_i} were determined by a weighted linear least-squares fit of the data.[7,8]

The gases used were Ar (99.998%, Linde) and N_2 (99.998%, Airco) obtained from the liquid, BCl_3 (99.9%, Matheson), N_2O (99.99%, Matheson), N_2O (99.0%, Linde), SO_2 (99.98%, Matheson), SO_2 (99.98%, Linde), and O_2 (5.0% in Ar, certified; Scott).

Results

The measured rate coefficients k_i of reactions 1 and 2 at the various temperatures used are shown in Figure 1. They are summarized in Tables I and II along with the observed reaction zone length, total pressure P, total concentration [M], maximum oxidant concentration $[\text{SO}_2]_{\text{max}}$ or $[\text{N}_2\text{O}]_{\text{max}}$, fluorescence intensity F (a measure of [BCl] at the start of the reaction zone), and average velocity $\bar{v}$. Variation in the experimental conditions was used to check the accuracy of the k_i measurements, as secondary reactions of potential other species produced in the Ar + BCl discharge, i.e., B, BCl, BCl_2, Cl, and Cl_2, could have produced BCl in the reaction zone. If this had occurred, k_i measurements would have shown dependences on reaction zone length, $\bar{v}$, and P. Our reported k_i values (Tables I and II) may be seen to be independent of these quantities by examining plots of $[k(T) -$
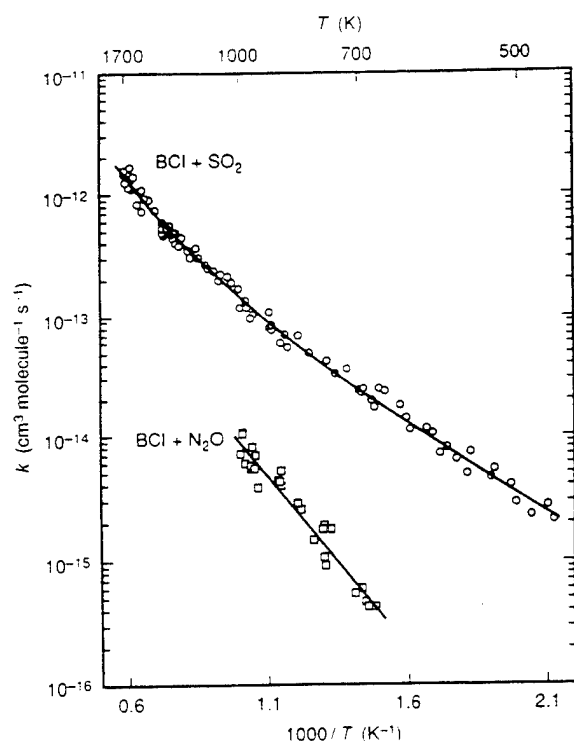
Figure 1. Arrhenius plots of experimental rate coefficients for the BCl + SO₂ (open circles) and BCl + N₂O (open squares) reactions. The full lines represent the experimental rate coefficient expressions.

$k_i]/k(T)$, where $k(T)$ are the fitted rate coefficient expressions given below, vs the experimental parameters; for each case, the k_i data are randomly scattered about the zero line of the ordinate.

BCl + SO₂ Reaction. The 85 rate coefficient measurements of this reaction were obtained over the temperature range 470–1690 K (Table I). In this study, LIF radiation was observed in the absence of BCl at temperatures above about 1300 K. For each measurement with BCl, the intensity of this radiation was subtracted from the signal. The interference was observed to increase as the reaction tube temperature was raised and as the [SO₂] increased. Since SO₂ as well as SO, generated from thermal dissociation of SO₂, absorb in the 260–280-nm region,[9] both could have contributed to this background radiation. There was also an a priori possibility that SO, produced by reaction 1, could have interfered with the rate coefficient measurements. This would have resulted in decreased k_1 values. However, since the measured rate coefficients are independent of the [SO₂] ranges and the initial [BCl] concentrations, cf. Table I, and since plots of ln [BCl]ᵣₑₗₐₜᵢᵥₑ vs [SO₂] are linear, we conclude that fluorescence from SO did not significantly affect the measurements. Furthermore, BCl was monitored at four different wavelengths, cf. Table I, all of which gave similar results.

The k_1 measurements were fitted to the expression $k(T) = AT^n \exp(-E/RT)$ using a three-parameter nonlinear regression analysis.[10] The value of n, determined from the fit, was rounded to one decimal place, and a two-parameter nonlinear regression analysis was done. The resulting expression is

$$k_1(470\text{–}1690 \text{ K}) = 7.7 \times 10^{-22}(T/\text{K})^{3.0} \times$$
$$\exp(-1680 \text{ K}/T) \text{ cm}^3 \text{ molecule}^{-1} \text{ s}^{-1} \quad (3)$$

with variance and covariance matrix elements[11]

$$(\sigma_A/A)^2 = 0.00142, \quad \sigma_E^2 = 1164 \text{ K}^2, \quad \sigma_{AE}/A = 1.193 \text{ K}$$
$$(4)$$

This method is advantageous, because it prevents round-off errors in the value of n in the final fit and simplifies the error analysis. Combining the covariance matrix elements by the propagation of errors technique yields $\pm 2\sigma_k$ precision limits of 8% at 470 K,

3% at 1080 K, and 4% at 1690 K. Allowing 10% uncertainty associated with the flow profile factor[7] and a conservative 20% for further systematic errors yields $\pm 2\sigma_k$ confidence limits of 24% at 470 K and 23% at 1080 and 1690 K.

BCl + N₂O Reaction. Preliminary measurements showed a dependence of k_2 on the average flow velocity, indicating that continued BCl production in the reaction zone was occurring. Addition of 50–500 ppm of O₂ just downstream from the microwave discharge removed this dependence, and this procedure was therefore adopted. In Table II, the rate coefficient measurements on reaction 2 over the temperature range 670–1000 K are summarized. Above about 1000 K the measured rate coefficients were observed to be dependent on pressure, suggesting that decomposition of N₂O is interfering with the measurements. Hence these are not included in the table. The k_2 measurements were fitted to the Arrhenius expression $k(T) = A \exp(-E/RT)$ to give

$$k_2(670\text{–}1000 \text{ K}) = 5.1 \times 10^{-12} \times$$
$$\exp(-6340 \text{ K}/T) \text{ cm}^3 \text{ molecule}^{-1} \text{ s}^{-1} \quad (5)$$

with matrix elements

$$(\sigma_A/A)^2 = 0.0764, \quad \sigma_E^2 = 56400 \text{ K}^2, \quad \sigma_{AE}/A = 65.1 \text{ K} \quad (6)$$

Combining these matrix elements by the propagation of errors technique yields $\pm 2\sigma_k$ precision limits of 18% at 670 K, 7% at 830 K, and 10% at 1000 K and $\pm 2\sigma_k$ confidence limits of 28% at 670 K, 24% at 830 K, and 25% at 1000 K.

Model-Based Transition-State Theory (MTST)

Recently,[3] we developed a method for applying transition-state theory to reactions of metal-containing species. As in CTST, the rate coefficient is given by[12]

$$k(T) = \frac{k_B T}{h} \frac{q^*}{q_A q_B} \exp(-\Delta E^*/RT) \quad (7)$$

where ΔE^* is the difference in zero-point levels of the transition state and the reactants, q^* is the partition function for the transition state, and q_A and q_B are partition functions for the reactants. In the MTST method, we use molecular models to estimate the vibrational frequencies and rotational constants that are needed to evaluate q^*. For the molecular model, we assume that harmonic restoring forces oppose changes in bond lengths, angles between valence bonds, and dihedral angles. The potential energy V is thus given by[13]

$$2V = \sum_i F_{ri}\Delta r_i^2 + \sum_j F_{\theta j}\Delta\theta_j^2 + \sum_k F_{\tau k}\Delta\tau_k^2 \quad (8)$$

where F_r, F_θ, and F_τ are force constants for changes in internuclear distances r, valence angles θ, and dihedral angles τ from their respective equilibrium values. As described previously,[3] the MTST approach is suitable for reactions with transition states which arise from an early crossing of neutral and ionic potential surfaces, particularly for many oxidation reactions of metal-containing species. For such transition states, one can make reasonably good estimates of the geometrical parameters and force constants based on Hammond's postulate.[14] For example, for an exothermic reaction it can be assumed that the internuclear distances, valence angles, and force constants of the transition states are closely related to those properties of the reactants. The parameters required by the treatment that cannot be obtained from properties of the reactants are estimated,[3] such that the calculated vibrational frequencies of transition states are in good agreement with ab initio computations[15-17] on similar reactions. We have shown[18] that for transition states of eight reactions, one of the reactants being a B- or Al-containing species in each case, calculated vibrational frequencies show an average difference with ab initio results of less than about 100 cm⁻¹. With such

## TABLE I: Summary of Rate Coefficient Measurements for BCl + SO2[a]

reaction zone length (cm)	P (mbar)	[M] (10^{17} cm^{-3})	[SO2]$_{max}$ (10^{15} cm^{-3})	F^b	$\bar{v}$ (m s^{-1})	T (K)	$k \pm \sigma_k$ (cm^3 molecule^{-1} s^{-1})
20	40.5	2.2	0.6	25^c	35	1308	4.35 ± 0.33 (−13)^d
10	40.6	2.2	1.1	19^c	36	1316	4.80 ± 0.35 (−13)
10	64.1	3.6	1.2	55^c	34	1295	4.91 ± 0.37 (−13)
20	64.0	3.6	0.6	49^c	34	1296	3.93 ± 0.32 (−13)
20	27.9	1.2	0.5	27^c	91	1622	1.33 ± 0.12 (−12)
10	27.9	1.2	1.0	38^c	92	1637	1.65 ± 0.13 (−12)
20	48.7	2.2	0.4	21^c	53	1626	1.38 ± 0.13 (−12)
10	48.7	2.2	0.8	40^c	52	1623	1.40 ± 0.11 (−12)
10	31.7	3.2	5.3	33^c	18	723	3.62 ± 0.36 (−14)
20	31.6	3.3	5.4	15^c	18	702	2.43 ± 0.23 (−14)
20	82.4	9.6	8.0	27^c	12	621	1.13 ± 0.08 (−14)
20	31.2	1.4	1.0	37^e	101	1628	1.11 ± 0.09 (−12)
20	31.6	1.4	1.0	27^e	101	1651	1.15 ± 0.09 (−12)
10	53.9	2.4	0.8	24^e	66	1650	1.46 ± 0.16 (−12)
10	62.0	2.7	0.7	8^f	34	1685	1.24 ± 0.11 (−12)
10	29.3	1.3	1.3	17^f	72	1691	1.45 ± 0.13 (−12)
10	29.5	1.3	0.7	23^f	71	1691	1.56 ± 0.12 (−12)
20	33.5	2.7	3.4	25^f	28	903	8.02 ± 0.72 (−14)
20	67.6	5.5	1.1	17^f	18	895	7.69 ± 0.58 (−14)
20	22.5	1.8	2.7	44^f	55	904	1.08 ± 0.11 (−13)
20	23.6	1.8	2.9	24	33	953	1.03 ± 0.09 (−13)
10	46.1	3.5	2.9	12	17	962	9.68 ± 0.78 (−14)
10	28.6	2.1	2.6	21	37	977	1.35 ± 0.14 (−13)
10	44.9	3.3	3.2	20	30	975	1.19 ± 0.10 (−13)
10	78.9	5.7	2.8	14	17	999	1.19 ± 0.10 (−13)
10	27.6	1.5	1.5	14	66	1377	5.99 ± 0.91 (−13)
10	85.2	4.5	1.0	16	29	1368	4.62 ± 0.48 (−13)
10	54.2	2.9	1.2	24	40	1375	4.91 ± 0.49 (−13)
10	54.2	2.9	1.2	4^e	40	1375	5.26 ± 0.40 (−13)
20	25.7	1.4	0.6	9^e	82	1329	5.23 ± 0.69 (−13)
20	25.7	1.4	1.2	39	82	1329	5.53 ± 0.54 (−13)
20	59.1	3.3	0.5	76	42	1311	4.89 ± 0.39 (−13)
20	33.5	1.8	0.6	88	50	1346	5.37 ± 0.45 (−13)
20	20.1	1.0	1.0	50	98	1472	9.18 ± 0.82 (−13)
20	62.2	3.2	0.6	68	49	1430	7.36 ± 0.59 (−13)
20	39.5	1.9	0.8	44	60	1507	9.35 ± 0.81 (−13)
20	34.5	1.6	0.5	31	59	1554	1.06 ± 0.07 (−12)
10	34.6	1.6	1.6	34	60	1570	8.37 ± 0.60 (−13)
10	94.6	4.5	1.2	63	35	1535	7.33 ± 0.53 (−13)
10	58.2	2.6	0.9	20	44	1602	1.38 ± 0.16 (−12)
10	79.9	3.8	0.7	15	31	1536	1.09 ± 0.11 (−12)
10	19.7	1.4	2.5	31	38	1003	1.69 ± 0.19 (−13)
10	41.1	2.9	1.8	38	27	1041	2.10 ± 0.18 (−13)
10	55.3	3.9	3.3	48	29	1027	1.89 ± 0.12 (−13)
10	66.3	4.5	1.6	35	19	1073	2.20 ± 0.22 (−13)
20	46.7	3.1	1.1	34	27	1080	2.00 ± 0.18 (−13)
20	25.9	1.6	0.8	32	35	1138	2.65 ± 0.25 (−13)
20	30.5	2.0	1.7	53	57	1102	2.39 ± 0.17 (−13)
20	39.6	2.5	1.1	32	35	1126	2.46 ± 0.26 (−13)
10	39.7	2.4	2.6	56	37	1187	3.61 ± 0.27 (−13)
10	89.3	5.5	1.4	45	21	1171	3.02 ± 0.18 (−13)
10	50.3	3.0	1.5	43	21	1212	3.01 ± 0.22 (−13)
10	32.1	1.8	2.3	66	42	1258	4.49 ± 0.34 (−13)
20	32.0	1.8	1.2	33	43	1277	3.77 ± 0.30 (−13)
20	44.1	2.6	1.7	52	46	1226	3.45 ± 0.22 (−13)
20	19.9	1.8	3.2	37	30	802	4.99 ± 0.51 (−14)
20	60.7	5.8	2.6	17	16	762	4.20 ± 0.30 (−14)
20	39.7	3.9	5.0	29	19	746	3.33 ± 0.25 (−14)
20	49.0	5.1	4.4	13	11	696	2.32 ± 0.27 (−14)
10	49.1	5.1	8.7	15	11	692	2.48 ± 0.16 (−14)
10	83.2	9.6	6.2	13	8	627	1.41 ± 0.11 (−14)
20	28.5	4.0	9.6	11	10	523	5.40 ± 0.50 (−15)
20	79.8	12.3	15.5	12	6	471	2.12 ± 0.19 (−15)
20	63.3	9.6	15.9	19	6	476	2.77 ± 0.17 (−15)
20	63.3	9.1	15.2	18	6	503	2.87 ± 0.26 (−15)
20	57.7	8.5	10.5	53	9	490	2.31 ± 0.22 (−15)
20	85.4	12.2	15.0	7	6	508	4.05 ± 0.53 (−15)
20	63.9	8.8	14.0	24	7	527	4.65 ± 0.46 (−15)
20	35.4	4.7	11.1	12	9	548	7.37 ± 0.62 (−15)
20	56.1	7.2	12.7	17	8	563	6.48 ± 0.39 (−15)
20	48.4	6.1	10.7	25	9	575	8.00 ± 0.62 (−15)
20	54.7	7.2	8.4	38	11	552	4.94 ± 0.60 (−15)
20	47.1	5.7	8.2	36	12	600	1.16 ± 0.09 (−14)
20	55.6	6.9	7.9	31	12	583	7.22 ± 0.50 (−15)
10	85.3	10.4	11.9	21	8	592	1.05 ± 0.13 (−14)
10	47.6	5.2	7.3	55	13	668	2.45 ± 0.20 (−14)
10	77.1	8.8	8.7	34	11	635	1.79 ± 0.23 (−14)
10	40.9	4.5	5.6	93	17	657	2.34 ± 0.26 (−14)
20	20.0	2.1	5.3	84	18	674	1.73 ± 0.19 (−14)
20	24.8	2.6	6.1	21	16	678	1.98 ± 0.16 (−14)
20	20.6	1.7	3.4	37	28	897	8.38 ± 0.72 (−14)
20	51.1	4.3	4.3	51	22	854	5.48 ± 0.33 (−14)
20	39.5	3.3	4.7	32	20	872	6.12 ± 0.48 (−14)
10	39.5	3.3	4.8	46	20	859	7.04 ± 0.68 (−14)
10	76.2	6.7	3.3	32	15	826	6.93 ± 0.55 (−14)

[a] The measurements are reported in the sequence in which they were obtained. [b] In arbitrary units. Unless otherwise indicated, BCl was monitored at the 272.0-nm transition. [c] BCl was monitored at the 272.16-nm transition. [d] Should be read as (4.35 ± 0.33) × 10^{-13} cm^3 molecule^{-1} s^{-1}. [e] BCl was monitored at the 266.0-nm transition. [f] BCl was monitored at the 272.21-nm transition.

estimated geometrical parameters and force constants, we obtain the vibrational frequencies by a normal coordinate analysis of the molecular model, which procedure has been described in detail by Pauling and Wilson.[19] Finally, rotational constants are calculated from the eigenvalues of the inertia tensor.[18]

Discussion

BCl + SO2 Reaction. The thermochemically accessible channels of reaction 1

$$BCl + SO_2 \rightarrow OBCl + SO \qquad (1a)$$

$$\rightarrow BO_2 + SCl \qquad (1b)$$
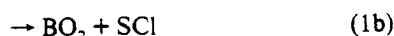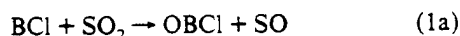
are 245 and 26 kJ mol^{-1} exothermic, respectively, at 0 K.[20-22] Channel 1b is probably inhibited by a substantial energy barrier, as all of the reactant bonds must be broken and reformed. In contrast, we expect channel 1a to have a slight barrier as only the O–SO bond is broken in the reaction. In channel 1a, formation of SO($^3\Sigma^-$), the ground state, is forbidden by the spin rule; however, formation of SO($^1\Delta$)[23] is both exothermic (by 169 kJ mol^{-1}) and spin allowed. The MTST calculations which follow are based on the formation of this state. Table III summarizes the rotational constants and vibrational frequencies for the transition state. The

first two terms of eq 7 are computed at several temperatures in the range 500–2000 K and fitted to the expression AT^n. An estimate of the barrier height is made by equating eqs 3 and 7 at 735 K, the midpoint of the T^{-1} range investigated, which yields 24.1 kJ mol^{-1}. The present calculations lead to the expression

$$k_{MTST} = 5.19 \times 10^{-19}(T/K)^{2.26} \times$$
$$\exp(-2902\ K/T)\ cm^3\ molecule^{-1}\ s^{-1} \qquad (9)$$

Figure 2 compares the MTST calculations with the recommended $k_1(T)$ expression, and they are in good agreement over the 470–1690 K range. This agreement suggests that channel 1a, for which the MTST calculations are based, is the dominant pathway. In a related paper,[3] we attempted to make rate coefficient measurements on the homologous AlCl + SO2 reaction. We failed to observe any significant disappearance of AlCl by reaction with SO2, indicating that the AlCl reaction has a much lower rate coefficient than the BCl + SO2 reaction. The lower rate coefficient is consistent with the reaction being at least 110 kJ mol^{-1} endothermic.[20,22]

BCl + N2O Reaction. The abstraction pathway of reaction 2

$$BCl + N_2O \rightarrow OBCl + N_2 \qquad (2a)$$
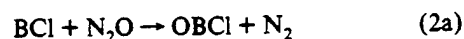
is 631 kJ mol^{-1} exothermic at 0 K.[20,22] Similarly to our investigation of the above treatment of BCl + SO2, we investigate

TABLE II: Summary of Rate Coefficient Measurements for BCl + N₂O[a]

reaction zone length (cm)	P (mbar)	[M] $(10^{17}$ cm$^{-3})$	$[N_2O]_{max}$ $(10^{15}$ cm$^{-3})$	F^b	$\bar{v}$ (m s^{-1})	T (K)	$k \pm \sigma_k$ (cm^3 molecule^{-1} s^{-1})
20	42.3	4.5	23.2	15	13	674	4.28 ± 0.40 (−16)[c]
20	36.3	3.4	16.1	58	18	771	1.94 ± 0.34 (−15)
20	36.3	3.5	16.4	59	18	756	1.78 ± 0.14 (−15)
20	84.6	8.7	50.2	27	11	709	5.50 ± 0.73 (−16)
20	84.8	8.9	51.4	24	11	691	4.64 ± 0.31 (−16)
20	40.7	3.0	12.2	35	24	982	6.07 ± 0.59 (−15)
20	78.8	6.1	27.8	23	20	939	3.88 ± 0.69 (−15)
20	59.1	4.3	23.2	42	24	997	7.14 ± 0.64 (−15)
20	99.2	7.3	16.1	27	18	989	1.08 ± 0.07 (−14)
20	99.4	7.3	16.1	26	18	989	1.06 ± 0.09 (−14)
20	40.5	3.8	20.7	45	21	768	9.14 ± 0.97 (−16)
20	40.5	3.8	20.6	35	21	772	1.80 ± 0.42 (−15)
20	77.2	7.3	39.3	37	11	770	1.07 ± 0.10 (−15)
20	55.1	5.0	24.6	42	12	792	1.48 ± 0.12 (−15)
20	56.8	5.0	28.7	76	20	822	2.59 ± 0.39 (−15)
20	56.8	5.0	28.5	79	20	829	2.89 ± 0.28 (−15)
20	51.7	4.3	19.8	43	15	872	4.01 ± 0.43 (−15)
20	51.7	4.3	19.7	38	15	879	4.42 ± 0.40 (−15)
20	42.0	3.2	17.6	84	25	945	7.09 ± 0.60 (−15)
20	42.0	3.2	17.4	72	25	956	8.23 ± 0.57 (−15)
20	78.1	5.9	22.2	29	13	960	5.56 ± 0.43 (−15)
20	78.1	5.9	22.2	33	13	961	5.74 ± 0.39 (−15)
20	55.7	5.9	40.2	39	11	687	4.29 ± 1.04 (−16)
20	55.7	5.8	39.7	28	11	696	5.95 ± 1.06 (−16)
10	53.7	4.5	27.2	24	16	873	5.22 ± 0.45 (−15)
10	53.7	4.4	27.1	20	16	877	4.27 ± 0.52 (−15)
10	47.1	3.6	23.0	21	25	950	5.45 ± 0.74 (−15)

[a] The measurements are reported in the sequence in which they were obtained. [b] In arbitrary units. For each measurement, BCl was monitored at the 272.0-nm transition. [c] Should be read as (4.28 ± 0.40) × 10^{-16} cm^3 molecule^{-1} s^{-1}.

TABLE III: Transition-State Parameters for ClBOSO[a]

geometrical parameter[a,b]		force constant[c]	
r(ClB)	1.72	F_r(ClB)	3.5
r(BO)	1.94	F_r(BO)	−2.0
r(OS)	1.43	F_r(OS)	5.15
r(SO)	1.43	F_r(SO)	10.3
θ(ClBO)	120°	F_θ(ClBO)	0.2
θ(BOS)	120°	F_θ(BOS)	0.6
θ(OSO)	120°	F_θ(OSO)	1.68
τ(ClBOS)	0°	F_τ(ClBOS)	0.02
τ(BOSO)	90°	F_τ(BOSO)	0.02

|	
rotational constants $(B_1B_2B_3)$	7.95×10^{-4} cm^{-3}
vibrational frequencies ν_i	50, 65, 122, 237, 520, 839, 896, 1300 cm^{-1}

[a] We assume trans arrangements for the atoms in the ClBOS and BOSO groups. [b] Units of r are 10^{-10} m. [c] Units of F_r are 10^2 N m^{-1}; units of F_θ and F_τ are 10^{-18} N m rad^{-2}.

the kinetics of this reaction path using MTST with the parameters summarized in Table IV. The first two terms of eq 7 are computed in the 500–2000 K range and fitted to the expression AT^n. Using eqs 5 and 7 at the mid T^{-1} point 802 K, we back out a barrier height of 53.2 kJ mol^{-1}, which combines with the calculated A and n values to give

$$k_{MTST} = 7.98 \times 10^{-18}(T/K)^{2.01} \times$$
$$\exp(-6399 \text{ K}/T) \text{ cm}^3 \text{ molecule}^{-1} \text{ s}^{-1} \quad (10)$$

As shown in Figure 2, eq 10 is roughly in agreement with the recommended $k_2(T)$ expression in the 670–1000 K temperature range. We obtained similar results in a previous study[3] of the homologous AlCl + N₂O reaction. The two reactions are closely related in that both have fairly large activation barriers and both reactions have exothermic channels leading to O-atom abstraction.

BCl + O₂ Reaction. The abstraction reaction

$$BCl + O_2 \rightarrow OBCl + O \quad (11)$$
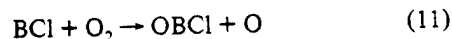
is 298 kJ mol^{-1} exothermic at 0 K.[20,22] We again calculate transition-state parameters, which are summarized in Table V, for the abstraction channel. By equating the MTST expression
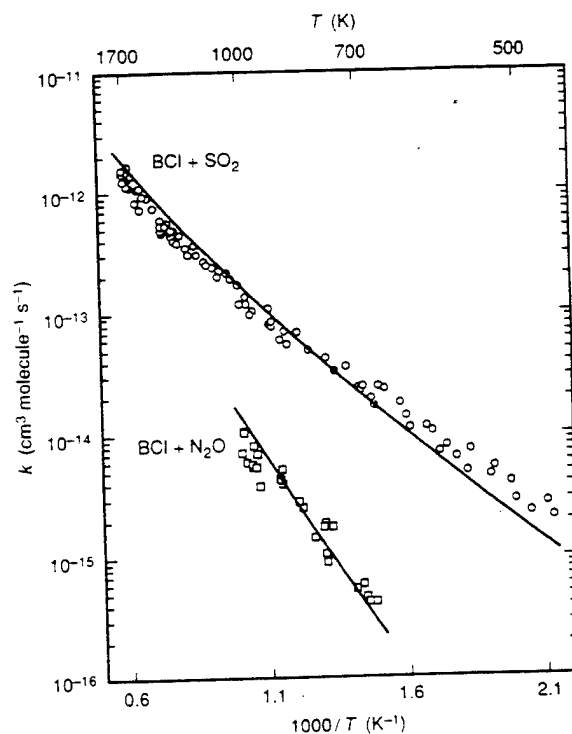

Figure 2. Arrhenius plots of experimental rate coefficients for the BCl + SO₂ (open circles) and BCl + N₂O (open squares) reactions. The full lines represent the rate coefficient expressions for the O-atom abstraction channels, as calculated by the MTST method.

to the experimental rate coefficient expression[1] at 820 K, we calculate a barrier height of 31.0 kJ mol^{-1}, which yields

$$k_{MTST} = 5.17 \times 10^{-17}(T/K)^{1.77} \times$$
$$\exp(-3730 \text{ K}/T) \text{ cm}^3 \text{ molecule}^{-1} \text{ s}^{-1} \quad (12)$$

As shown in Figure 3, eq 12 is in good agreement with the experimental measurements. In contrast to the present study,

TABLE IV: Transition-State Parameters for ClBONN[+]

geometrical parameter[a,b]		force constant[c]	
r(ClB)	1.72	F_r(ClB)	3.5
r(BO)	1.94	F_r(BO)	−2.0
r(ON)	1.18	F_r(ON)	5.85
r(NN)	1.13	F_r(NN)	18.7
θ(ClBO)	120°	F_θ(ClBO)	0.2
θ(BON)	90°	F_θ(BON)	0.6
θ(ONN)	160°	F_θ(ONN)	0.67
τ(ClBON)	0°	F_τ(ClBON)	0.02
τ(BONN)	0°	F_τ(BONN)	0.02
rotational constants ($B_1B_2B_3$)		2.46×10^{-3} cm^{-3}	
vibrational frequencies ν_i		58, 123, 170, 292, 596, 839, 996, 2221 cm^{-1}	

[a] We assume trans arrangements for the atoms in the ClBON and BONN groups. [b] Units of r are 10^{-10} m. [c] Units of F_r are 10^2 N m^{-1}; units of F_θ and F_τ are 10^{-18} N m rad^{-2}.

TABLE V: Transition-State Parameters for ClBOO[+]

geometrical parameter[a,b]		force constant[c]	
r(ClB)	1.72	F_r(ClB)	3.5
r(BO)	1.94	F_r(BO)	−2.0
r(OO)	1.21	F_r(OO)	5.9
θ(ClBO)	120°	F_θ(ClBO)	0.2
θ(BOO)	120°	F_θ(BOO)	0.6
τ(ClBOO)	0°	F_τ(ClBOO)	0.02
rotational constants ($B_1B_2B_3$)		1.00×10^{-2} cm^{-3}	
vibrational frequencies ν_i		75, 131, 317, 841, 1116 cm^{-1}	

[a] We assume a trans arrangements for the atoms in the ClBOO. [b] Units of r are 10^{-10} m. [c] Units of F_r are 10^2 N m^{-1}; units of F_θ and F_τ are 10^{-18} N m rad^{-2}.
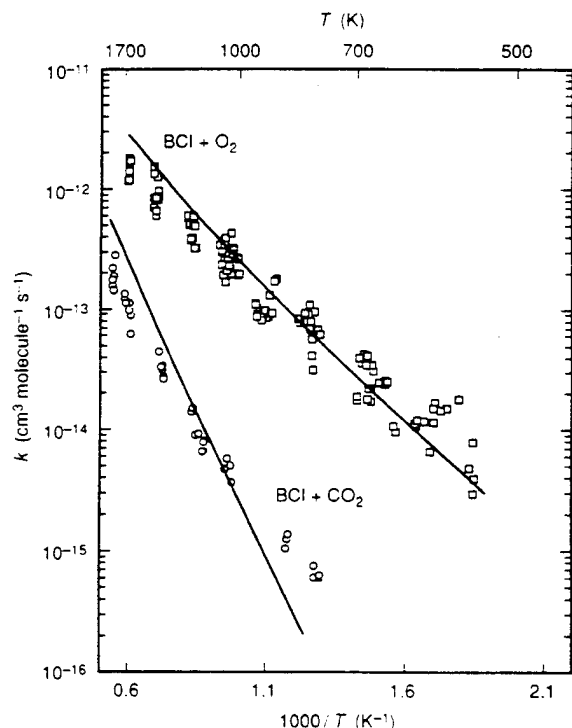

Figure 3. Arrhenius plots of measurements of the rate coefficients for the BCl + O₂ (open squares) and BCl + CO₂ (open circles) reactions from previous studies.[1,2] The full lines represent rate coefficient expressions for the O-atom abstraction channels, as calculated by the MTST method.

we previously found[3] that the AlCl + O₂ reaction MTST calculations, which were based on an O-atom abstraction mechanism, were inconsistent with experiments. The AlCl + O₂ reaction differs from the analogous BCl reaction in that formation of the abstraction products OAlCl + O is an endothermic process with a barrier[3] of at least 66 kJ mol^{-1}. On the basis of the ab

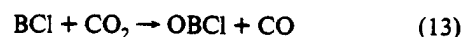**TABLE VI: Transition-State Parameters for ClBOCO[+]**

geometrical parameter[a,b]		force constant[c]	
r(ClB)	1.72	F_r(ClB)	3.5
r(BO)	1.94	F_r(BO)	−2.0
r(OC)	1.16	F_r(OC)	8.0
r(CO)	1.16	F_r(CO)	16.0
θ(ClBO)	120°	F_θ(ClBO)	0.2
θ(BOC)	90°	F_θ(BOC)	0.6
θ(OCO)	160°	F_θ(OCO)	0.79
τ(ClBOC)	0°	F_τ(ClBOC)	0.02
τ(BOCO)	0°	F_τ(BOCO)	0.02
rotational constants ($B_1B_2B_3$)		2.26×10^{-3} cm^{-3}	
vibrational frequencies ν_i		57, 122, 169, 303, 662, 842, 1117, 2185 cm^{-1}	

[a] We assume trans arrangements for the atoms in the ClBOC and BOCO groups. [b] Units of r are 10^{-10} m. [c] Units of F_r are 10^2 N m^{-1}; units of F_θ and F_τ are 10^{-18} N m rad^{-2}.

initio study by Chen, Hase, and Schlegel,[17] we suggested that the main channel of AlCl + O₂ reaction involves the formation of an adduct.

BCl + CO₂ Reaction. The O-atom abstraction reaction

$$BCl + CO_2 \rightarrow OBCl + CO \qquad (13)$$

is 266 kJ mol^{-1} exothermic at 0 K.[20,22] The calculated transition-state parameters for this path are summarized in Table VI. By equating the MTST expression to the experimental rate coefficient expression[2] at 1080 K, we calculate a barrier height of 73.2 kJ mol^{-1}, which gives

$$k_{MTST} = 1.23 \times 10^{-17}(T/K)^{2.05} \times$$

$$\exp(-8804 \text{ K}/T) \text{ cm}^3 \text{ molecule}^{-1} \text{ s}^{-1} \quad (14)$$

Figure 3 shows a comparison of eq 14 with experimental data from the previous study.[2] The calculations are in approximate agreement with experiment over the 770–1830 K range. A comparison can be made between the BCl and AlCl reactions with CO₂. As is the case for the BCl and AlCl reactions with O₂, the BCl + CO₂ reaction has an exothermic abstraction channel while the channel leading to formation of OAlCl + CO has an enthalpy barrier of at least 98 kJ mol^{-1}. Because the abstraction channel for the AlCl + CO₂ reaction is endothermic, other channels resulting in adduct formation can dominate, especially at low temperatures.[3]

Conclusions

Kinetic measurements on BCl reactions with oxygen-containing oxidants have been made over wide temperature ranges. We used a TST-based method to calculate pre-exponentials for four BCl reactions and obtained good agreement with experiments. We showed that for these reactions rate coefficients can be reasonably well predicted over a range of temperatures, given a rate coefficient measurement at a single temperature to obtain the E factor. For exothermic processes, i.e., the N₂O reactions, AlCl and BCl behave similarly, as may be expected for cogeners. The observed differences for the other reactions are in accord with the thermochemistry.

References and Notes

(1) Slavejkov, A. G.; Rogowski, D. F.; Fontijn, A. *Chem. Phys. Lett.* **1988**, *143*, 26.

(2) Slavejkov, A. G.; Futerko, P. M.; Fontijn, A. *23rd Symposium (International) on Combustion*; The Combustion Institute: Pittsburgh, 1991, p 155.

(3) Futerko, P. M.; Fontijn, A. *J. Phys. Chem.* **1993**, *97*, 7222.

(4) Benson, S. W. *Thermochemical Kinetics*, 2nd ed.; Wiley: New York, 1976.

(5) Fontijn, A.; Futerko, P. M. In *Gas-Phase Metal Reactions*; Fontijn, A., Ed.; Elsevier: Amsterdam, 1992; Chapter 6.

(6) Herzberg, G.; Hushley, W. *Can. J. Res. Sec A.* **1941**, *19*, 127.

(7) Fontijn, A.; Felder, W. In *Reactive Intermediates in the Gas Phase*; Setser, D. W., Ed.; Academic Press: New York. 1979; Chapter 2.

(8) Irvin, J. A.; Quickenden, T. I. *J. Chem. Educ.* **1983**, *60*, 711.

(9) Pearse, R. W. B.; Gaydon, A. G. *The Identification of Molecular Spectra*, 4th ed.; Wiley: New York, 1976.

(10) Press, W. H.; Flannery, B. P.; Teukolsky, S. A.; Vetterling, W. T. *Numerical Recipes*; Cambridge University: Cambridge, 1986.

(11) Wentworth, W. E. *J. Chem. Educ.* **1965**, *42*, 96; **1965**, *42*, 162.

(12) Laidler, K. J. *Chemical Kinetics*, 3rd ed.; Harper and Row: New York. 1987; p 94.

(13) Herzberg, G. *Molecular Spectra and Molecular Structure. II. Infrared and Raman Spectra of Polyatomic Molecules*; Van Nostrand: New York, 1945; pp 168–186.

(14) Hammond, G. S. *J. Am. Chem. Soc.* **1955**, *77*, 334.

(15) Marshall, P.; Fontijn, A.; Melius, C. F. *J. Chem. Phys.* **1987**, *86*, 5540.

(16) Marshall, P.; O'Connor, P. B.; Chan, W-T.; Kristof, P. V.; Goddard, J. D. In *Gas-Phase Metal Reactions*; Fontijn, A., Ed.; Elsevier: Amsterdam, 1992; Chapter 8.

(17) Chen, W.; Hase, W. L.; Schlegel, H. B., work in progress communicated to us by H. B. Schlegel.

(18) Futerko, P. M.; PhD Thesis, Rensselaer Polytechnic Institute, 1993; Section 5.2.4.

(19) Pauling, L.; Wilson, E. B., Jr. *Introduction to Quantum Mechanics*; Dover: New York, 1963; pp 282–288.

(20) Based on atomization energies at 0 K from data in *JANAF Thermochemical tables, J. Phys. Chem. Ref. Data* **1985**, *14*, Supplement No. 1.

(21) Based on the G2 atomization energy at 0 K for SCl in Curtiss, L. A.; Raghavachari, K.; Trucks, G. W.; Pople, J. A. *J. Chem. Phys.* **1991**, *94*, 7221.

(22) Based on G2 atomization energies at 0 K for BCl, OBCl, and OAlCl in Chen, W.; Hase, W. L.; Schlegel, H. B. in *Gas-Phase Metal Reactions*; Fontijn, A., Ed.; Elsevier: Amsterdam, 1992; Chapter 9.

(23) Huber, K. P.; Herzberg, G. *Molecular Spectra and Molecular Structure. IV. Constants of Diatomic Molecules*; Van Nostrand: New York, 1979.

Activation barriers for series of exothermic homologous reactions. IV. Comparison of measurements to theory for reactions of s^2p^1 atoms with N_2O

David P. Belyung, Peter M. Futerko,[a] and Arthur Fontijn[b]

High-Temperature Reaction Kinetics Laboratory, The Isermann Department of Chemical Engineering, Rensselaer Polytechnic Institute, Troy, New York 12180-3590

The kinetics of the $Al+N_2O\rightarrow AlO+N_2$ reaction has been studied in a high-temperature fast-flow reactor (HTFFR). The expression $k(520-1030$ K$)=4.6\times10^{-12}$ $(T/K)^{0.5}\exp(-778$ K/T$)$ cm^3 molecule^{-1} s^{-1} has been derived from a nonlinear regression analysis of the measured rate coefficients. 2σ precision limits are about $\pm5\%$ and accuracy limits are estimated to be about $\pm23\%$. Combining the data with a 296 K literature measurement yields $k(296-1030$ K$)=5.8\times10^{-15}$ $(T/K)^{1.37}\exp(-90.4$ K/T$)$ cm^3 molecule^{-1} s^{-1}, with 2σ estimated accuracy limits of about $\pm27\%$. The semiempirical approach used previously to predict activation barriers for s^1 and s^2 metal atom reactions with N_2O has been modified to allow predictions of group 13 atom reactions with N_2O. The activation barriers for the B, Ga, In, and Tl atom reactions are calculated from the experimental activation barrier of the $Al+N_2O$ reaction. © *1995 American Institute of Physics.*

I. INTRODUCTION

In the first paper[1] of this series it was shown that the experimental activation barriers E, and as a result the rate coefficients of reactions of ground state s^1 and s^2 metal atoms with N_2O, are closely related to the sums of the $s-p$ promotion energies and ionization potentials of the atoms. E was defined by

$$k(T)=AT^n\exp(-E/RT) \tag{1}$$

which expression gave the best correlations for $n=0.5$. A semiempirical treatment was developed to calculate E for all the s^1 and s^2 metal atoms reactions with N_2O, using the experimentally determin⸗ ᵻ activation barrier of the $Cu+N_2O$ reaction. In the second paper,[2] the treatment was refined for s^1 metals for which the reaction coordinate had to be taken as a variable instead of a constant. In the third paper,[3] the treatment for s^2 metals was further modified and reactions with O_2 were considered. Here, the calculations are extended to reactions of $Z(s^2p^1)$ atoms with N_2O, where the barrier heights for the group are determined from measurements on the $Al+N_2O$ reaction, reported here.

II. EXPERIMENT

A. Technique

The measurements on

$$Al+N_2O\rightarrow AlO+N_2 \tag{2}$$

for which[4] ΔH°_{298} is -345 kJ mol^{-1}, were performed in an HTFFR (high-temperature fast-flow reactor). This facility[5,6] and the operational procedures[7] have been described in detail. Briefly, a vertical mullite (McDanel MV-30) reaction tube (60 cm long, 2.2 cm i.d.) was radiatively heated to the desired temperature by columns of resistively heated SiC rods inside an insulated, water-cooled vacuum housing. Al vapor was produced by resistively heating an Al-wetted W coil in a flow of Ar carrier gas. Mixtures of N_2O in Ar, at volume flow rates of between 2% and 7% of the main Ar flow, were injected into the Al/Ar gas stream through a movable inlet. The total molar flow rate of gas through the inlet was kept constant during a given rate coefficient measurement. Further downstream, relative Al concentrations were determined by laser-induced fluorescence (LIF) or atomic resonance absorption spectrometry (ARAS). ARAS was used as a check on the LIF results. These two optical measurement techniques have an important difference. LIF measures the concentration of Al at the axis of the reactor, whereas ARAS measures the average concentration over the full width of the reactor. Comparison thus also gives an indication of the effect, if any, of the flow profile. For the LIF measurements a pulsed Lambda Physik EMG 101 excimer/FL2002 dye laser in combination with a KDP doubling crystal was used. The Al $(^2S-^2P°)$ transition at 265.2 nm was pumped and the fluorescence intensity was measured through a 262 nm (26 nm full width at half-maximum) filter by an EMI 9813 QA photomultiplier tube (PMT), connected to a Data Precision Analogic 6000/620 100 MHz transient digitizer. For the ARAS experiments a hollow cathode lamp was used to generate the Al line radiation at 309.3 nm and the transmitted radiation intensity was monitored with a monochromator in combination with the PMT connected to a Keithley 614 electrometer.

Rate coefficient measurements were made in the stationary inlet mode[7] at observed reaction zone lengths of 10 or 20 cm, under pseudo-first-order conditions with Al as the minor reactant. $[Al]_{relative}$ is defined as $[Al]/[Al]_i$; where $[Al]_i$ is the concentration of Al at the lowest $[N_2O]$ used. The $[N_2O]$ was typically varied by a factor of 5. In LIF, $[Al]_{relative}\propto F/F_i$, where F_i is the initial fluorescence and F the fluorescence in the presence of N_2O. In ARAS, the Lambert–Beer law gives

$[Al]_{relative} \propto \ln(I_0/I)$, where I_0 is the light intensity passing through the reactor without Al present and I is the intensity with Al atoms. Rate coefficients, k_i, were obtained from the slope of linear plots of $\ln[Al]_{relative}$ vs $[N_2O]$. A weighted linear regression was used to determine k_i and σ_{k_i} for each measurement.[8]

The gases used were 99.998% Ar from the liquid Ar (Linde), and 0.53% N_2O (99.99%) in Ar (99.999%) from Matheson, the calibration of which was checked against pure N_2O.[9]

B. Results and discussion

The measured rate coefficients k_i and the experimental conditions under which they were obtained are summarized in Table I. The parameters varied include: total pressure P, corresponding to total concentration $[M]$, initial fluorescence intensity F or initial percentage absorption (both a measure of initial [Al]), average gas velocity $\bar{v}$, and reaction zone length. Our reported k_i values were determined to be independent of these parameters by examining plots of $[k(T) - k_i]/k(T)$, where $k(T)$ is obtained from Eq. (3) below vs the particular parameter. For each parameter the k_i data were found to be randomly scattered about the zero line of the ordinate. Figure 1 shows the k_i data taken. The range of temperatures covered is 520–1030 K. The lower limit was determined by the heating of the Ar bath gas by the Al source. The upper limit was set by the onset of potential dissociation of N_2O.[10]

A weighted nonlinear fit[11] of the data to Eq. (1) with $n = 0.5$ yields

$k(520-1030 \text{ K})$

$$= 4.6 \times 10^{-12}(T/K)^{0.5}$$

$$\times \exp(-6.469/RT)\text{cm}^3 \text{ molecule}^{-1} \text{ s}^{-1}, \qquad (3)$$

where E is expressed in kJ mol^{-1}. The covariance matrix elements[12] are calculated to be $\sigma_A^2 = 5.02 \times 10^{-3} \ A^2$, $\sigma_{AE} = 4.84 \times 10^{-3} \ AE$, and $\sigma_E^2 = 4.83 \times 10^{-3} \ E^2$. These yield $\pm 2\sigma_k$ precision limits varying from $\pm 2\%$ to $\pm 7\%$. Fitting only the LIF results would have led to a $k(T)$ expression 2%–11% higher than Eq. (3), while considering only the ARAS data yields an expression 10%–13% lower. The later set consists of less data and is therefore less precise. Nonetheless, this suggests a small systematic difference, well within the $\pm 20\%$ systematic errors and $\pm 10\%$ flow profile factor uncertainty always allowed for in this type of work.[6,7,10,13] Using these factors leads to accuracy intervals varying from $\pm 22\%$ to $\pm 24\%$. The fit is shown in Fig. 1.

The only previously reported kinetic measurements on the Al+N$_2$O reaction resulted in a $k(296 \text{ K})$ of $(11 \pm 1) \times 10^{-12}$ cm^3 molecule^{-1} s^{-1}. It was obtained by Mitchell and co-workers using their static cell laser-photolysis, laser-fluorescence technique.[14] Their uncertainty value pertains to precision only. Allowing for possible systematic errors of similar magnitude as in our work, leads to $(11 \pm 2$ to $3) \times 10^{-12}$ cm^3 molecule^{-1} s^{-1}. Extrapolation of Eq. (3) to 296 K yields $(5.8 \pm 1.8) \times 10^{-12}$ cm^3 molecule^{-1} s^{-1}. The joint uncertainty limits thus do not quite

overlap. The value of $n = 0.5$ in Eq. (3) was chosen for uniformity with the work on the s^1 and s^2 metals,[1,2] and may not be the best choice here. Also extrapolation over a large range of T^{-1}, i.e., from (1.9 to 3.4)$\times 10^{-3}$ is a somewhat uncertain procedure. There is no reason to doubt either data set. Indeed, we recently[15] made measurements on the Cr+N$_2$O reaction in a MHTP (metals high-temperature photochemistry reactor) from 278 to 1150 K, which showed excellent agreement with the static cell results at 298 and 348 K,[16] as well as with a shock tube study[17] from 1130 to 2570 K. In the same work we reported similar agreement between a MHTP study of the Cr+HCl reaction from 811 to 1414 K and HT-FFR measurements from 880 to 1449 K. As the various techniques for studies of elementary metal atom reactions are showing good agreement, see also Refs. 5 and 18, it appears justified to combine the two sets of results for the present reaction. Using the fitting procedures given above leads to

$k(296-1030 \text{ K})$

$$= 5.8 \times 10^{-15}(T/K)^{1.37}$$

$$\times \exp(-0.752/RT)\text{cm}^3 \text{ molecule}^{-1} \text{ s}^{-1} \qquad (4)$$

with $\sigma_A^2 = 3.19 \ A^2$, $\sigma_{An} = -0.428 \ A$, $\sigma_{AE} = 2.86 \ AE$, $\sigma_n^2 = 7.86 \times 10^{-2}$, $\sigma_{nE} = -0.382 \ E$, and $\sigma_E^2 = 2.71 \ E^2$ are yielding $\pm 2\sigma_k$ precision limits from $\pm 3\%$ to $\pm 21\%$ and accuracy limits from $\pm 23\%$ to $\pm 31\%$. Figure 2 shows that this expression leads, in the temperature range of the present measurements, to a fit nearly as good as that resulting from Eq. (3).

III. THEORY

A. Activation barriers of $Z(s^2 p^1)$+N$_2$O($X \ ^1\Sigma^+$) reactions using semiempirical configuration interaction (SECI) theory

Following the treatment of Ref. 1, the wave function ψ of the activated complex (NNOZ)‡ can be taken as the linear superposition of three wave functions ψ_1, ψ_2, and ψ_3, corresponding to the properties of three resonating structures. These result, respectively, from the covalent ground–ground state interaction, a covalent interaction where a valence s electron is promoted to a p state, and an ionic interaction between the positively charged atom and negatively charged N$_2$O. Thus,

$$\psi = c_1\psi_1 + c_2\psi_2 + c_3\psi_3, \qquad (5)$$

where c_k ($k = 1,2,3$) are the expansion coefficients. The height of the barrier is

$$E = \int \psi^* H \psi \, d\tau. \qquad (6)$$

According to the variation principle,[19] the wave function ψ for the system is that for which E is at a minimum. This condition can be expressed as a set of simultaneous linear equations,

$$\sum_{k=1}^{3} c_k(H_{lk} - \Delta_{lk}E) = 0, \quad l = 1,2,3. \qquad (7)$$

TABLE I. Summary of rate coefficient measurements of Al+N$_2$O.[a]

Reaction zone length (cm)	P (mbar)	$[M]$ (10^{17} cm^{-3})	$[N_2O]_{max}$ (10^{12} cm^{-3})	F (arbitrary units)	Initial Al absorption (%)	$\bar{v}$ (m s^{-1})	T (K)	$k \pm \sigma_k$ (cm^3 molecule^{-1} s^{-1})
20	18.2	2.1	3.7	84		28	623	4.49±0.42 (−11)[b]
20	18.2	2.1	3.6	69		28	634	4.33±0.43 (−11)
20	18.2	2.0	3.5	62		29	646	4.33±0.40 (−11)
20	34.6	3.7	3.8	52		27	672	4.73±0.47 (−11)
20	34.6	3.7	3.9	51		26	670	4.35±0.40 (−11)
10	34.5	3.9	4.0	70		26	646	4.25±0.46 (−11)
10	16.6	1.9	5.0	17		21	629	4.75±0.65 (−11)
20	44.9	4.4	2.6	47		17	745	5.11±0.40 (−11)
20	44.9	4.2	2.6	57		18	765	5.41±0.45 (−11)
20	44.7	4.2	2.5	42		18	771	5.91±0.46 (−11)
20	34.1	3.9	2.5	46		18	640	4.39±0.45 (−11)
20	34.2	3.8	4.1	72		19	655	4.12±0.36 (−11)
20	20.3	2.2	2.9	102		35	665	3.46±0.37 (−11)
10	47.9	4.5	6.0	49		17	767	5.29±0.39 (−11)
10	47.9	4.5	6.0	52		17	771	5.44±0.45 (−11)
10	28.3	2.6	4.4	68		29	776	5.59±0.50 (−11)
10	54.4	5.0	6.0	51		17	796	6.31±0.54 (−11)
10	52.9	4.4	4.1	68		18	864	7.52±0.75 (−11)
20	48.7	3.8	4.6	47		22	928	6.76±0.53 (−11)
20	48.4	3.8	3.2	29		22	927	7.18±0.48 (−11)
20	45.7	3.6	3.4	49		30	921	6.86±0.62 (−11)
20	49.3	3.9	4.2	38		30	915	7.28±0.54 (−11)
20	19.4	1.5	2.6	51		40	938	6.65±0.75 (−11)
20	23.7	1.8	3.8	57		47	931	6.71±0.80 (−11)
20	22.7	1.8	3.0	40		60	921	6.00±0.62 (−11)
20	22.6	2.1	3.1	34		33	784	5.77±0.57 (−11)
20	22.6	2.1	3.9	36		33	789	4.22±0.35 (−11)
20	25.8	2.4	4.5	31		34	792	5.07±0.66 (−11)
20	31.0	2.8	4.2	26		36	796	5.01±0.51 (−11)
10	20.0	1.9	4.9	43		31	774	4.37±0.55 (−11)
10	20.0	1.9	5.7	34		31	775	3.72±0.44 (−11)
10	34.2	3.2	7.1	21		25	775	3.53±0.45 (−11)
20	21.7	3.0	4.7	37		27	516	2.40±0.26 (−11)
20	28.9	3.5	5.8	44		22	601	2.52±0.25 (−11)
20	17.3	1.9	12.9	57		47	671	3.19±0.38 (−11)
20	17.3	1.9	12.9	56		47	671	2.93±0.32 (−11)
10	17.3	1.9	13.2	62		46	656	3.58±0.41 (−11)
10	16.0	1.8	13.6	68		45	656	3.61±0.59 (−11)
10	20.8	2.2	12.2	63		50	675	4.96±0.47 (−11)
20	16.1	1.4	9.1	24		57	826	4.57±0.49 (−11)
20	16.1	1.4	10.8	48		57	826	4.56±0.48 (−11)
20	14.7	1.3	11.1	46		55	834	6.05±0.66 (−11)
20	14.7	1.3	10.9	32		56	847	5.97±0.76 (−11)
10	14.7	1.3	11.4	34		54	813	4.17±0.57 (−11)
10	14.7	1.3	13.1	39		54	812	4.53±0.74 (−11)
10	14.7	1.2	12.0	56		58	881	5.95±0.87 (−11)
10	14.7	1.2	11.8	47		60	896	6.53±0.74 (−11)
10	14.8	1.2	11.8	44		60	906	4.94±0.66 (−11)
10	14.8	1.2	11.6	28		61	917	6.16±0.78 (−11)
20	16.1	1.3	9.7	52		63	913	7.58±0.82 (−11)
20	16.1	1.3	11.3	69		63	909	7.22±0.75 (−11)
20	19.8	1.6	9.3	35		66	901	7.55±0.68 (−11)
20	19.9	1.6	9.3	26		66	900	7.94±0.70 (−11)
20	26.0	2.5	4.6		9	26	743	3.07±0.24 (−11)
20	39.5	3.8	4.8		25	21	751	4.09±0.40 (−11)
20	39.5	3.8	4.8		22	21	752	3.77±0.28 (−11)
20	16.4	1.7	8.2		21	50	681	3.91±0.41 (−11)
20	16.4	1.7	10.9		25	51	683	3.51±0.35 (−11)
10	16.3	1.9	17.5		24	47	632	3.35±0.37 (−11)
10	17.2	2.2	13.9		16	49	568	3.01±0.34 (−11)
10	17.3	2.2	27.7		31	49	574	2.50±0.30 (−11)
20	17.2	2.1	27.3		28	50	580	2.31±0.24 (−11)
20	17.2	2.1	16.4		21	50	582	2.66±0.31 (−11)
20	16.8	1.3	8.1		15	51	963	5.63±0.58 (−11)
20	20.3	1.5	7.4		14	56	991	6.36±0.55 (−11)
20	20.3	1.5	7.4		15	56	992	6.63±0.59 (−11)
20	19.2	1.4	7.1		26	77	996	7.71±0.70 (−11)
10	19.5	1.5	11.1		15	74	968	6.03±0.65 (−11)
10	19.5	1.5	18.4		20	74	967	5.57±0.55 (−11)
20	32.8	3.8	8.4		16	19	627	3.46±0.29 (−11)
20	37.9	2.7	4.6		15	26	1024	5.62±0.39 (−11)
20	37.9	2.7	4.6		17	26	1029	5.75±0.47 (−11)

[a]The measurements are reported in the sequence in which they were obtained.
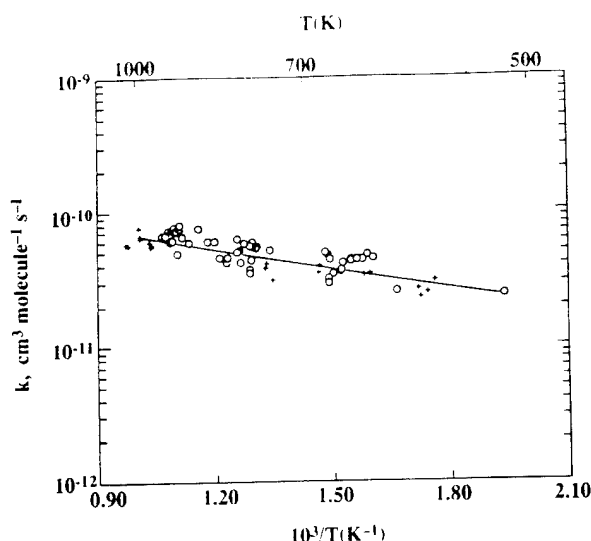[b]Should be read as (4.49±0.42)×10^{-11}.

FIG. 1. Arrhenius plot of the rate coefficient data of $Al+N_2O$ reaction: ○—LIF used as the monitoring technique, +—ARAS used as the monitoring technique.

FIG. 2. Arrhenius plot of all the rate coefficient data for $Al+N_2O$ reaction: ○—Present work, □—Parnis, Mitchell, Kanigan, and Hackett (Ref. 12).

Here H_{lk} represents the interaction–energy integrals and Δ_{lk} the overlap integrals, which are defined as

$$H_{lk}=\int \psi_l^* H \psi_k \, d\tau, \quad \Delta_{lk}=\int \psi_l^* \psi_k \, d\tau. \tag{8}$$

The overlap integrals are approximately equal to zero, $\Delta_{lk}=0$ for $l \ne k$, because each of the three resonating structures are distinctly different from the others. This, along with normalization of Eq. (5), results in $\Delta_{kk}=\int \psi_k^* \psi_k \, d\tau=1$ and

$$\sum_{k=1}^{3} c_k^2=1, \tag{9}$$

where the c_k^2 represent the fraction of character contributed by the respective structures to the activated complex. Similarly, Eq. (7) reduces to the secular equation

$$\begin{vmatrix} H_{11}-E & H_{12} & H_{13} \\ H_{12} & H_{22}-E & H_{23} \\ H_{13} & H_{23} & H_{33}-E \end{vmatrix}=0. \tag{10}$$

H_{11} is the energy of the $Z(s^2p^1)+N_2O(X \, ^1\Sigma^+)$ interaction. The barrier height for this structure $q(s^2p^1)$ equals H_{11}. For each series of homologous reactions q is constant; it is the one quantity to be determined from experiment in these treatments. The second structure results from the attractive covalent interaction of $Z(s^1p^2)$ with N_2O where spin conservation requires N_2O to be in a triplet state, whereas for the s^1 and s^2 metals N_2O is in a singlet state in the second structure. The barrier to form this structure includes the promotion energy PE of $Z(s^2p^1)$ to the $Z(s^1p^2)$ state and the excitation energy of $N_2O(X \, ^1\Sigma^-)$ to the first $N_2O(^3\Sigma^+)$ state, minus the amount by which the interaction is attractive. Following the previous work[1,2] this term is estimated to be $q(s^2p^1)/2$. Thus,
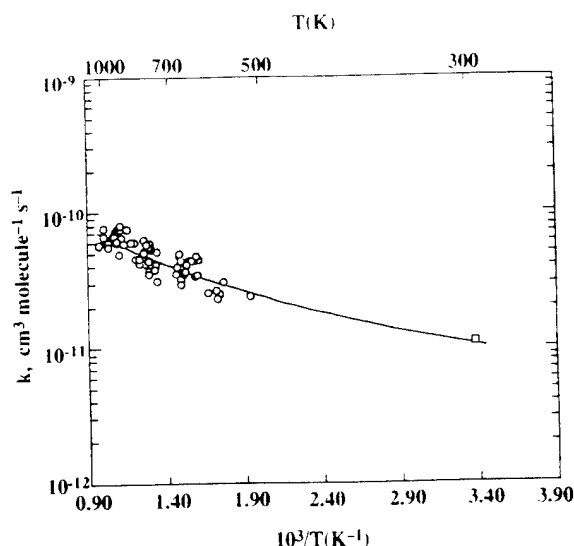
$$H_{22}=PE+q(s^2p^1)/2. \tag{11}$$

The third structure results from the ionic interaction of $Z^+(s^2)+N_2O^-(^2\Pi)$, which involves the attractive Coulomb and the repulsive Born potential between these species. The energy of the barrier resulting from this structure is evaluated as before[2]

$$H_{33}=IP-EA-\frac{e^2}{R_0}\frac{\delta-1}{\delta}. \tag{12}$$

where IP is the ionization potential of Z, EA is the vertical electron affinity of N_2O, e is the elementary charge, R_0 is the sum of the univalent radii of Z^+ and O^-, and δ is the average Born exponent of Z^+ and O^-. Values for these properties and PE along with their sources are given in Table II.

The interaction–energy integrals are estimated to be equal to those for the alkali, alkaline earth, and transition

TABLE II. Physical properties used to calculate energy integrals for group 13 atom reactions with N_2O.

Z	PE (kJ mol^{-1})	IP−EA (kJ mol^{-1})	R_0 (10^{-8} cm)	δ
B	345[a]	1018[b]	2.23[c]	6.0[d]
Al	347	795	2.53	7.0
Ga	455	796	2.58	8.0
In	419	776	2.78	8.5
Tl	541	807	3.05	9.5

[a]The values correspond to the lowest $s-p$ promotion energy obtained from the atomic energy levels in Ref. 24.
[b]Values are obtained from the ionization potentials in Ref. 25 and the vertical electron affinity of N_2O, −217 kJ mol^{-1}, which corresponds to the N_2O negative-ion-state $^2\Pi$ from Ref. 26.
[c]Univalent radii are derived from the effective ionic radii in Ref. 27. The univalent radius of O^- is taken to be 1.76×10^{-8} cm.
[d]The average Born exponent equals $(\delta_1+7)/2$ where the value of 7 is the Born exponent of O^- and the δ_1 value is that of Z^+ taken from Ref. 28.

TABLE III. Comparison of experimental and calculated activation barriers for group 13 atom reactions with N_2O.

Z	c_1^2 (fraction)	c_2^2 (fraction)	c_3^2 (fraction)	A (cm^3 molecule^{-1} s^{-1})	E_{calc} (kJ mol^{-1})	E_{expt} (kJ mol^{-1})	T_{range} (K)	
B	0.85	0.09	0.06	8.4×10^{-12}	21.3	22.1[b]	300	Ref. 20[d]
Al	0.79	0.09	0.12	4.6×10^{-12a}	6.5	6.5	520–1030	This work
Ga	0.81	0.06	0.13	5.9×10^{-12}	14.3	14.4[c]	296	Ref. 21[d]
In	0.81	0.07	0.12	6.3×10^{-12}	13.4			
Tl	0.87	0.04	0.09	7.1×10^{-12}	26.7			

[a]Experimental value of the Al+N_2O reaction; A coefficients for all other reactions are calculated using simple collision theory.
[b]This E_{expt} value is obtained from the 300 K rate coefficient and the A coefficient of column 4.
[c]This E_{expt} value is obtained from the 296 K rate coefficient and the A coefficient of column 4.
[d]Reference from which the experimental data were obtained.

metal atom reactions.[2] Thus H_{12} and H_{13} are equal to β and H_{23} is equal to $\beta/2$, where $\beta = -107.9$ kJ mol^{-1}.

B. Results and discussion

The value of $q(s^2p^1)$ is chosen such that the height of the barrier E of Eq. (10) equals the experimental activation barrier E_{expt} of the Al+N_2O reaction (Sec. II B). From Eq. (3) this yields $q(s^2p^1) = 85.7$ kJ mol^{-1}. Using this value, and Eqs. (7) and (9), the activation barriers E and the fraction of character contributed by each structure can now be calculated for the other boron group atoms. The results of these calculations are given in Table III. Table III also shows the comparison of the calculated activation barriers to the derived experimental activation barriers E_{expt}. For B and Ga, these experimental activation barriers are determined by setting the rate coefficients found in room temperature studies[20,21] equal to $AT^{0.5}\exp(-E/RT)$ in which the A are

taken as the values given by simple collision theory[22] $R_0^2(8\pi k_B/\mu)^{0.5}$. Here, k_B is the Boltzmann constant and μ the reduced mass. The predicted barriers for B and Ga are within 0.7 kJ mol^{-1} of the derived experimental values, using the lowest $s-p$ promotion energies. Using instead the activation barrier from the combined experimental rate coefficient expression, Eq. (4), yields values within 1.2 kJ mol^{-1} of the predicted values. This confirms that varying the value of n has little influence on the accuracy of the predictions. The E_{expt} for In and Tl+N_2O could not be estimated because no experimental data are available for these reactions.

In the present treatment, Sec. III A, we assumed the lowest $s-p$ promotion. The activation barriers were also computed using the lowest $p-s$ promotion energies and the average of the promotion energies $[(s-p)+(p-s)]/2$. In all cases the calculated activation barriers were too high for boron and too low for gallium, indicating that the lowest $p-s$ promotion energies do not correlate with the activation barrier of these atoms.

In Fig. 3 the experimental and calculated activation barriers of the present work are compared to those for the s^1 and s^2 metals atom N_2O reactions.[1,2] As can be seen, good agreement between theory and experiment is obtained for all three groups.[23] Each group shows a linear increase of the activation barrier with the sums of the ionization potentials and $s-p$ promotion energies, which properties determine the energies of the resonating structures, cf. Eqs. (11) and (12). As the magnitude of IP+PE increases, the resonance interaction between these structures and the activated complex weakens, thereby increasing the barrier E.

In summary, the semiempirical treatment, applied to s^1 and s^2 metal atom reactions with N_2O, has been extended to s^2p^1 atoms by modifications to the treatment and use of the experimental barrier from one s^2p^1 atom reaction, namely Al+N_2O. Comparison to the experimental data available in the literature indicates good agreement between theory and experiment.
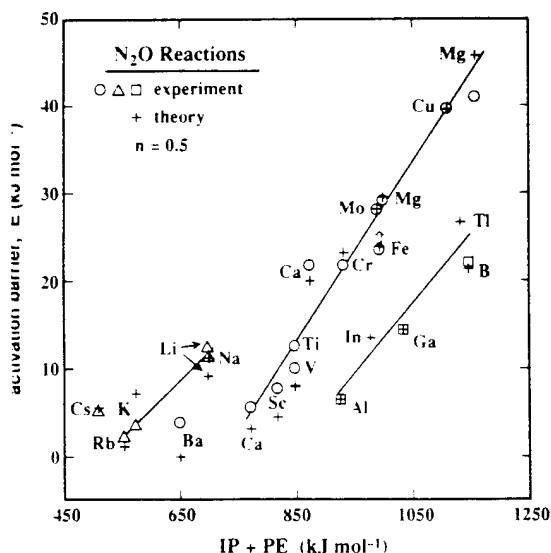

FIG. 3. Plot of the experimental and calculated activation barriers (crosses) of Z−N_2O→ZO+N_2 reactions vs the sums of the $s-p$ promotion energies and ionization potentials of Z. Alkali metal (open triangles), alkaline earth, and transition metal (open circles), and boron group (open squares) atom reactions are distinguished.

[1] P. M. Futerko and A. Fontijn, J. Chem. Phys. **95**, 8065 (1991).

[2] P. M. Futerko and A. Fontijn, J. Chem. Phys. **97**, 3861 (1992).

[3] P. M. Futerko and A. Fontijn, J. Chem. Phys. **98**, 7004 (1993).

[4] The reaction enthalpy is obtained from the enthalpies at 298 K in *JANAF Thermochemical Tables*, 3rd ed. (Dow Chemical Company, Midland, MI); J. Phys. Chem. Ref. Data **14**, Suppl. 1 (1985).

[5] A. Fontijn and P. M. Futerko, *Gas-Phase Metal Reactions*, edited by A. Fontijn, (North-Holland, Amsterdam, 1992). Chap. 6.

[6] A. G. Slavejkov, P. M. Futerko, and A. Fontijn, *23rd Symposium (International) on Combustion* (The Combustion Institute, Pittsburgh, 1990), p. 155.

[7] A. Fontijn and W. Felder, *Reactive Intermediates in the Gas Phase. Generation and Monitoring*, edited by D. W. Setser (Academic, New York, 1979), Chap. 2.

[8] J. A. Irvin and T. I. Quickenden, J. Chem. Ed. **60**, 711 (1983).

[9] A. S. Narayan, P. M. Futerko, and A. Fontijn, J. Phys. Chem. **96**, 290 (1992).

[10] P. M. Futerko, A. G. Slavejkov, and A. Fontijn, J. Phys. Chem. **97**, 11950 (1993).

[11] W. H. Press, B. P. Flannery, S. A. Teukolsky, and W. T. Vetterling, *Numerical Recipes* (Cambridge University, Cambridge, 1986), Chap. 14.

[12] W. E. Wentworth, J. Chem. Ed. **42**, 96, 162 (1965).

[13] A. Fontijn and W. Felder, J. Phys. Chem. **83**, 24 (1979).

[14] J. M. Parnis, S. A. Mitchell, T. S. Kanigan, and P. A. Hackett, J. Phys. Chem. **93**, 8045 (1989).

[15] A. Fontijn, A. S. Blue, A. S Narayan, and P. N. Bajaj, Combust. Sci. Technol. (in press).

[16] J. M. Parnis, S. A. Mitchell, and P. A. Hackett, J. Phys. Chem. **94**, 8152 (1990).

[17] V. N. Smirnov and I. S. Zaslonko (private communication to A. Fontijn, 1992).

[18] L. Lian, S. A. Mitchell, and D. M. Rayner, J. Phys. Chem (in press).

[19] L. Pauling, *The Nature of the Chemical Bond and the Structure of Molecules and Crystals*, 3rd. ed. (Cornell University Press, Ithaca, 1960), pp. 589–591.

[20] T. G. DiGiuseppe and P. Davidovits, J. Chem. Phys. **74**, 3287 (1981).

[21] S. A. Mitchell, P. A. Hackett, D. M. Rayner, and M. Cantin, J. Phys. Chem. **90**, 6148 (1986).

[22] P. W. Atkins, *Physical Chemistry*, 3rd ed. (Freeman, New York, 1986), p. 738.

[23] This figure includes two updated experimental activation barriers from those given in Ref. 1. The Cr activation barrier has recently been determined (Ref. 15) to be 21.7 kJ mol^{-1}. The Ti barrier has been determined as 12.5 kJ mol^{-1} by M. L. Campbell and R. E. McClean, J. Phys. Chem. **97**, 7942 (1993).

[24] C. E. Moore, *Atomic Energy Levels as Derived from the Analyses of Optical Spectra*, Natl. Bur. Stand. (U. S.), Circ. 467, Vol. I (1949) and Vol. II (1952).

[25] C. E. Moore, *Ionization Potentials and Ionization Limits Derived from the Analysis of Optical Spectra*, Natl. Stand. Ref. Data Ser., Natl. Bur. Stand. (U. S.), 34 (1970).

[26] P. J. Chantry, J. Chem. Phys. **51**, 3369 (1969).

[27] R. D. Shannon, Acta Crystallogr. Sec. A **32**, 751 (1976).

[28] L. Pauling, *The Nature of the Chemical Bond and the Structure of Molecules and Crystals*, 3rd ed. (Cornell University Press, Ithaca, NY, 1960), p. 509.

The AlO + O$_2$ Reaction System Over A Wide Temperature Range.

David P. Belyung and Arthur Fontijn*

High-Temperature Reaction Kinetics Laboratory, The Isermann Department of Chemical Engineering, Rensselaer Polytechnic Institute, Troy, NY 12180-3590

—

(Received

The kinetics of the AlO + O$_2$ reaction system has been studied in a high-temperature fast-flow reactor (HTFFR) from 7 to 100 mbar. The relative AlO concentrations were monitored by laser-induced fluorescence at the B$^2\Sigma$–X$^2\Sigma$ and C$^2\Pi$–X$^2\Sigma$ transitions. Below about 1000 K the AlO consumption is pressure-dependent, i.e. leading initially to AlO$_3$, with log k(305-1010 K) = $-25.36 - 1.69$ log (T / K) cm^6 molecule^{-2} s^{-1}, as obtained by weighted linear regression. At higher temperatures the system becomes pressure-independent with AlO$_2$ and O as the likely products. For this process k(1200-1690 K) = 7.7 x 10^{-10} exp (-10008 K / T) cm^3 molecule^{-1} s^{-1}. The accuracy estimates are discussed in the text. The reactions are suggested to proceed through an OAlOO addition complex of similar structure as identified in solid matrices.

INTRODUCTION

Reactions of aluminum species play a role in many high-temperature environments.[1-4] We have studied a large number of Al, AlCl and AlO reactions over wide temperature ranges, by use of the HTFFR (high-temperature fast-flow reactor) technique.[5-8] Two early studies of the AlO + O_2 system, at respectively 1400 and 300 K,[9,10] suggested a temperature-independent rate coefficient, attributed to abstraction

$$AlO + O_2 \rightarrow AlO_2 + O \qquad (1)$$

This interpretation, which indicates no activation energy, is in conflict with some subsequent information, such as the currently recommended endothermicity[11] for reaction (1), $\Delta H° = 96 \pm 40$ kJ mol^{-1}. Recently, we showed that several reactions, which were considered in the literature to proceed by simple abstraction, i.e. AlO + CH_4 and Cr + O_2, to be more complex.[6,12] The earlier AlO + O_2 measurements could have similarly hidden an addition process, as they showed considerable scatter. Since then the HTFFR technique has been much improved.[5,13] A re-investigation of the AlO/O_2 system thus was indicated. We demonstrate here that there are in fact two reactions, reaction (1) which under the present conditions dominates above 1200 K, and an addition reaction

$$AlO + O_2 + Ar \rightarrow AlO_3 + Ar \qquad (2)$$

which dominates below 1000 K.

TECHNIQUE

The HTFFR facility used in this work and the data handling procedures have been previously described.[5,14] Briefly, a vertical mullite (McDanel MV-30) reaction tube (60 cm long, 2.2 cm i.d.), was heated to the desired temperature by resistively heated SiC rods inside an insulated, water-cooled

vacuum housing. AlO was produced by several methods. At room temperature and for a few checks at 547 K, production was achieved by passing Ar with approximately 100 ppm of trimethyl aluminum (TMA) and 1 ppm of O_2 through a microwave discharge. This technique was limited to reaction zone pressures from 7 to 28 mbar and could not be used at higher temperatures. For the other experiments Al vapor was produced by resistively heating an Al-wetted W coil in a flow of Ar carrier gas. A trace of oxidizer, 0.5% N_2O or 5% O_2 in Ar, at $\simeq 4 \times 10^{-3}\%$ of the main Ar flow, was passed through a Pt tube to a location just downstream from the vapor source to rapidly convert Al to AlO.[5,8,15,16] This production technique limited observations at 547 K to $P \leq 32$ mbar due to the condensation of Al and AlO on the reactor walls, but at higher temperatures allowed observations up to 100 mbar, i.e. over the full normal HTFFR pressure range. For the $T \geq 850$ K experiments only the 5% O_2 was used.

Downstream from the AlO production zone, O_2/Ar mixtures at flow rates between 1% and 8% of the main Ar flow rate were introduced through a movable inlet at 10 or 20 cm upstream from the observation windows. There, relative AlO concentrations were measured by laser-induced fluorescence (LIF). A pulsed Lambda Physik EMG 101 excimer / FL 2002 dye laser in combination with a KDP doubling crystal was employed. Just before the reactor window, the laser beam passed through two light baffles,[17] made of metallic concentric brass cones with 4 and 2.5 mm diam. exits respectively, to reduce scattered light in the reactor. Two transitions, $B^2\Sigma–X^2\Sigma$ and $C^2\Pi–X^2\Sigma$ were used. For the former, AlO is pumped on the 464.8 nm (1,0) band and the fluorescence is observed through a 482nm (20 nm full width at half maximum) interference filter, i.e. mainly at the 486.6 nm (1,1) band.[18] The $B^2\Sigma–X^2\Sigma$ system could only be used up to 1200 K because of interference by background radiation from the reactor walls. For measurements above 1200 K and for a comparison near 826 K the weaker LIF from the $C^2\Pi–X^2\Sigma$ (0,0) transition at 302.2 nm[18] was used in combination with a 301nm (11 nm full width at half maximum) interference filter. The fluorescence was detected by an EMI 9813QA photomultiplier tube, connected to a Data Precision Analogic 6000/620 100 MHz transient digitizer.

The gases used were Ar (99.998%) from the liquid (Linde), O_2 (99.6%) from Linde, O_2 (99.98%) from Matheson and 5% O_2 (99.99%) in Ar (99.995%) from Scott. The rate coefficients obtained with these O_2 sources were indistinguishable. The 5% O_2 and 0.5% O_2 (99.99%) in Ar (99.995%) from Matheson, 0.5% N_2O (99.99%) in Ar (99.995%) from Matheson, and TMA (98%) from the liquid TMA (Johnson Matthey) were used for AlO production.

Measurements were made under pseudo-first-order conditions, $[AlO] << [O_2]$, in the stationary inlet mode.[19] Rate coefficients k_i, in second order units, for a given temperature, pressure, and average velocity were obtained by using five O_2 concentrations providing variation by a factor of about 5. k_i and σ_{ki} were calculated by applying a weighted linear regression[20] to plots of ln $[AlO]_{relative}$ vs. $[O_2]$. These yielded straight lines with slopes equal to $-k_i t$, where t is reaction time.

RESULTS

The measurements are divided into two sets. In one, the measurements were made at varying pressures at temperatures near 305, 547, 826, or 1010 K to evaluate the temperature dependence of the pressure-dependent reaction. In the other, T > 1200 K, where pressure-independent rate coefficients were obtained, the temperature was randomly varied up to 1690 K.

305-1010 K MEASUREMENTS

The k_i measurements obtained in this range, and the conditions under which they were obtained, are assembled in Table I and show a pressure dependence. At each temperature, to determine if the data were dependent on parameters other than [M], plots of the residuals $[k_i - k(M)]/k(M)$ versus an individual parameter were examined. Here, k(M) is the fitting expression for that particular temperature, eqs. 3, 4, or 5 below. These plots showed that the third-order rate coefficients are independent of initial fluorescence intensity F (a measure of initial [AlO]), average gas velocity $\bar{v}$, and observed reaction zone length.

There were slight variations in temperature for each group of measurements. The standard deviation of these were computed[21] for each data set and combined, by a propagation of error method,[22] with an estimated maximum $\sigma_T = \pm 2\%\ T$ for systematic errors. The resulting standard deviations for each average temperature are shown in Table II.

The 305 K measurements are near the high-pressure limit as evidenced by the leveling off of the k_i vs. [M] plot, Fig. 1. These data were fitted using Marquardt's method,[23] with a fall-off expression from Troe:[24]

$$\log k(M) = \log\left(\frac{k_{2,0}[M]}{1 + k_{2,0}[M]/k_{2,\infty}}\right) + \frac{\log F_c}{1 + [\log(k_{2,0}[M]/k_{2,\infty})]^2} \tag{3}$$

Here $k_{2,0}$ is the third-order rate coefficient for reaction (2), $k_{2,\infty}$ is the high-pressure second-order rate coefficient, and F_c is a broadening factor. Eq. (3) yields $k_{2,0} = 5.1 \times 10^{-30}\ cm^6\ molecule^{-2}\ s^{-1}$, $k_{2,\infty} = 1.1 \times 10^{-12}\ cm^3\ molecule^{-1}\ s^{-1}$, and $F_c = 0.752$. To estimate $\sigma_{k_{2,0}}$ a nonlinear fit[23] of the data was made with only the first term of eq. 3. From this the elements of the covariance matrix were calculated[25] and $\sigma_{k_{2,0}}$ was found to be 0.34 $k_{2,0}$, Table II.

At 547 and 826 K linear k_i vs. [M] plots were obtained, Figs 2 and 3. The k_i were fitted with an expression purely proportional to pressure,

$$k(M) = k_{2,0}\ [M] \tag{4}$$

From the fits[23] the covariance matrices were calculated[25] and the $\sigma_{k_{2,0}}$ obtained, Table II. The 547 K measurements allowed comparison of the various AlO production techniques. As shown in Fig. 2 no influence of the method used is evident. At 826 K higher pressures could be studied than at 547 K, due

to the improved efficiency of the production technique. The larger [AlO] at this temperature also made it convenient to compare the LIF results from the $B^2\Sigma-X^2\Sigma$ transition to those of the $C^2\Pi-X^2\Sigma$ transition. This is done in Fig. 3, which shows the independence of the transition used.

The data at 1010 K display linear behavior with an intercept indicative of a pressure-independent channel, Fig. 4. These data were fitted with a simple linear expression

$$k(M) = k_1 + k_{2,0} [M] \tag{5}$$

using a linear least-squares algorithm.[20] In this eq. k_1 is the second-order rate coefficient. This algorithm also yielded $\sigma_{k_{2,0}}$ and σ_{k_1}.

The temperature dependence of the third-order rate coefficients is shown in Fig. 5. The rate coefficients decrease with increasing temperature, typical behavior for an association reaction. The data were fitted with a $\log k_{2,0} = \log A_{2,0} + n \log(T/K)$ expression using a linear least squares fit[20] with the transformation $\sigma_T = 2.303\, T\sigma_{\log T}$ which yields

$$\log k_{2,0}\,(305-1010\ \text{K}) = -25.36 - 1.69\ \log\,(T/K)\ \text{cm}^6\ \text{molecule}^{-2}\ \text{s}^{-1}. \tag{6}$$

The variance and covariance matrix elements[25] are $\sigma^2_{\log A2,0} = 1.45$, $\sigma_{\log A2,0\,n} = -0.508$, and $\sigma^2_n = 0.178$. Using these variances and covariance the $2\sigma_{k_{2,0}}$ precision limits are calculated to vary from $\pm76\%$ at 305 K, decreasing to a minimum of $\pm22\%$ at 700 K, and increasing again to $\pm37\%$ at 1010 K. Using a $\pm10\%$ uncertainty in the reactor flow profile,[19,26] along with a conservative $\pm20\%$ for possible systematic errors, yields confidence intervals varying from $\pm79\%$ to $\pm31\%$.

1200 - 1690 K MEASUREMENTS

The 1200 K to 1690 K data are assembled in Table III. Residual plots showed no dependence on pressure, initial fluorescence intensity F, average gas velocity $\bar{v}$, and reaction zone length. As a precaution, in determining the parameters of the $k_1(T)$ expression below, only measurements at low enough pressures to insure less than 20% contribution from the extrapolated third-order reaction eq. 6 were used. These measurements are shown in Fig. 6 and show a strong positive temperature dependence with no significant curvature. Applying a linear regression fit[23] to

$$k_1(T) = A\exp(-E\ K/\ T)\ \text{yields}$$

$$k_1(1200 - 1690\ K) = 7.7 \times 10^{-10} \exp(-10008\ K\ /\ T)\ cm^3\ molecule^{-1}\ s^{-1}. \qquad (7)$$

A nearly identical expression was obtained by (i) fitting all the data and (ii) by subtracting the termolecular component from all the data and fitting the results. In both cases the activation energy was within 6% of the value shown in eq. 7. Equation 7 has variances and covariance[25] of $\sigma_A^2 = 0.182\ A^2$, $\sigma_{AE} = 2.54 \times 10^2\ A$, and $\sigma_E^2 = 3.59 \times 10^5$, which yields precision limits varying from $\pm 9\%$ to $\pm 17\%$ depending upon temperature. The resulting estimated accuracy limit is $\pm 26\%$ when the same systematic errors as above are considered. The k_1 from the 1010 K measurements (above) was not used as the associated uncertainly was considered to be too large.

DISCUSSION

The results of the negative temperature dependence of reaction (2) and the positive dependence of reaction (1) is that the AlO consumption rate coefficients, calculated on a second order basis, pass through a minimum which occurs at around 800 - 1000 K at the pressures used. Comparison of the k_1 data at 300 K (Table I) to those at 1400 K (Table III) shows little difference. Thus the temperature independence indicated for reaction (1) in the previous work[10] was based on a coincidence. The actual measurements from the present and previous[9,10] work are in reasonable agreement as can be seen in

Figs. 5 and 6. For the comparison in Fig. 5 the individual second-order rate coefficients from ref. 10 were divided by the pressure and averaged. There now is also no conflict between the endothermicity for reaction (1) of 96 ± 40 kJ mol^{-1} and the activation energy of 83 ± 10 kJ mol^{-1} obtained from eq. 7.

The type of results obtained here can be fitted to a general scheme of the kind:

$$AlO + O_2 \rightleftharpoons AlO_3^* \xrightarrow{M} AlO_3$$
$$\downarrow$$
$$AlO_2 + O$$

(8)
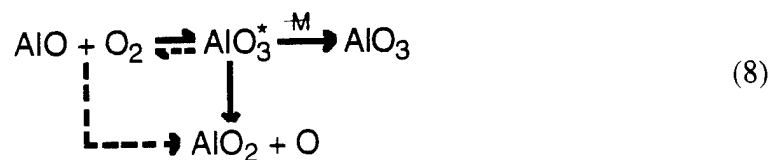
, where the dotted lines indicate the less likely channels. The path leading to AlO_3 appears a straight forward termolecular mechanism. The chemically activated intermediate AlO_3^* is also likely to be the precursor of the $AlO_2 + O$ reaction products of the high-temperature second-order process, as the pre-exponential of the $k_1(T)$ expression, 7.7×10^{-10} cm^3 molecule^{-1} s^{-1}, appears rather too large for a diatomic radical - diatomic radical direct abstraction reaction.[27] Certainty with regard to the mechanism of the relative importance of direct and indirect bimolecular processes is, however, generally difficult to establish.[28]

The large pre-exponential of $k_1(T)$ also suggests that the AlO_3^* complex once formed will not significantly re-dissociate to the reactants AlO and O_2. This in contrast to the exothermic iso-electronic $BO + O_2$ reaction system for which no pressure dependence and a negative activation energy was found.[29] This suggests[29,30] a reaction involving an activated complex which is not significantly pressure stabilized. The mechanism for that reaction can be summarized by

$$BO + O_2 \rightleftharpoons BO_3^* \longrightarrow BO_2 + O$$

(9)
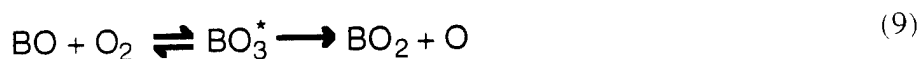
There have apparently not been any direct gas-phase observations of AlO_3 species. However, the $Al + O_2$ and $Al + O_3$ reactions when carried out in solid matrices have been shown to yield a product[31,32] $OAlO_2$ that is also the likely product for AlO, O_2 addition. The matrix work further suggested that a major isomer of this structure is a branched ring compound $O\text{-}Al\overset{O}{\underset{O}{\diamond}}$. This is the same configuration as an SCF/CI calculation has indicated for the BO_3^* intermediate of eq. 9.[29] AlO has been observed to form gaseous addition complexes with other molecules. Thus, chemiluminescense observations in the visible on the $Al + CO_2 + O_3$ reaction system have given evidence for the formation of $OAlCO_2$.[33] Also, room temperature kinetic measurements have found that the reactions of AlO with CO_2 and C_2H_4 have pressure-dependent pseudo-second-order rate coefficients.[34] These CO_2 and C_2H_4 observations show an interesting difference with the present $AlO + O_2$ findings, in that they display a non-zero intercept, indicative of a contribution of second-order process at room temperature. That work was done at bath gas N_2O pressures of 270 to 800 mbar. Since in the present work at pressures an order of magnitude lower, with a less efficient bath gas, Ar, the second-order component did not become evident till about 1000 K this may suggest a rather stable $OAlO_2$ adduct.

ACKNOWLEDGMENTS

REFERENCES

1 Park, C. *Atmos. Environ.* **1976**, *10*, 693.

2 Ogle, R. A.; Beddow, J. K.; Chen, L. D.; Butler, P. B. *Combust. Sci. Technol.* **1988**, *61*, 75.

3 Neville, M.; Quann, R. J.; Haynes, B. S.; Sarofim, A. F. *18th Symposium (International) on Combustion*; The Combustion Institute, Pittsburgh, 1981, p. 1267.

4 Cernichard, J.; Guelin, M. *Astron. Astrophys.* **1987**, *183*, L10.

5 Fontijn, A.; Futerko, P. M. in: *Gas-Phase Metal Reactions*; A. Fontijn, Ed.; North-Holland: Amsterdam, 1992, Chapter 6.

6 Belyung, D. P.; Fontijn, A.; Marshall, P. *J. Phys. Chem.* **1993**, *97*, 3456.

7 Futerko, P. M.; Fontijn, A. *J. Phys. Chem.* **1993**, *97*, 7222.

8 Belyung, D. P.; Futerko, P. M.; Fontijn, A. *J. Chem. Phys.* **1995**, *102*, 155.

9 Felder, W.; Fontijn, A. *J. Chem. Phys.* **1976**, *64*, 1977.

10 Fontijn, A.; Felder, W.; Houghton, J. J. *16th Symposium (International) on Combustion*; The Combustion Institute, Pittsburgh, 1977, p. 871.

11 Chase, M. W.; Jr., Davies, C. A.; Downey, Jr.; Frurip, D. J.; McDonald, R. A.; Syverup, A.N.; *JANAF Thermochemical Tables*, *J. Phys. Chem. Ref. Data* **1985**, *14*, supplement No.1.

12 Narayan, A. S.; Slavejkov, A. G.; Fontijn, A. *24th Symposium (International) on Combustion*; The Combustion Institute, Pittsburgh, 1992, p. 727.

13 Slavejkov, A. G.; Futerko, P. M.; Fontijn, A. *23rd Symposium (International) on Combustion*; The Combustion Institute, Pittsburgh, 1990, p. 155.

14 Slavejkov, A. G.; Stanton. C. T.; Fontijn, A. *J. Phys. Chem.* **1990**, *94*, 3347 and references therein.

15 Garland, N. L. in: *Gas-Phase Metal Reactions*; A. Fontijn, Ed.; North-Holland: Amsterdam, 1992, Chapter 5.

16 Garland, N. L.; Nelson, H. H. *Chem. Phys. Lett.* **1992**, *191*, 269.

17 Bowen, T. S.; Anderson, W. R. *Memorandum report BRL-MR-3935*, U. S. Army Laboratory Command Ballistic Research Laboratory, Aberdeen proving ground, Maryland, August 1991.

18 Pearse, R. W. B.; Gaydon, A. G. *The Identification of Molecular Spectra*; Chapman and Hall: London, 1976; p 41.

19 Fontijn, A.; Felder, W. In *Reactive Intermediates in the Gas Phase. Generation and Monitoring*, Setser D. W., Ed.; Academic Press: New York, 1979; Chapter 2.

20 Irvin J. A.; Quickenden I. T. *J. Chem. Educ.* **1983**, *60*, 711.

21. Bevington, P. R. *Data Reduction and Error Analysis for the Physical Sciences*; McGraw Hill: New York, 1969; Chapter 2.

22 Bevington, P. R.*Data Reduction and Error Analysis for the Physical Sciences*; McGraw Hill: New York, 1969; Chapter 4.

23. Press, W. H.; Flannery, B. P.; Teukolsky, S. A.; Vetterling, W. T. *Numerical Recipes*; Cambridge University: Cambridge, 1986; Chapter 14.

24 Troe, J. *J. Phys. Chem.* **1979**, *83*, 114.

25 Wentworth,W. E. *J. Chem Educ.* **1965**, *42*, 96, 162.

26 Fontijn, A.; Felder, W. *J. Phys. Chem.* **1979**, *83*, 24.

27 Howard, M. J.; Smith, I. W. M. *Prog. Reaction Kinetics* **1983**, *12*, 55.

28 Troe, J. *J. Chem. Soc. Faraday Trans.* **1994**, *90*, 2303.

29 Stanton, C. T.; Garland, N. L.; Nelson, H. H. *J. Phys. Chem.* **1991**, *95*, 8741.

30 Golden, D. M. *J. Phys. Chem.* **1979**, *83*, 108.

31 Andrews, L.; Borkholder, T. R.; Yustein, J. T. *J. Phys. Chem.* **1992**, *96*, 10182.

32 Sonchik, S. M.; Andrews, L.; Carlson, K. D. *J. Phys. Chem.* **1983**, *87*, 2004.

33 McQuaid, M.; Woodward, J. R.; Gole, J. L. *J. Phys. Chem.* **1988**, *92*, 252.

34 Parnis, J. M.; Mitchell, S. A.; Kanigan, T. S.; Hackett, P. A. *J. Phys. Chem.* **1989**, *93*, 8045.

TABLE I

Summary of Rate Coefficient Measurements on the AlO + O_2 reaction taken below 1050 K

Reaction zone length (cm)	P (mbar)	[M] (10^{17} cm^{-3})	[O_2] max (10^{15} cm^{-3})	F (arbitary units)	$\bar{v}$ (m s^{-1})	T (K)	$k_i \pm \sigma_{k_i}$ (cm^3 molecule^{-1} s^{-1})
20	19.7	4.75	0.2g	42	18	301	6.28 ± 1.21 (-13)[a,b]
10	19.9	4.75	0.6g	66	18	301	5.08 ± 0.98 (-13)[b]
10	10.5	2.52	1.1g	21	30	303	4.05 ± 1.17 (-13)[b]
20	10.5	2.52	0.7g	27	30	303	3.78 ± 1.09 (-13)[b]
10	10.4	2.49	0.7g	14	18	303	5.69 ± 1.69 (-13)[b]
10	7.1	1.68	1.0g	27	34	304	4.48 ± 1.80 (-13)[b]
20	7.1	1.68	0.7g	30	28	304	4.08 ± 1.64 (-13)[b]
20	6.8	1.62	0.6g	23	21	305	2.84 ± 1.18 (-13)[b]
10	6.9	1.65	1.4g	34	36	305	3.58 ± 1.46 (-13)[b]
10	27.6	6.56	0.2g	25	15	305	7.04 ± 1.20 (-13)[b]
20	27.9	6.60	0.2g	23	15	306	6.80 ± 1.16 (-13)[b]
20	6.9	1.64	0.7g	34	36	306	4.22 ± 1.72 (-13)[b]
20	14.7	3.47	0.4h	51	21	306	5.81 ± 1.32 (-13)[b]
20	14.7	3.47	0.3g	47	21	306	4.92 ± 1.12 (-13)[b]
10	27.9	6.58	0.3h	24	15	307	5.91 ± 1.00 (-13)[b]
20	27.9	6.58	0.2h	28	15	307	6.93 ± 1.18 (-13)[b]
10	14.7	3.46	0.6h	57	21	307	5.80 ± 1.32 (-13)[b]
10	14.7	3.46	0.6g	60	21	307	5.30 ± 1.22 (-13)[b]

Table I, continued

20	26.8	3.71	0.9[g]	22	21	523	3.85 ± 0.68 (-13)[d]
10	32.4	4.45	1.4[g]	26	23	527	3.94 ± 0.65 (-13)[d]
10	13.9	1.89	2.5[g]	106	25	532	1.47 ± 0.35 (-13)[c]
10	25.7	3.50	2.6[g]	74	22	533	2.55 ± 0.45 (-13)[d]
10	20.9	2.77	2.1[g]	19	36	537	2.94 ± 0.57 (-13)[c]
10	26.7	3.60	2.0[g]	29	22	537	3.95 ± 0.70 (-13)[c]
10	20.9	2.77	2.1[g]	27	36	547	1.99 ± 0.38 (-13)[c]
10	32.4	4.27	0.8[g]	14	24	550	3.67 ± 0.62 (-13)[c]
20	20.5	2.69	1.0[g]	25	39	553	3.05 ± 0.58 (-13)[c]
20	14.1	1.85	1.2[g]	34	26	553	2.13 ± 0.50 (-13)[c]
20	7.2	0.94	1.9[g]	28	61	558	1.48 ± 0.59 (-13)[c]
20	20.9	2.69	1.0[g]	22	37	563	2.62 ± 0.50 (-13)[c]
20	7.5	0.95	2.3[g]	74	59	569	1.60 ± 0.61 (-13)[b]
10	15.5	1.96	2.4[g]	25	32	573	1.99 ± 0.44 (-13)[b]
10	21.6	1.98	6.9[g]	115	26	789	1.00 ± 0.19 (-13)[c]
20	21.5	1.93	3.4[g]	52	27	805	1.39 ± 0.26 (-13)[c]
10	42.1	3.78	1.2[i]	59	25	808	1.97 ± 0.30 (-13)[e]
10	58.9	5.22	0.7[i]	35	14	818	3.36 ± 0.50 (-13)[e]
20	42.0	3.72	1.2[i]	51	26	819	2.67 ± 0.41 (-13)[e]
20	41.5	3.66	0.8[i]	79	25	820	2.57 ± 0.39 (-13)[e]
10	79.2	6.99	0.8[i]	38	13	821	3.80 ± 0.55 (-13)[f]
20	80.2	7.07	0.8[i]	20	17	823	4.15 ± 0.61 (-13)[c]
20	17.9	1.56	3.1[g]	39	59	832	1.64 ± 0.33 (-13)[e]
10	27.3	2.37	8.0[g]	51	29	837	1.05 ± 0.18 (-13)[d]
20	102.6	8.88	0.5[i]	16	14	838	4.05 ± 0.61 (-13)[c]

Table I, continued

20	19.7	1.70	4.5g	54	62	841	1.76 ± 0.34 (-13)[f]
20	11.1	0.95	3.4g	45	66	843	8.51 ± 2.35 (-14)[d]
20	27.1	2.32	5.0g	26	31	844	1.03 ± 0.18 (-13)[e]
20	58.3	5.00	0.4g	27	15	845	3.19 ± 0.46 (-13)[e]
20	36.4	2.69	2.5g	40	23	982	1.30 ± 0.21 (-13)[e]
20	54.8	4.03	1.6h	39	30	986	2.46 ± 0.37 (-13)[e]
10	54.5	3.99	3.2h	42	30	989	1.79 ± 0.26 (-13)[e]
20	54.4	3.98	1.6g	40	30	990	2.06 ± 0.30 (-13)[e]
20	40.1	2.93	1.7h	33	27	993	1.69 ± 0.26 (-13)[e]
10	67.2	4.90	2.4g	66	23	994	2.26 ± 0.33 (-13)[e]
10	36.3	2.64	6.8g	30	42	996	1.59 ± 0.25 (-13)[e]
10	55.3	4.01	3.2g	47	30	999	2.15 ± 0.32 (-13)[e]
20	66.7	4.82	1.6g	39	23	1001	2.25 ± 0.33 (-13)[e]
10	37.2	2.69	2.0g	33	25	1001	1.42 ± 0.22 (-13)[e]
10	20.7	1.49	7.6g	44	69	1002	1.08 ± 0.20 (-13)[e]
10	36.3	2.62	8.4g	38	42	1003	1.35 ± 0.22 (-13)[e]
10	72.6	5.25	1.7g	33	18	1003	1.81 ± 0.26 (-13)[e]
10	40.5	2.92	4.1h	28	28	1006	1.13 ± 0.18 (-13)[e]
20	13.9	1.00	3.7g	55	114	1006	1.15 ± 0.27 (-13)[e]
20	36.1	2.60	3.4g	26	43	1007	1.76 ± 0.28 (-13)[e]
10	50.7	3.64	3.5g	36	19	1008	1.11 ± 0.17 (-13)[e]
20	36.3	2.60	3.4g	29	42	1009	1.66 ± 0.26 (-13)[e]
10	54.4	3.90	2.4g	48	23	1010	1.89 ± 0.28 (-13)[e]
20	20.5	1.47	4.1g	54	70	1013	1.04 ± 0.20 (-13)[e]
20	37.2	2.64	1.0g	24	26	1019	1.88 ± 0.29 (-13)[e]

Table I, end

20	72.5	5.15	0.5g	21	18	1021	2.66 ± 0.39 (−13)c
20	81.7	5.80	1.6g	25	23	1021	2.33 ± 0.34 (−13)c
10	22.5	1.60	8.2g	35	43	1023	1.04 ± 0.19 (−13)c
10	22.5	1.59	6.6g	25	43	1025	8.68 ± 1.58 (−14)c
20	11.3	0.80	5.1h	63	104	1029	9.73 ± 2.65 (−14)c
20	11.3	0.80	5.1g	58	104	1031	1.00 ± 0.27 (−13)c
20	22.5	1.57	4.1g	31	44	1038	8.36 ± 1.51 (−14)c
20	22.3	1.55	4.1g	38	44	1043	1.05 ± 0.19 (−13)c
20	50.9	3.54	0.9g	24	20	1043	1.62 ± 0.24 (−13)c

a) Should be read as $(6.28 \pm 1.21) \times 10^{-13}$.

b) AlO produced by microwave-discharge of TMA with subsequent reaction with 0.5% O_2 and LIF using the $B^2\Sigma - X^2\Sigma$ transition.

c) AlO produced by vaporization of Al with subsequent reaction with 5% O_2 and LIF using the $B^2\Sigma - X^2\Sigma$ transition.

d) AlO produced by vaporization of Al with subsequent reaction with 0.5% N_2O and LIF using the $B^2\Sigma - X^2\Sigma$ transition.

e) AlO produced by vaporization of Al with subsequent reaction with 5% O_2 and LIF using the $C^2\Pi - X^2\Sigma$ transition.

f) AlO produced by vaporization of Al with subsequent reaction with 0.5% N_2O and LIF using the $C^2\Pi - X^2\Sigma$ transition.

g) Used UHP (99.98%) O_2.

h) Used Zero grade (99.6%) O_2.

i) Used 5% O_2 in Ar.

TABLE II

Summary of Third-Order Rate Coefficients for the $AlO/O_2/Ar$ Reaction System.

$\overline{T} \pm \sigma_T$ (K)	N^a	P range (mbar)	[M] range (10^{17} cm^{-3})	$k_{2,0} \pm \sigma_{k_{2,0}}$ (cm^6 molecule^{-2} s^{-1})
305 ± 6	18	6.8 - 27.9	1.6 - 6.6	$5.1 \pm 1.7(-30)^b$
547 ± 19	14	7.2 - 32.4	0.9 - 4.5	$9.1 \pm 0.5(-31)$
826 ± 24	15	11.1 - 102.6	1.0 - 8.9	$5.7 \pm 0.3(-31)$
1010 ± 26	30	11.3 - 81.7	0.8 - 5.8	$3.0 \pm 0.4(-31)$

a) N is the number of k_i measurements at this temperature.

b) Should be read as $(5.1 \pm 1.7) \times 10^{-30}$ cm^6 molecule^{-2} s^{-1}

TABLE III
Summary of Rate Coefficient Measurements on the AlO + O_2 reaction taken above 1200 K

Reaction zone length (cm)	P (mbar)	|M| (10^{17} cm^{-3})	|O_2|max (10^{15} cm^{-3})	F (arbitary units)	$\bar{v}$ (m s^{-1})	T (K)	$k_i \pm \sigma_{k_i}$ (cm^3 molecule^{-1} s^{-1})	
20	14.7	0.89	2.6	24	89	1198	1.47 ± 0.34	(-13)[a]
20	20.1	1.21	3.0	29	80	1202	1.90 ± 0.37	(-13)
20	16.1	0.97	2.5	24	95	1209	1.71 ± 0.37	(-13)
20	40.7	2.38	1.2	31	42	1239	2.28 ± 0.35	(-13)
20	20.1	1.17	3.1	22	75	1242	1.80 ± 0.35	(-13)
20	72.6	4.22	0.9b	18	30	1246	2.85 ± 0.41	(-13)
20	23.2	1.34	1.1	23	58	1253	2.03 ± 0.37	(-13)
20	66.4	3.84	0.7b	32	27	1253	2.18 ± 0.32	(-13)
10	66.1	3.81	0.4b	18	27	1258	3.50 ± 0.52	(-13)
20	54.1	3.08	0.7	25	26	1273	2.49 ± 0.37	(-13)
20	54.4	3.10	0.7	24	26	1273	2.86 ± 0.42	(-13)
20	87.0	4.94	1.4	72	14	1278	2.57 ± 0.38	(-13)
10	47.2	2.67	1.0	33	26	1279	3.72 ± 0.55	(-13)
10	67.3	3.81	1.5	24	21	1281	2.33 ± 0.34	(-13)
10	42.1	2.38	2.0	29	25	1284	2.12 ± 0.32	(-13)
10	21.9	1.23	1.4	115	52	1286	5.04 ± 0.92	(-13)
10	55.9	3.13	2.7	29	23	1291	1.99 ± 0.29	(-13)
20	18.1	1.02	1.5	136	64	1294	2.83 ± 0.57	(-13)
10	31.5	1.76	0.6	36	40	1296	5.03 ± 0.81	(-13)

Table III, end

20	47.1	2.62	0.5	50	26	1301	4.63 ± 0.68	(-13)
10	72.5	4.03	2.2	27	29	1303	3.38 ± 0.49	(-13)
10	41.7	2.31	1.9	36	33	1307	1.83 ± 0.28	(-13)
20	31.5	1.74	0.6	27	40	1308	4.52 ± 0.74	(-13)
20	21.7	1.18	1.0	22	47	1333	6.65 ± 1.24	(-13)
10	40.5	2.14	1.0	22	24	1372	3.45 ± 0.53	(-13)
20	21.6	1.11	0.9	15	45	1414	4.70 ± 0.89	(-13)
10	53.1	2.72	0.4	24	29	1414	1.02 ± 0.16	(-12)
20	23.5	1.18	0.4	18	57	1446	6.44 ± 1.17	(-13)
20	28.4	1.41	0.3	21	42	1461	1.58 ± 0.27	(-12)
20	15.7	0.77	0.2	18	57	1479	1.32 ± 0.29	(-12)
10	31.6	1.51	0.6	16	28	1516	8.56 ± 1.42	(-13)
20	31.5	1.50	0.2	12	28	1517	1.30 ± 0.22	(-12)
20	14.9	0.70	0.4	26	77	1537	1.08 ± 0.25	(-12)
20	54.8	2.56	0.1	42	35	1548	1.96 ± 0.29	(-12)
20	13.9	0.63	0.3	26	71	1588	2.36 ± 0.56	(-12)
20	14.9	0.68	1.4	27	66	1588	9.22 ± 2.11	(-13)
10	53.2	2.41	0.5	20	29	1596	9.58 ± 1.45	(-13)
20	39.1	1.77	0.2	35	33	1597	1.17 ± 0.18	(-12)
10	31.5	1.38	0.1	37	31	1648	2.63 ± 0.43	(-12)
20	31.5	1.35	0.1	20	31	1689	2.51 ± 0.41	(-12)

a) Should be read as $(1.47 \pm 0.34) \times 10^{-13}$.
b) Used 5% O_2 in Ar.; otherwise used UHP (99.98%) O_2.

FIGURE CAPTIONS

FIG. 1. Plot of k_i vs. [M] for the AlO/O_2/Ar reaction system at $\overline{T}$ = 305 K

(O) individual rate coefficients

(–) Troe fit of measurements, eq. 3

FIG. 2. Plot of k_i vs. [M] for the AlO/O_2/Ar reaction system at $\overline{T}$ = 547 K

(O) vaporization of Al and 5% O_2 used to produce AlO

(+) vaporization of Al and 0.5% N_2O used to produce AlO

(□) microwave discharge of TMA and 0.5% O_2 used to produce AlO

(–) Proportional fit of measurements, eq. 4

FIG. 3. Plot of k_i vs. [M] for the AlO/O_2/Ar reaction system at $\overline{T}$ = 826 K

(O) Measurements taken using the $C^2\Pi$–$X^2\Sigma$ transition with LIF

(□) Measurements taken using the $B^2\Sigma$–$X^2\Sigma$ transition with LIF

(–) Proportional fit of measurements, eq. 4

FIG. 4. Plot of k_i vs. [M] for the AlO/O_2/Ar reaction system at $\overline{T}$ = 1010 K

(O) Measurements taken using O_2 (99.98%) from Matheson

(□) Measurements taken using O_2 (99.6%) from Linde

(–) Linear fit of measurements eq. 5

FIG. 5. Plot of the third-order rate coefficient data of the AlO + O_2 reaction. Uncertainties shown are

$\pm 2\sigma$ precision.

(Δ) Current study

(–) Best fit to current study, eq. 6

(●) Calculated from ref. 10

FIG. 6. Arrhenius plot of the second-order rate coefficient data of the AlO + O_2 reaction.

($\triangle$) Individual rate coefficients
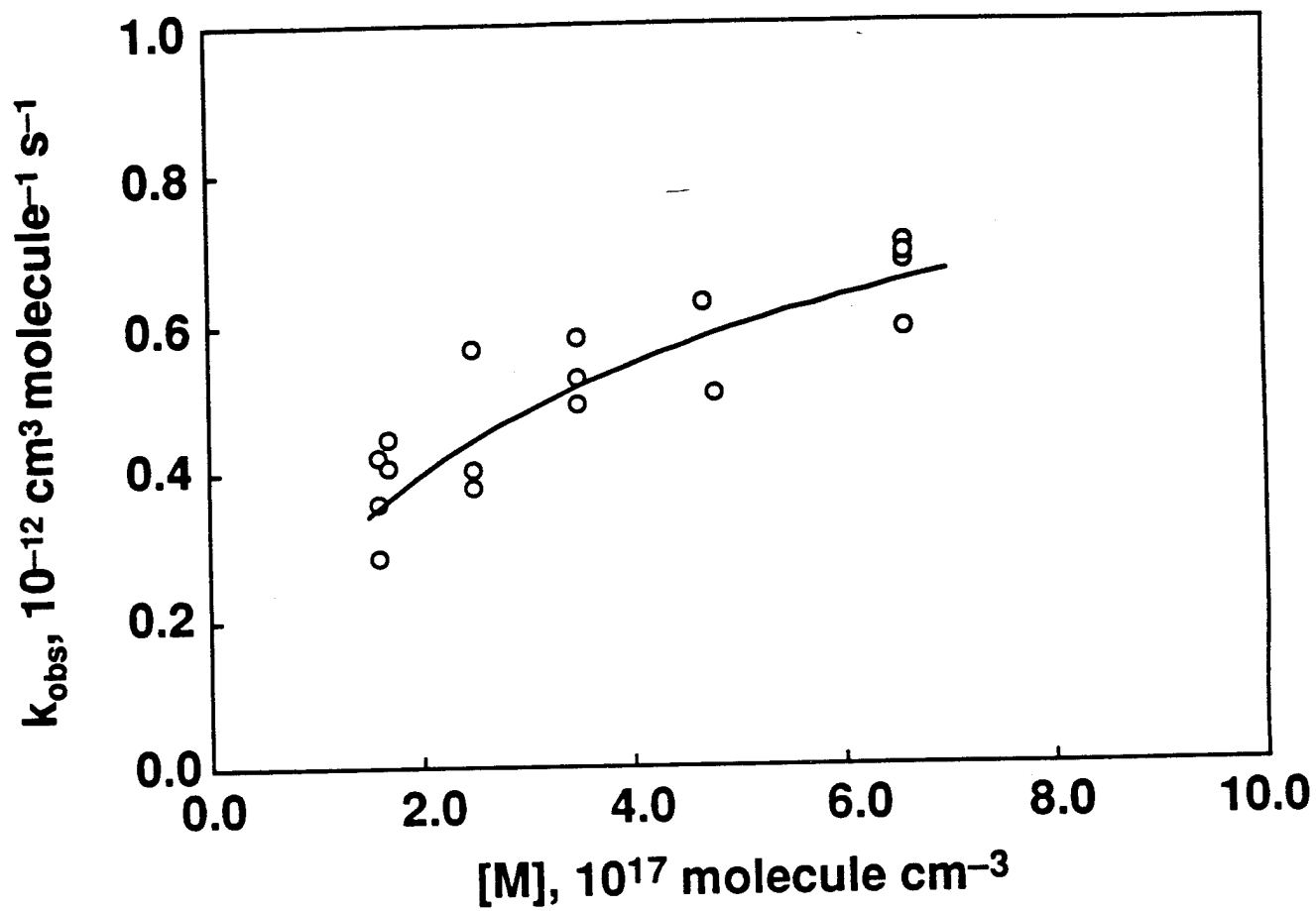
($-$) Arrhenius fit to data, eq. 7

($\bullet$) Recommendation from ref. 9

Figure 1
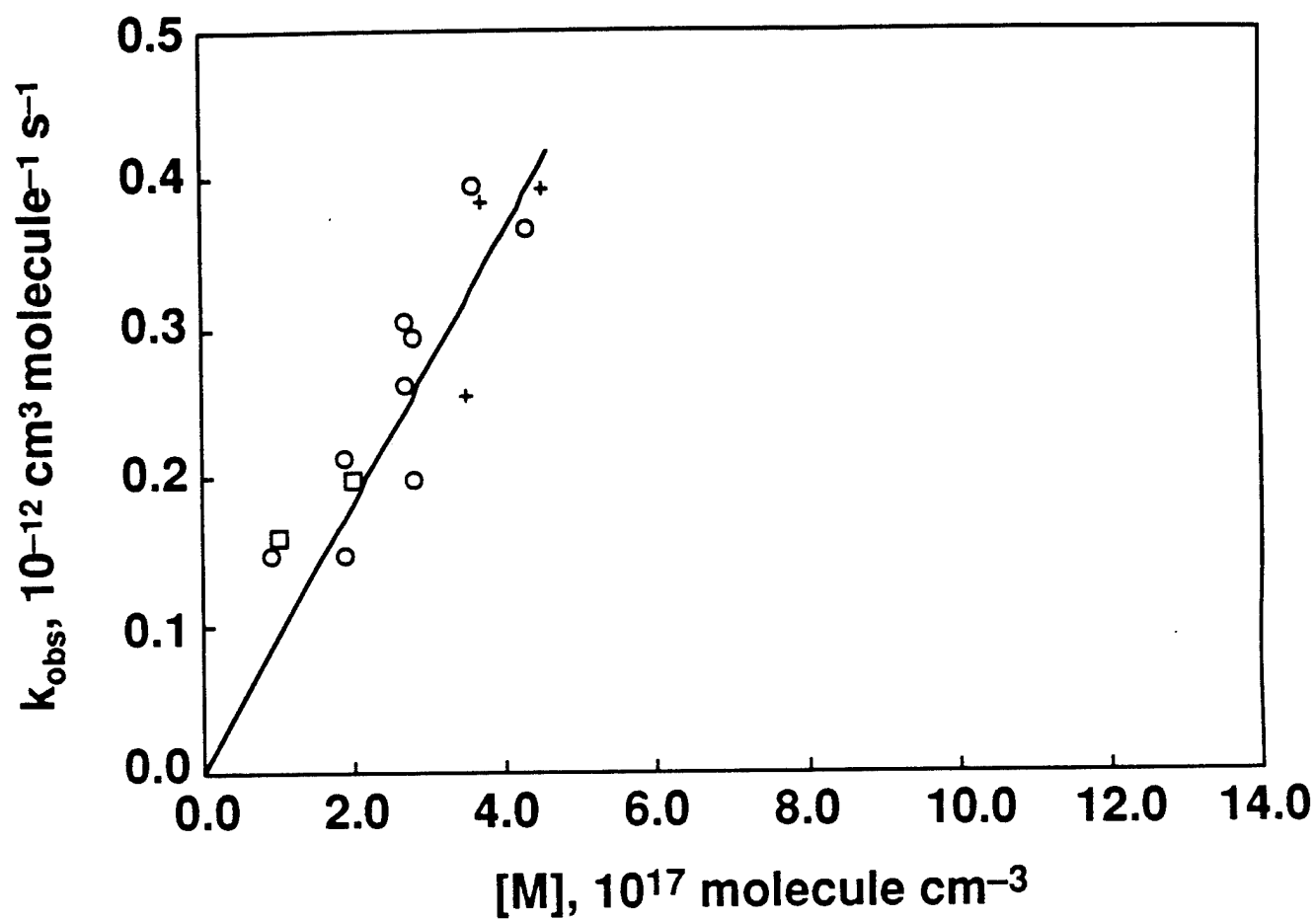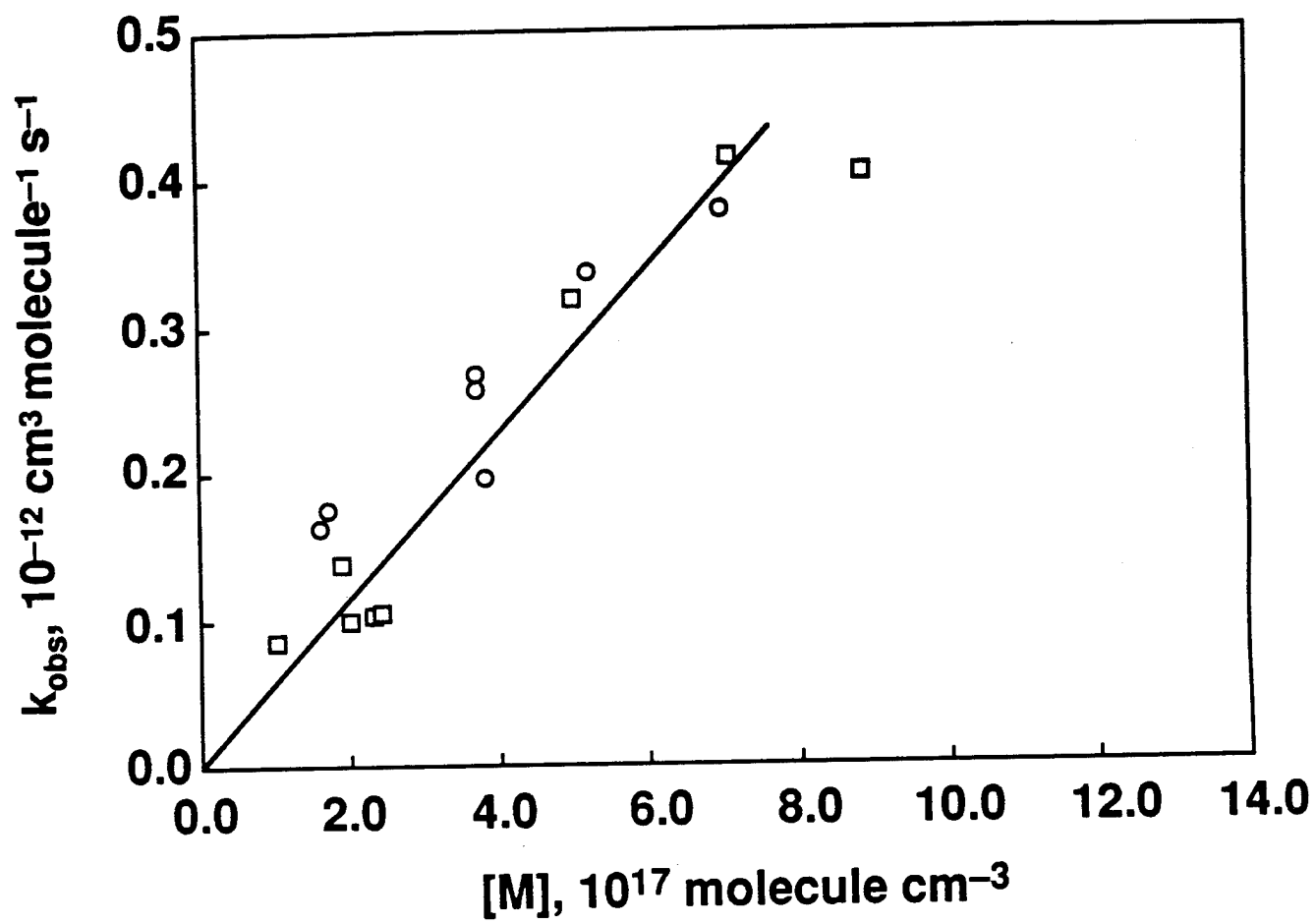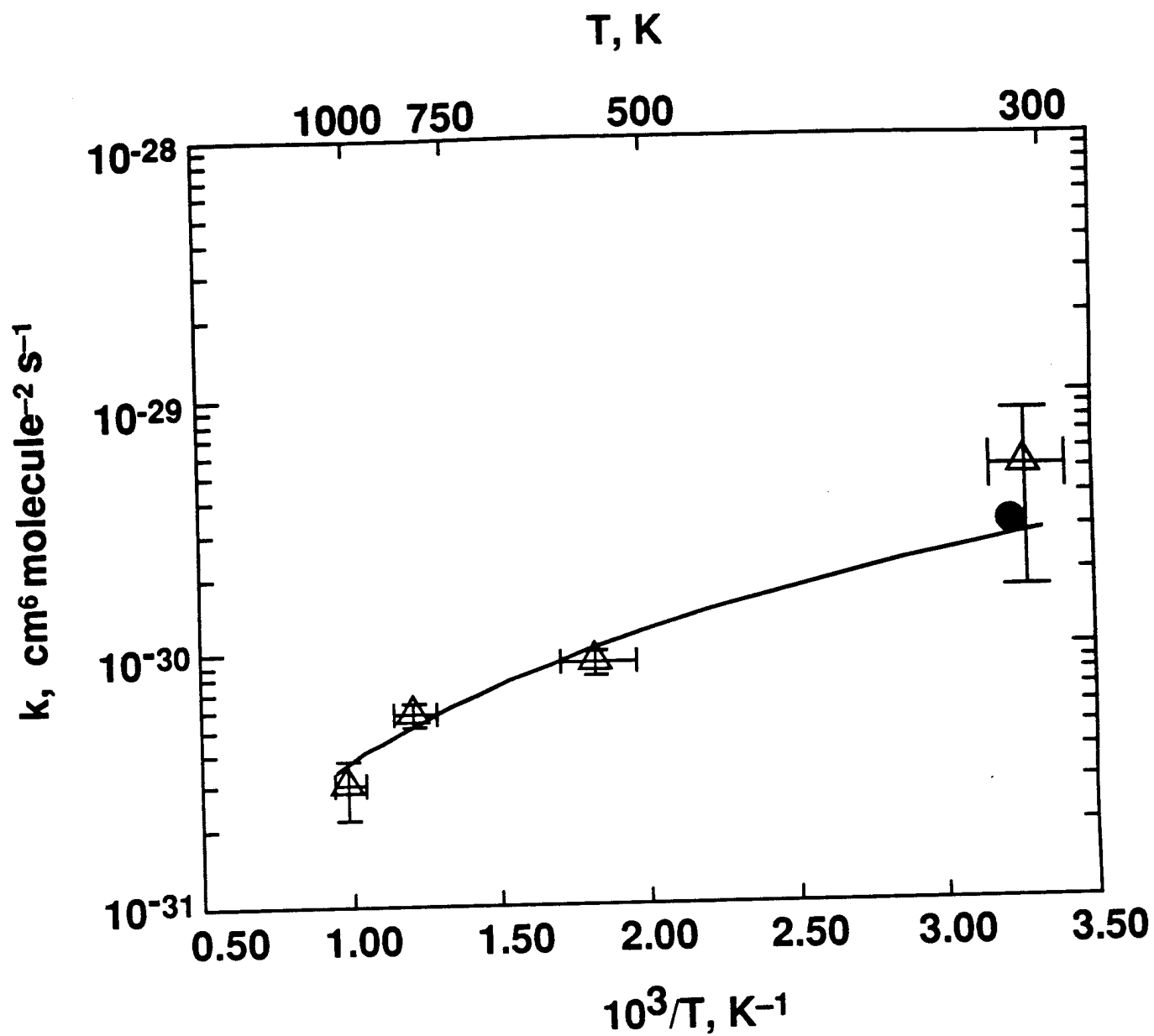
Figure 2

Figure 3

Figure 4

Figure 5

Figure 6